Expanded geographic distribution and dietary strategies of the earliest Oldowan hominins and *Paranthropus*

One Sentence Summary: The 3.032-2.581 Ma Oldowan sites from Nyayanga evidence hippo butchery, plant processing, and the first *Paranthropus* from SW Kenya.

Thomas W. Plummer*[1,2,3,4], James S. Oliver[5], Emma M. Finestone[6,7], Peter W. Ditchfield[8], Laura C. Bishop[9,10], Scott A. Blumenthal[4,11,12], Cristina Lemorini[13], Isabella Caricola[13,14], Shara E. Bailey[3,15], Andy I.R. Herries[16,17], Jennifer A. Parkinson[4,18], Elizabeth Whitfield[9], Fritz Hertel[19], Rahab N. Kinyanjui[4,20,21], Thomas H. Vincent[9], Youjuan Li[22,23], Julien Louys[24], Stephen R. Frost[11], David R. Braun[25,26], Jonathan S. Reeves[26], Emily D.G. Early[4,27], Blasto Onyango[20], Raquel Lamela-Lopez[2,3], Frances L. Forrest[28,29], Huaiyu He[30], Timothy P. Lane[9], Marine Frouin[31], Sébastien Nomade[32,33], Evan P. Wilson[2,3], Simion K. Bartilol[34], Nelson Kiprono Rotich[35], Richard Potts[4,20]

[1] Department of Anthropology, Queens College, Flushing, NY, USA
[2] The CUNY Graduate Center, New York, NY, USA
[3] New York Consortium in Evolutionary Primatology, New York, NY, USA
[4]Human Origins Program, National Museum of Natural History, Smithsonian Institution, Washington DC, USA
[5] Anthropology Section, Illinois State Museum Springfield, IL, USA
[6] The Cleveland Museum of Natural History, Cleveland, OH, USA
[7] Department of Archeology, Max Planck Institute for the Science of Human History, Jena, Germany
[8] School of Archeology, University of Oxford, Oxford, United Kingdom
[9] Research Centre in Evolutionary Anthropology and Paleoecology, School of Biological and Environmental Sciences, Liverpool John Moores University, Liverpool, UK
[10] The Sino-British College, University of Shanghai for Science and Technology, Shanghai, P.R. China
[11] Department of Anthropology, University of Oregon, Eugene, OR, United States
[12] University of British Columbia, Vancouver, BC, Canada
[13] LTFAPA Laboratory, Department of Classics, Sapienza University of Rome, Rome, Italy
[14] School of History, Classics and Archeology, Newcastle University, Newcastle upon Tyne, United Kingdom
[15] Department of Anthropology, New York University, New York, NY, USA
[16] The Australian Archaeomagnetism Laboratory, Dept. Archaeology and History, La Trobe University, Melbourne Campus, 3086, Bundoora, VIC, Australia
[17] Paleo-Research Institute, University of Johannesburg, Johannesburg South Africa
[18] Department of Anthropology, University of San Diego, San Diego, CA, USA
[19] California State University, Northridge, CA, USA
[20] National Museums of Kenya, Nairobi, Kenya
[21] Max Planck Institute for Geoanthropology, Jena, Germany
[22] Department of Geoscience, University of Wisconsin-Madison, Madison, WI, USA
[23] Institute of Geology, China Earthquake Administration, Beijing, China

[24] Australian Research Centre for Human Evolution, Griffith University, Brisbane, Australia
[25] George Washington University, Washington DC, USA
[26] Max Planck Institute for Evolutionary Anthropology, Leipzig, Germany
[27] Arizona Museum of Natural History, Mesa, AZ, USA
[28] Department of Sociology and Anthropology, Fairfield University, Fairfield, CT, USA
[29] American Museum of Natural History, New York, NY, USA
[30] Institute of Geology and Geophysics, Chinese Academy of Sciences, Beijing, China
[31] Department of Geosciences, Stony Brook University, Stony Brook, NY, USA
[32] Université de Versailles Saint-Quentin and Paris Saclay, Gif Sur Yvette, France
[33] Institut Pierre Simon Laplace, Guyancourt, France
[34] Institute of Nuclear Science and Technology, University of Nairobi, Nairobi, Kenya
[35] Institute of Nuclear Chemistry and Technology, Warsaw, Poland

Abstract

The oldest Oldowan tool sites, ca. 2.6 million years ago (Ma), have previously been confined to Ethiopia's Afar Triangle. We describe sites at Nyayanga, Kenya, dated to 3.032-2.581 Ma, and expand this distribution by over 1300 km. Furthermore, we found two hippopotamid butchery sites associated with mosaic vegetation and a C_4 grazer-dominated fauna. Tool flaking proficiency was comparable to younger Oldowan assemblages, but pounding activities were more common. Tool use-wear and bone damage indicate plant and animal tissue processing. *Paranthropus* sp. teeth, the first from southwestern Kenya, possessed carbon isotopic values indicative of a diet rich in C_4 foods. We argue that the earliest Oldowan was more widespread than previously known, used to process diverse foods including megafauna, and associated with *Paranthropus* from its onset.

The appearance of Oldowan tools ca. 2.6 million years ago (Ma) was a technological breakthrough that used systematically produced, sharp-edged flakes for cutting, and cobbles or cores for percussion (*1*). Although the Oldowan is often attributed to the genus *Homo*, multiple hominin taxa overlapped temporally and geographically with these early tools, and it is possible that other genera, such as *Paranthropus*, made and/or used them. Some have linked emergent Oldowan technology to the first access, or more efficient processing of nutrient-rich animal carcasses (e.g., *2*, *3*). Others have argued that plant food processing was the primary goal of early Oldowan stone tool usage, with increased carnivory (and butchery with stone tools) being added to the behavioral repertoire after 2 Ma (*4*, *5*). The evolutionary benefits connected with the emergence of Oldowan technology are unclear due to the paucity of late Pliocene Oldowan

sites, hitherto known only from the Afar Triangle of Ethiopia at Gona and Ledi-Geraru, localities found approximately 50 km away from each other (*6, 7*). Here we report 3.032 - 2.595 Ma deposits at Nyayanga, Kenya, that expand the geographic range of the earliest Oldowan by more than 1300 km and the range of *Paranthropus* by approximately 230 km to southwestern Kenya. Archeological findings demonstrate that hominins used tools to butcher a variety of animals, including megafauna, and process diverse plants at the Oldowan's inception.

Nyayanga (0° 23.909'S, 34° 27.115'E) is an archeological and paleontological locality on the western shoreline of the Homa Peninsula (Fig. 1A) [materials and methods 1, see *(8)*]. The peninsula is located on the southern margin of the Winam Gulf of Lake Victoria, within the E-W oriented Nyanza Rift between the two main branches of the East African Rift System *(9)*. It is dominated by the Homa Mountain carbonatite complex, which on its flanks bears alluvial, fluvial, and lacustrine sediments ranging in age from 6 Ma through the Holocene *(10–13)*. Sediments at Nyayanga are exposed in a 40,000 m^2 amphitheater and a gully that can be traced for 500 m upslope (Fig. 1). Excavations and surface collection focused on the top half of the oldest bed (NY-1), which yielded Oldowan artifacts, *Paranthropus* sp. fossils, and faunal fossils in overbank deposits from a westward-flowing paleochannel [materials and methods 2, see *(8)*].

The age of the Nyayanga Beds is constrained by (U-Th)/He dating of apatite crystals, magnetostratigraphy, lithostratigraphic correlation with the Rawi Fm, and biostratigraphy. (U-Th)/He apatite crystal dating yielded ages of 2.87 +/- 0.79 Ma and 2.98 +/- 0.50 Ma from two tuffaceous silts in NY-1 (fig. S1 and table S1) [materials and methods 3, see *(8)*]. Magnetostratigraphic sampling was carried out on the Excavation 3 slope and in Trenches 9 and 11 (Fig. 1) [materials and methods 4, see *(8)*]. The Nyayanga sequence shows reversed polarity in Unit A, intermediate normal to normal polarity from basal to middle NY-1, normal polarity

from middle NY-1 through NY-2, intermediate normal polarity in the base of NY-3, and reversed polarity at the top of NY-3 (Fig. 1, fig. S2 and table S2). The (U-Th)/He apatite crystal dates suggest the normal interval corresponds to the C2An.1n Gauss Subchron between 3.032 and 2.595 Ma *(14)*. This is similarly indicated by the lithostratigraphic correlation of the Nyayanga Beds with the Rawi Fm, which was also deposited during the C2An.1n Subchron *(13)*. Biostratigraphy (materials and methods 6, see *(8)*) is consistent with a late Pliocene age, including more archaic examples of two pig species, the suid *Metridiochoerus andrewsi* and the tetraconodont *Notochoerus* cf. *scotti*, than the nearby ca. 2 Ma locality of Kanjera South *(13)*, as well as an equid sample composed exclusively of hipparionin (*Eurygnathohippus* sp.) fossils. The latter indicates a date prior to the 2.3 Ma dispersal of *Equus* across Africa *(15)*. Acknowledging the wide 1σ uncertainty, the combination of (U-Th)/He apatite crystal dates, biostratigraphy, and the transitional nature of the magnetostratigraphy of lower NY-1, supports deposition early in the temporal range of the C2An.1n Subchron.

Three hundred thirty artifacts were recovered from the upper half of NY-1; 135 were recovered in situ from Excavations 3 and 5 and 195 were recovered from the surface (materials and methods 7, see *(8)*). The overall technological attributes of tools, such as core and flake sizes and the number of flake scars on cores, are similar to other Oldowan assemblages (Fig. 2A and table S4). Nyayanga hominins efficiently removed flakes from cores using unifacial, bifacial, and multifacial reduction that is also comparable to technology at other Oldowan localities (*7*). The presence of cortical flakes and hammerstones with battering damage is consistent with on-site flake production through hard hammer percussion. Artifacts were manufactured from a diverse array of raw materials, including rhyolite, quartzite, and quartz. The Nyayanga assemblage is unique in containing a high frequency of cores (20.6%, N=68) (Fig. 2B) and a

large percentage of artifacts preserving evidence of percussive activities (7.0%, n=23) (Fig. 2C).

A total of 1,776 bones was recovered in situ from NY-1 in Excavation 3 (n=1580) and Excavation 5 (n=196). The most common taxa in Excavations 3 and 5 are hippopotamids (57.1% and 61.9% of the NISP, respectively) followed by bovids (19.2% and 22.2% of the NISP, respectively) (fig. S4 and tables S5, S6) [materials and methods 8, see *(8)*]. The high in situ frequencies of animals preferring near-water habitats (e.g., hippopotamids, turtles, crocodilians, cane rats [Thryonomyidae]) reflect a riparian depositional context. Bone surface preservation was highly variable, but more than 85% of the sample in both excavations showed no or minimal weathering, consistent with rapid burial by fluvial sediments (fig. S7).

Hippopotamid butchery is documented in both Excavation 3 and Excavation 5. A minimum of two hippopotamid individuals was recovered from Excavation 3 (fig. S5). The more complete individual is composed of 241 bone fragments from across the skeleton, including a large axial bone concentration likely marking its death site. Stone tools (n=42) were closely associated with the skeleton, including several tools recovered in direct physical contact with hippo bones. Despite the varied bone preservation, one hippo rib fragment exhibits a deep cutmark with clearly preserved internal striations (Fig. 3B), and three stone flakes (detached pieces) exhibit use-wear indicative of butchery (see below).

In Excavation 5, thirty-nine hippopotamid bones, likely from a single individual, were found spatially associated with 14 artifacts (fig. S6). One cluster of bones consisted of girdle elements (scapula, innominate), appendicular elements (proximal half of tibia, calcaneum), a flake, and a split cobble with percussion damage. The anterior tuberosity of the tibia has a series of 4 short, parallel cutmarks (Fig. 3A). A second cluster of bones, located 2 m away, consists of a broken humerus, a flake, a rib fragment, and a manuport. The non-anatomical placement of

these bones, some with hominin damage, and associated artifacts (one with use-wear indicative of butchery; see below) in a fine silt suggests that the bones may have been moved by hominins while butchering the carcass.

Tool-damaged bones of non-hippopotamid taxa were also found in the excavations and eroding out of NY-1 in the amphitheater. A size 3 bovid scapular spine fragment with cut marks was found eroding from an in situ context at about the same level as the Excavation 5 hippopotamid (Fig. 3C). Other bones from NY-1 with cut marks or percussion damage show that hominins were consuming both meat and marrow (Fig. 3D), a finding supported by use-wear analysis (see below). Overall frequencies of hominin damage from the excavations are low, 0.9% and 1.9% at Excavations 3 and 5, respectively (table S7). In part, this reflects poor surface preservation of many of the fossils as well as fragmentation of ribs.

Use-wear observed on 30 quartz, quartzite, granite, carbonatite, and rhyolite tools from NY-1 confirm hominin processing of faunal remains and plant tissue (materials and methods 9, see *(8)*). Use-wear found on 6 pounded pieces (*16*) and 17 flaked pieces (i.e., cores) show macro- and micro-traces related to pounding activities (fig. S8). Percussive stone tools were heavily utilized, showing deep pits and developed polishes and striations at low and high magnification, which based on modern experiments require at least several hours of use to emerge. Based on experimental analogues (figs. S9, S10 and tables S8, S10) the quartzite and rhyolite Oldowan percussive tools at Nyayanga were used to process soft (e.g., soft tubers, vegetables, or fruits) and hard (e.g., fibrous tubers or woody parts) plant tissues (fig. S11 and table S11). Macro- and micro-traces related to cutting and scraping on 6 detached pieces (i.e. flakes) and 1 flaked piece show that similar materials were being cut and pounded (fig. S12 and tables S9, S12). Five quartz detached pieces from Excavation 3 show traces indicative of

underground storage organ, wood, and animal processing. A rhyolite flaked piece from Excavation 5 and a NY-1 surface collected detached piece also have use-wear related to butchery (fig. S12 and table S12).

Stable carbon isotopic analysis of pedogenic carbonates, dietary reconstruction using tooth enamel isotopes, and bovid taxonomic frequencies indicate that hominin activities took place in a wooded grassland to grassy woodland/bushland/shrubland along a stream channel within a mesic savanna biome characterized by an abundance of C_4 grasses and herbaceous plants (figs. S13-S17 and tables S13-S14) [materials and methods 10-12, see *(8)*]. Similar C_4 grazer-dominated ecosystems are documented at the Ethiopian sites of Ledi-Geraru (~2.8 Ma) (*17*) and Mille-Logya (~2.8 Ma to ~2.4 Ma) (*18*), indicating that early representatives of both *Paranthropus* and *Homo* were found in substantially open ecosystems. The riparian setting, nearby freshwater spring, and ecotone with open habitats provided Nyayanga hominins with a diverse array of plant and animal foods, shelter, and potable water.

Two hominin individuals from Bed NY-1 are assigned to *Paranthropus* sp. (Fig. 4) [materials and methods 13, see *(8)*]. KNM-NG 77315 is a relatively complete left upper molar, probably M^2, from surface collection, with a crown area above the range of *P. boisei* and *P. robustus* samples (tables S17, S18). KNM-NG 77316 is a nearly complete lingual portion of a left lower molar, probably M_1, found in situ in Excavation 3 spatially associated with Oldowan artifacts and a butchered hippopotamid. The Nyayanga *Paranthropus* teeth have an average $\delta^{13}C_{enamel}$ value of -0.7 ± 0.4‰ (Fig. 4C), which demonstrates a heavy reliance on C_4 foods. Thus, the emergence of C_4 specialist diets coincided with the appearance of at least one major aspect of robust masticatory morphology (large post-canine teeth) relatively early in the evolution of *Paranthropus* (contra (*19*)).

Paranthropus molar KNM-NG 77316 from the Excavation 3 hippopotamid butchery site is a clear association of a hominin fossil with artifacts, raising the possibility that *Paranthropus* made and/or co-opted stone tools. Although its skull anatomy was not preserved, Nyayanga *Paranthropus* was megadont and had flat molars with poor shearing capability. However, its specialized gnathic morphology may not have precluded tool use. Extraoral cutting and pounding using stone tools could have provided access to carcasses and within bone nutrients, and made plant and animal tissue easier to chew and digest (*20*), potentially allowing *Paranthropus* to expand its diet. While not found at Nyayanga, *Homo* was also present in eastern Africa at about the time of Nyayanga deposition (*21*), so the Nyayanga artifacts cannot be definitively attributed to a specific hominin genus.

Deposits at Nyayanga dated between 3.032-2.581 Ma show that at its earliest onset the Oldowan was geographically more widely dispersed than previously known, a finding consistent with a recently described ca. 2.4 Ma Oldowan site in North Africa (*22*). Nyayanga artifacts were used to cut, scrape, and pound large mammal and plant tissue, demonstrating that at its emergence Oldowan tools were used in a variety of actions to access a broad array of food types. By 2 Ma Oldowan sites are found from northern to southern Africa in both grassy and wooded habitats (*23*), suggesting that one of the key attributes of the technology was the flexibility to process foods with different physical properties in a diversity of habitats.

The behaviors preserved at Nyayanga are at least 600,000 years older than prior evidence of megafaunal carcass and plant processing, and substantially predate the increase in absolute brain size documented in the genus *Homo* after 2 Ma (*24*). The late Pliocene expanded geography of the earliest Oldowan, and new evidence of its use in diverse tasks, amplifies our

understanding of the adaptive advantage of early stone technology in hominin diet and foraging ecology.

References and Notes

1. N. Toth, K. Schick, An overview of the cognitive implications of the Oldowan Industrial Complex. *Azania: Archaeological Research in Africa*. **53**, 3–39 (2018), DOI: https://doi.org/10.1080/0067270X.2018.1439558.

2. M. J. Rogers, S. Semaw, in *Sourcebook of Paleolithic transitions* (Springer, 2009), pp. 155–171.

3. I. Cáceres, N. Kandi, M. Sahnouni, Z. Harichane, J. van der Made, in *Proceedings of the II Meeting of African Prehistory Burgos 15–16 April, 2015.* (Consorcio CENIEH Burgos, Spain, 2017), pp. 173–196.

4. M. Domínguez-Rodrigo, B. Martinez-Navarro, Taphonomic analysis of the early Pleistocene (2.4 Ma) faunal assemblage from AL 894 (Hadar, Ethiopia). *Journal of Human Evolution*. **62**, 315–327 (2012), DOI: https://doi.org/10.1016/j.jhevol.2010.01.010.

5. E. Hovers, in *Developments in Quaternary Sciences* (Elsevier, 2012), vol. 16, pp. 51–68.

6. S. Semaw, P. Renne, J. W. Harris, C. S. Feibel, R. L. Bernor, N. Fesseha, K. Mowbray, 2.5-million-year-old stone tools from Gona, Ethiopia. *Nature*. **385**, 333–336 (1997), DOI: https://doi.org/10.1038/385333a0.

7. D. R. Braun, V. Aldeias, W. Archer, J. R. Arrowsmith, N. Baraki, C. J. Campisano, A. L. Deino, E. N. DiMaggio, G. Dupont-Nivet, B. Engda, Earliest known Oldowan artifacts at> 2.58 Ma from Ledi-Geraru, Ethiopia, highlight early technological diversity. *Proceedings of the National Academy of Sciences*. **116**, 11712–11717 (2019), DOI: https://doi.org/10.1073/pnas.1820177116.

8. Materials and methods 1 to 13 are provided as supplementary materials.

9. M. J. Le Bas, *Carbonatite-nephelinite volcanism: an African case history* (Wiley London, 1977).

10. A. K. Behrensmeyer, R. Potts, T. Plummer, L. Tauxe, N. Opdyke, T. Jorstad, The Pleistocene locality of Kanjera, Western Kenya: stratigraphy, chronology and paleoenvironments. *Journal of Human Evolution*. **29**, 247–274 (1995), DOI: https://doi.org/10.1006/jhev.1995.1059.

11. P. Ditchfield, J. Hicks, T. Plummer, L. C. Bishop, R. Potts, Current research on the Late Pliocene and Pleistocene deposits north of Homa Mountain, southwestern Kenya. *Journal of Human Evolution*. **36**, 123–150 (1999), DOI: https://doi.org/10.1006/jhev.1998.0255.

12. T. Plummer, L. C. Bishop, P. Ditchfield, J. Hicks, Research on Late Pliocene oldowan sites at kanjera south, Kenya. *Journal of Human Evolution*. **36**, 151–170 (1999).

13. L. C. Bishop, T. W. Plummer, D. R. Braun, P. W. Ditchfield, E. Goble Early, F. Hertel, C. Lemorini, J. S. Oliver, R. Potts, T. Vincent, E. Whitfield, R. Kinyanjui, in *African Palaeoecology and Human Origins*, S. C. Reynolds, R. Bobe, Eds. (Cambridge University Press, Cambridge, In Press).

14. J. G. Ogg, in *Geologic Time Scale 2020* (Elsevier, 2020), pp. 159–192.

15. R. L. Bernor, M. J. Armour-Chelu, H. Gilbert, T. M. Kaiser, E. Schulz, in *Cenozoic mammals of Africa*, L. Werdelin, B. Sanders, Eds. (University of California Press, Berkeley, CA, 2010), pp. 685–722.

16. G. L. Isaac, J. W. K. Harris, E. M. Kroll, in *Koobi Fora Research Project, Volume 5: Plio-Pleistocene Archeology* (Clarendon Press, Oxford, 1997).

17. E. N. DiMaggio, C. J. Campisano, J. Rowan, G. Dupont-Nivet, A. L. Deino, F. Bibi, M. E. Lewis, A. Souron, D. Garello, L. Werdelin, Late Pliocene fossiliferous sedimentary record and the environmental context of early Homo from Afar, Ethiopia. *Science*. **347**, 1355–1359 (2015), DOI: https://doi.org/10.1126/science.aaa1415.

18. Z. Alemseged, J. G. Wynn, D. Geraads, D. Reed, W. A. Barr, R. Bobe, S. P. McPherron, A. Deino, M. Alene, M. J. Sier, Fossils from Mille-Logya, Afar, Ethiopia, elucidate the link between Pliocene environmental changes and Homo origins. *Nature Communications*. **11**, 1–12 (2020), DOI: https://doi.org/10.1038/s41467-020-16060-8.

19. J. G. Wynn, Z. Alemseged, R. Bobe, F. E. Grine, E. W. Negash, M. Sponheimer, Isotopic evidence for the timing of the dietary shift toward C4 foods in eastern African Paranthropus. *Proceedings of the National Academy of Sciences*. **117**, 21978–21984 (2020), DOI: https://doi.org/10.1073/pnas.2006221117.

20. K. D. Zink, D. E. Lieberman, Impact of meat and Lower Palaeolithic food processing techniques on chewing in humans. *Nature*. **531**, 500–503 (2016), DOI: https://doi.org/10.1038/nature16990.

21. B. Villmoare, W. H. Kimbel, C. Seyoum, C. J. Campisano, E. N. DiMaggio, J. Rowan, D. R. Braun, J. R. Arrowsmith, K. E. Reed, Early Homo at 2.8 Ma from Ledi-Geraru, Afar, Ethiopia. *Science*. **347**, 1352–1355 (2015), DOI: https://doi.org/10.1126/science.aaa1343.

22. M. Sahnouni, J. M. Parés, M. Duval, I. Cáceres, Z. Harichane, J. Van der Made, A. Pérez-González, S. Abdessadok, N. Kandi, A. Derradji, 1.9-million-and 2.4-million-year-old artifacts and stone tool–cutmarked bones from Ain Boucherit, Algeria. *Science*. **362**, 1297–1301 (2018), DOI: https://doi.org/10.1126/science.aau0008.

23. T. Plummer, Flaked stones and old bones: biological and cultural evolution at the dawn of technology. *American Journal of Physical Anthropology*. **125**, 118–164 (2004), DOI: https://doi.org/10.1002/ajpa.20157.

24. S. C. Antón, R. Potts, L. C. Aiello, Evolution of early Homo: An integrated biological perspective. *Science*. **345** (2014), doi:https://doi.org/10.1126/science.1236828, DOI: https://doi.org/10.1126/science.1236828.

25. N. J. Van der Merwe, F. T. Masao, M. K. Bamford, Isotopic evidence for contrasting diets of early hominins Homo habilis and Australopithecus boisei of Tanzania. *South African Journal of Science*. **104**, 153–155 (2008), DOI: https://hdl.handle.net/10520/EJC96776.

26. T. D. White, S. H. Ambrose, G. Suwa, D. F. Su, D. DeGusta, R. L. Bernor, J.-R. Boisserie, M. Brunet, E. Delson, S. Frost, Macrovertebrate paleontology and the Pliocene habitat of Ardipithecus ramidus. *Science*. **326**, 67–93 (2009), DOI: https://doi.org/10.1126/science.1175822.

27. T. E. Cerling, E. Mbua, F. M. Kirera, F. K. Manthi, F. E. Grine, M. G. Leakey, M. Sponheimer, K. T. Uno, Diet of Paranthropus boisei in the early Pleistocene of East Africa. *Proceedings of the National Academy of Sciences*. **108**, 9337–9341 (2011), DOI: https://doi.org/10.1073/pnas.1104627108.

28. T. E. Cerling, F. K. Manthi, E. N. Mbua, L. N. Leakey, M. G. Leakey, R. E. Leakey, F. H. Brown, F. E. Grine, J. A. Hart, P. Kaleme, Stable isotope-based diet reconstructions of Turkana Basin hominins. *Proceedings of the National Academy of Sciences*. **110**, 10501–10506 (2013), DOI: https://doi.org/10.1073/pnas.1222568110.

29. M. Sponheimer, Z. Alemseged, T. E. Cerling, F. E. Grine, W. H. Kimbel, M. G. Leakey, J. A. Lee-Thorp, F. K. Manthi, K. E. Reed, B. A. Wood, Isotopic evidence of early hominin diets. *Proceedings of the National Academy of Sciences*. **110**, 10513–10518 (2013), DOI: https://doi.org/10.1073/pnas.1222579110.

30. N. E. Levin, Y. Haile-Selassie, S. R. Frost, B. Z. Saylor, Dietary change among hominins and cercopithecids in Ethiopia during the early Pliocene. *Proceedings of the National Academy of Sciences*. **112**, 12304–12309 (2015), DOI: https://doi.org/10.1073/pnas.1424982112.

31. J. R. Robinson, J. Rowan, C. J. Campisano, J. G. Wynn, K. E. Reed, Late Pliocene environmental change during the transition from Australopithecus to Homo. *Nature Ecology & Evolution*. **1**, 1–7 (2017), DOI: https://doi.org/10.1038/s41559-017-0159.

32. T. Lüdecke, O. Kullmer, U. Wacker, O. Sandrock, J. Fiebig, F. Schrenk, A. Mulch, Dietary versatility of Early Pleistocene hominins. *Proceedings of the National Academy of Sciences*. **115**, 13330–13335 (2018), DOI: https://doi.org/10.1073/pnas.1809439115.

33. J. E. Martin, T. Tacail, J. Braga, T. E. Cerling, V. Balter, Calcium isotopic ecology of Turkana Basin hominins. *Nature Communications*. **11**, 1–7 (2020), DOI: https://doi.org/10.1038/s41467-020-17427-7.

34. S. Semaw, M. J. Rogers, S. W. Simpson, N. E. Levin, J. Quade, N. Dunbar, W. C. McIntosh, I. Cáceres, G. E. Stinchcomb, R. L. Holloway, Co-occurrence of Acheulian and Oldowan artifacts with Homo erectus cranial fossils from Gona, Afar, Ethiopia. *Science Advances*. **6**, eaaw4694 (2020), DOI: https://doi.org/10.1098/rspb.2020.2604.

35. M. M. Skinner, M. G. Leakey, L. N. Leakey, F. K. Manthi, F. Spoor, Hominin dental remains from the Pliocene localities at Lomekwi, Kenya (1982–2009). *Journal of Human Evolution*. **145**, 102820 (2020), DOI: https://doi.org/10.1016/j.jhevol.2020.102820.

36. M. Pickford, The geology and palaeontology of the Kanam erosion gullies (Kenya). *Mainzer Geowissenschaftliche Mitteilungen*. **16**, 209–226 (1987).

37. S. R. Frost, T. Plummer, L. C. Bishop, P. Ditchfield, J. Ferraro, J. Hicks, Partial cranium of Cercopithecoides kimeui Leakey, 1982 from Rawi Gully, Southwestern Kenya. *American Journal of Physical Anthropology*. **122**, 191–199 (2003), DOI: https://doi.org/10.1002/ajpa.10279.

38. Y. Li, H. He, T. W. Plummer, P. W. Ditchfield, C. Deng, Z. Guo, R. Potts, Exploration of apatite (UTh)/He geochronological analysis of volcanic units in fossil-bearing strata of the Homa Peninsula, southwestern Kenya. *Palaeogeography, Palaeoclimatology, Palaeoecology*. **579**, 110599 (2021), DOI: https://doi.org/10.1016/j.palaeo.2021.110599.

39. N. J. Evans, J. P. Byrne, J. T. Keegan, L. E. Dotter, Determination of uranium and thorium in zircon, apatite, and fluorite: Application to laser (U-Th)/He thermochronology. *Journal of Analytical Chemistry*. **60**, 1159–1165 (2005), DOI: https://doi.org/10.1007/s10809-005-0260-1.

40. A. M. Kinyua, T. Plummer, N. Shimizu, W. Melson, R. Potts, Provenance of Kanjera Fossils by X-Ray Fluorescence and Ion Microprobe Analyses. *Advances in X-ray Analysis*. **35**, 1165–1173 (1991), DOI: https://doi.org/10.1154/S0376030800013458.

41. S. Ohde, Instrumental neutron activation analysis of carbonatites from Homa Mountain, Kenya. *Journal of Radioanalytical and Nuclear Chemistry*. **260**, 213–218 (2004), DOI: https://doi.org/10.1023/B:JRNC.0000027084.87098.74.

42. D. Otwoma, J. P. Patel, S. Bartilol, A. O. Mustapha, Estimation of annual effective dose and radiation hazards due to natural radionuclides in mount Homa, southwestern Kenya. *Radiation Protection Dosimetry*. **155**, 497–504 (2013), DOI: https://doi.org/10.1093/rpd/nct031.

43. A. I. R. Herries, M. Kovacheva, M. Kostadinova, Mineral magnetism and archaeomagnetic dating of a mediaeval oven from Zlatna Livada, Bulgaria. *Physics and Chemistry of the Earth, Parts A/B/C*. **33**, 496–510 (2008), DOI: https://doi.org/10.1016/j.pce.2008.02.021.

44. M. Kostadinova, N. Jordanova, D. Jordanova, M. Kovacheva, Preliminary study on the effect of water glass impregnation on the rock-magnetic properties of baked clay. *Studia Geophysica et Geodaetica*. **48**, 637–646 (2004), DOI: https://doi.org/10.1023/B:SGEG.0000037475.67953.9b.

45. J. L. Kirschvink, The least-squares line and plane and the analysis of palaeomagnetic data. *Geophysical Journal International*. **62**, 699–718 (1980), DOI: https://doi.org/10.1111/j.1365-246X.1980.tb02601.x.

46. R. A. Fisher, Dispersion on a sphere. *Proceedings of the Royal Society of London. Series A. Mathematical and Physical Sciences*. **217**, 295–305 (1953), DOI: https://doi.org/10.1098/rspa.1953.0064.

47. Y. Yamamoto, O. Ishizuka, M. Sudo, K. 4 Uto, 40Ar/39Ar ages and palaeomagnetism of transitionally magnetized volcanic rocks in the Society Islands, French Polynesia: Raiatea excursion in the upper-Gauss Chron. *Geophysical Journal International*. **169**, 41–59 (2007), DOI: https://doi.org/10.1111/j.1365-246X.2006.03277.x.

48. T. Harrison, *Paleontology and Geology of Laetoli: Human Evolution in Context: Volume 1: Geology, Geochronology, Paleoecology and Paleoenvironment* (Springer Science & Business Media, 2011).

49. A. L. Deino, in *Paleontology and geology of Laetoli: Human evolution in context* (Springer, Dordrecht, 2011), pp. 77–97.

50. M. Frouin, S. Huot, S. Kreutzer, C. Lahaye, M. Lamothe, A. Philippe, N. Mercier, An improved radiofluorescence single-aliquot regenerative dose protocol for K-feldspars. *Quaternary Geochronology*. **38**, 13–24 (2017), DOI: 10.1016/j.quageo.2016.11.004.

51. M. K. Murari, S. Kreutzer, M. Fuchs, Further investigations on IR-RF: Dose recovery and correction. *Radiation Measurements*. **120**, 110–119 (2018), DOI: 10.1016/j.radmeas.2018.04.017.

52. S. Nomade, A. Gauthier, H. Guillou, J.-F. Pastre, 40Ar/39Ar temporal framework for the Alleret maar lacustrine sequence (French Massif-Central): volcanological and

paleoclimatic implications. *Quaternary Geochronology*. **5**, 20–27 (2010), DOI: https://doi.org/10.1016/j.quageo.2009.07.001.

53. E. M. Niespolo, D. Rutte, A. L. Deino, P. R. Renne, Intercalibration and age of the Alder Creek sanidine 40Ar/39Ar standard. *Quaternary Geochronology*. **39**, 205–213 (2017), DOI: https://doi.org/10.1016/j.quageo.2016.09.004.

54. L. C. Bishop, in *Cenozoic mammals of Africa* (University of California Press, Berkeley, CA, 2010), vol. 821, pp. 821–842.

55. N. G. Jablonski, S. R. Frost, in *Cenozoic Mammals of Africa, eds Werdelin L, Sanders WJ* (Univ California Press, Berkeley, CA, 2010).

56. W. J. Sanders, E. Gheerbrant, J. M. Harris, H. Saegusa, C. Delmer, in *Cenozoic Mammals of Africa* (University of California Press, Berkeley, CA, 2010), pp. 161–251.

57. M. Dominguez-Rodrigo, T. R. Pickering, E. Baquedano, A. Mabulla, D. F. Mark, C. Musiba, H. T. Bunn, D. Uribelarrea, V. Smith, F. Diez-Martin, First partial skeleton of a 1.34-million-year-old Paranthropus boisei from Bed II, Olduvai Gorge, Tanzania. *PLoS One*. **8**, e80347 (2013), DOI: https://doi.org/10.1371/journal.pone.0080347.

58. M. G. Leakey, Extinct large colobines from the Plio-Pleistocene of Africa. *American Journal of Physical Anthropology*. **58**, 153–172 (1982), DOI: https://doi.org/10.1002/ajpa.1330580207.

59. J. M. Harris, F. H. Brown, M. G. Leakey, *Stratigraphy and paleontology of Pliocene and Pleistocene localities west of Lake Turkana, Kenya* (Natural History Museum of Los Angeles County, 1988).

60. N. P. Toth, thesis, University of California, Berkeley (1982).

61. N. Toth, Behavioral inferences from early stone artifact assemblages: an experimental model. *Journal of Human Evolution*. **16**, 763–787 (1987), DOI: https://doi.org/10.1016/0047-2484(87)90023-6.

62. D. Stout, S. Semaw, M. J. Rogers, D. Cauche, Technological variation in the earliest Oldowan from Gona, Afar, Ethiopia. *Journal of Human Evolution*. **58**, 474–491 (2010), DOI: https://doi.org/10.1016/j.jhevol.2010.02.005.

63. D. R. Braun, J. W. Harris, in *Oldowan: Rather more than smashing stones*, J. Moreno, R. Torcal, I. Saniz, Eds. (University of Barcelona Press, 2003), pp. 117–144.

64. D. R. Braun, Examining flake production strategies: examples from the Middle Paleolithic of Southwest Asia. *Lithic Technology*. **30**, 107–125 (2005), DOI: https://doi.org/10.1080/01977261.2005.11721029.

65. A. Mackay, A method for estimating edge length from flake dimensions: use and implications for technological change in the southern African MSA. *Journal of Archaeological Science*. **35**, 614–622 (2008), DOI: http://dx.doi.org/10.1016/j.jas.2007.05.013.

66. I. de la Torre, R. Mora, M. Domínguez-Rodrigo, L. de Luque, L. Alcalá, The Oldowan industry of Peninj and its bearing on the reconstruction of the technological skills of Lower Pleistocene hominids. *Journal of Human Evolution*. **44**, 203–224 (2003), DOI: https://doi.org/10.1016/S0047-2484(02)00206-3.

67. J. Mercader, P. Akuku, N. Boivin, R. Bugumba, P. Bushozi, A. Camacho, T. Carter, S. Clarke, A. Cueva-Temprana, P. Durkin, Earliest Olduvai hominins exploited unstable environments~ 2 million years ago. *Nature Communications*. **12**, 1–15 (2021), DOI: https://doi.org/10.1038/s41467-020-20176-2.

68. H. T. Bunn, thesis, University of California, Berkeley (1982).

69. H. T. Bunn, Archaeological evidence for meat-eating by Plio-Pleistocene hominids from Koobi Fora and Olduvai Gorge. *Nature*. **291**, 574–577 (1981), DOI: https://doi.org/10.1038/291574a0.

70. R. Potts, P. Shipman, Cutmarks made by stone tools on bones from Olduvai Gorge, Tanzania. *Nature*. **291**, 577–580 (1981), DOI: https://doi.org/10.1038/291577a0.

71. R. J. Blumenschine, C. W. Marean, S. D. Capaldo, Blind tests of inter-analyst correspondence and accuracy in the identification of cut marks, percussion marks, and carnivore tooth marks on bone surfaces. *Journal of Archaeological Science*. **23**, 493–507 (1996), DOI: https://doi.org/10.1006/jasc.1996.0047.

72. R. J. Blumenschine, M. M. Selvaggio, Percussion marks on bone surfaces as a new diagnostic of hominid behaviour. *Nature*. **333**, 763–765 (1988), DOI: https://doi.org/10.1038/333763a0.

73. T. R. Pickering, C. P. Egeland, Experimental patterns of hammerstone percussion damage on bones: implications for inferences of carcass processing by humans. *Journal of Archaeological Science*. **33**, 459–469 (2006), DOI: https://doi.org/10.1016/j.jas.2005.09.001.

74. J. S. Oliver, *Diagnosing bone fracture to assess early hominin behaviour, meat-eating, and socioecology at FLK-Zinjanthropus, Olduvai Gorge, Tanzania* (Liverpool John Moores University (United Kingdom), 2015).

75. Y. Fernandez-Jalvo, P. Andrews, *Atlas of taphonomic identifications: 1001+ images of fossil and recent mammal bone modification* (Springer, 2016).

76. M. Domínguez-Rodrigo, E. Baquedano, Distinguishing butchery cut marks from crocodile bite marks through machine learning methods. *Scientific Reports*. **8**, 1–8 (2018), DOI: https://doi.org/10.1038/s41598-018-24071-1.

77. L. R. Binford, *Bones: ancient men and modern myths* (Academic press, 2014).

78. M. M. Selvaggio, Carnivore tooth marks and stone tool butchery marks on scavenged bones: archaeological implications. *Journal of Human Evolution*. **27**, 215–228 (1994), DOI: https://doi.org/10.1006/jhev.1994.1043.

79. C. Delaney-Rivera, T. W. Plummer, J. A. Hodgson, F. Forrest, F. Hertel, J. S. Oliver, Pits and pitfalls: taxonomic variability and patterning in tooth mark dimensions. *Journal of Archaeological Science*. **36**, 2597–2608 (2009), DOI: https://doi.org/10.1016/j.jas.2009.08.001.

80. G. J. Linares Matás, J. Yravedra, ‘We hunt to share’: social dynamics and very large mammal butchery during the Oldowan–Acheulean transition. *World Archaeology*, 1–31 (2022), DOI: https://doi.org/10.1080/00438243.2022.2030793.

81. C. Lemorini, T. W. Plummer, D. R. Braun, A. N. Crittenden, P. W. Ditchfield, L. C. Bishop, F. Hertel, J. S. Oliver, F. W. Marlowe, M. J. Schoeninger, Old stones’ song: use-wear experiments and analysis of the Oldowan quartz and quartzite assemblage from Kanjera South (Kenya). *Journal of Human Evolution*. **72**, 10–25 (2014), DOI: https://doi.org/10.1016/j.jhevol.2014.03.002.

82. C. Lemorini, L. C. Bishop, T. W. Plummer, D. R. Braun, P. W. Ditchfield, J. S. Oliver, Old stones’ song—second verse: use-wear analysis of rhyolite and fenetized andesite artifacts from the Oldowan lithic industry of Kanjera South, Kenya. *Archaeological and Anthropological Sciences*. **11**, 4729–4754 (2019), DOI: https://doi.org/10.1007/s12520-019-00800-z.

83. C. Hamon, *Broyage et abrasion au Néolithique ancien. Caractérisation technique et fonctionnelle des outils en grès du Bassin parisien. British Archaeological Reports* (2006), vol. 1551.

84. M. J. Jackson, M. P. Hitchiner, *High performance grinding and advanced cutting tools* (Springer Science & Business Media, 2012).

85. J. L. Adams, S. Delgado, L. Dubreuil, C. Hamon, H. Plisson, R. Risch, F. Sternke, L. J. Costa, L. Eigeland, in *Functional analysis of macro-lithic artifacts.* (Archaeopress Oxford, 2009), pp. 43–66.

86. L. Dubreuil, D. Savage, S. Delgado-Raack, H. Plisson, B. Stephenson, I. de la Torre, in *Use-wear and residue analysis in archaeology* (Springer, 2015), pp. 105–158.

87. A. Pedergnana, A. Ollé, A. A. Evans, A new combined approach using confocal and scanning electron microscopy to image surface modifications on quartzite. *Journal of Archaeological Science: Reports*. **30**, 102237 (2020), DOI: https://doi.org/10.1016/j.jasrep.2020.102237.

88. V. Rots, Hafting and raw materials from animals: Guide to the identification of hafting traces on stone tools. *Anthropozoologica*. **43**, 43–66 (2008).

89. A. van Gijn, *Flint in focus: lithic biographies in the Neolithic and Bronze Age* (Sidestone Press, Leiden, 2010).

90. D. Stapert, Some natural surface modifications on flint in the Netherlands. *Palaeohistoria*, 7–41 (1976).

91. H. Plisson, M. Mauger, Chemical and mechanical alteration of microwear polishes: an experimental approach. *Helinium*. **28**, 3–16 (1988).

92. I. Levi-Sala, *Processes of polish formation on flint tool surface. British Archaeological Reports International Series, vol. 411. Archaeopress* (Oxford, 1988).

93. J. J. Flenniken, J. C. Haggarty, Trampling as an agency in the formation of edge damage: an experiment in lithic technology. *Northwest Anthropological Research Notes*. **13**, 208–214 (1979).

94. S. McBrearty, L. Bishop, T. Plummer, R. Dewar, N. Conard, Tools underfoot: human trampling as an agent of lithic artifact edge modification. *American Antiquity*. **63**, 108–129 (1998).

95. T. E. Cerling, J. Quade, Y. Wang, J. R. Bowman, Carbon isotopes in soils and palaeosols as ecology and palaeoecology indicators. *Nature*. **341**, 138–139 (1989), DOI: https://doi.org/10.1038/341138a0.

96. T. E. Cerling, J. G. Wynn, S. A. Andanje, M. I. Bird, D. K. Korir, N. E. Levin, W. Mace, A. N. Macharia, J. Quade, C. H. Remien, Woody cover and hominin environments in the past 6 million years. *Nature*. **476**, 51–56 (2011).

97. T. E. Cerling, J. M. Harris, Carbon isotope fractionation between diet and bioapatite in ungulate mammals and implications for ecological and paleoecological studies. *Oecologia*. **120**, 347–363 (1999), DOI: https://doi.org/10.1007/s004420050868.

98. B. H. Passey, T. F. Robinson, L. K. Ayliffe, T. E. Cerling, M. Sponheimer, M. D. Dearing, B. L. Roeder, J. R. Ehleringer, Carbon isotope fractionation between diet, breath CO2, and bioapatite in different mammals. *Journal of Archaeological Science*. **32**, 1459–1470 (2005), DOI: https://doi.org/10.1016/j.jas.2005.03.015.

99. T. E. Cerling, S. A. Andanje, S. A. Blumenthal, F. H. Brown, K. L. Chritz, J. M. Harris, J. A. Hart, F. M. Kirera, P. Kaleme, L. N. Leakey, Dietary changes of large herbivores in the Turkana Basin, Kenya from 4 to 1 Ma. *Proceedings of the National Academy of Sciences*. **112**, 11467–11472 (2015), DOI: https://doi.org/10.1073/pnas.1513075112.

100. J. V. Tejada-Lara, B. J. MacFadden, L. Bermudez, G. Rojas, R. Salas-Gismondi, J. J. Flynn, Body mass predicts isotope enrichment in herbivorous mammals. *Proceedings of the Royal Society B.* **285**, 20181020 (2018), DOI: https://doi.org/10.1098/rspb.2018.1020.

101. A. Zazzo, M. Balasse, B. H. Passey, A. P. Moloney, F. J. Monahan, O. Schmidt, The isotope record of short-and long-term dietary changes in sheep tooth enamel: implications for quantitative reconstruction of paleodiets. *Geochimica et Cosmochimica Acta*. **74**, 3571–3586 (2010), DOI: https://doi.org/10.1016/j.gca.2010.03.017.

102. B. J. Tipple, S. R. Meyers, M. Pagani, Carbon isotope ratio of Cenozoic CO2: A comparative evaluation of available geochemical proxies. *Paleoceanography*. **25** (2010), doi:https://doi.org/10.1029/2009PA001851, DOI: https://doi.org/10.1029/2009PA001851.

103. M. J. Kohn, Predicting animal δ18O: accounting for diet and physiological adaptation. *Geochimica et Cosmochimica Acta*. **60**, 4811–4829 (1996), DOI: https://doi.org/10.1016/S0016-7037(96)00240-2.

104. N. E. Levin, T. E. Cerling, B. H. Passey, J. M. Harris, J. R. Ehleringer, A stable isotope aridity index for terrestrial environments. *Proceedings of the National Academy of Sciences*. **103**, 11201–11205 (2006), DOI: https://doi.org/10.1073/pnas.0604719103.

105. S. A. Blumenthal, N. E. Levin, F. H. Brown, J.-P. Brugal, K. L. Chritz, J. M. Harris, G. E. Jehle, T. E. Cerling, Aridity and hominin environments. *Proceedings of the National Academy of Sciences*. **114**, 7331–7336 (2017), DOI: https://doi.org/10.1073/pnas.1700597114.

106. M. P. Veldhuis, E. S. Kihwele, J. Cromsigt, J. O. Ogutu, J. G. C. Hopcraft, N. Owen-Smith, H. Olff, Large herbivore assemblages in a changing climate: incorporating water dependence and thermoregulation. *Ecology Letters*. **22**, 1536–1546 (2019), DOI: https://doi.org/10.1111/ele.13350.

107. E. S. Kihwele, V. Mchomvu, N. Owen-Smith, R. S. Hetem, M. C. Hutchinson, A. B. Potter, H. Olff, M. P. Veldhuis, Quantifying water requirements of African ungulates through a combination of functional traits. *Ecological Monographs*. **90**, e01404 (2020), DOI: https://doi.org/10.1002/ecm.1404.

108. S. A. Blumenthal, T. E. Cerling, T. M. Smiley, C. E. Badgley, T. W. Plummer, Isotopic records of climate seasonality in equid teeth. *Geochimica et Cosmochimica Acta*. **260**, 329–348 (2019), DOI: https://doi.org/10.1016/j.gca.2019.06.037.

109. K. T. Uno, F. Rivals, F. Bibi, M. Pante, J. Njau, I. de la Torre, Large mammal diets and paleoecology across the Oldowan–Acheulean transition at Olduvai Gorge, Tanzania from stable isotope and tooth wear analyses. *Journal of Human Evolution*. **120**, 76–91 (2018), DOI: https://doi.org/10.1016/j.jhevol.2018.01.002.

110. J. Rowan, E. M. Locke, J. R. Robinson, C. J. Campisano, J. G. Wynn, K. E. Reed, Fossil Giraffidae (Mammalia, Artiodactyla) from Lee Adoyta, Ledi-Geraru, and Late Pliocene Dietary Evolution in Giraffids from the Lower Awash Valley, Ethiopia. *Journal of Mammalian Evolution*. **24**, 359–371 (2017), DOI: https://doi.org/10.1007/s10914-016-9343-z.

111. D. Geraads, Perissodactyla (Rhinocerotidae and Equidae) from Kanapoi. *Journal of Human Evolution*. **140**, 102373 (2020), DOI: https://doi.org/10.1016/j.jhevol.2017.07.013.

112. T. W. Plummer, E. M. Finestone, in *Rethinking Human Evolution*, J. H. Schwartz, Ed. (MIT Press, Cambridge, Massachusetts, 2018), pp. 267–296.

113. E. S. Vrba, *The significance of bovid remains as indicators of environment and predation patterns. In (AK Behrensmeyer & AP Hill, Eds) Fossils in the Making* (Chicago: University of Chicago Press, 1980).

114. P. Shipman, J. Harris, in *Evolutionary History of the'Robust'Australopithecines. F. Grine, eds. New York, Aldine de Gruyter* (1988), pp. 343–383.

115. F. Bibi, J. Rowan, K. Reed, Late Pliocene Bovidae from Ledi-Geraru (Lower Awash Valley, Ethiopia) and their implications for Afar paleoecology. *Journal of Vertebrate Paleontology*. **37**, e1337639 (2017), DOI: https://doi.org/10.1080/02724634.2017.1337639.

116. B. A. Wood, S. A. Abbott, Analysis of the dental morphology of Plio-pleistocene hominids. I. Mandibular molars: crown area measurements and morphological traits. *Journal of Anatomy*. **136**, 197 (1983), DOI: PMCID: PMC1171940.

117. B. A. Wood, S. A. Abbott, S. H. Graham, Analysis of the dental morphology of Plio-Pleistocene hominids. II. Mandibular molars--study of cusp areas, fissure pattern and cross sectional shape of the crown. *Journal of Anatomy*. **137**, 287 (1983), DOI: PMCID: PMC1262088.

118. B. A. Wood, C. A. Engleman, Analysis of the dental morphology of Plio-Pleistocene hominids. V. Maxillary postcanine tooth morphology. *Journal of Anatomy*. **161**, 1 (1988), DOI: PMCID: PMC1262088.

119. B. Asfaw, T. White, O. Lovejoy, B. Latimer, S. Simpson, G. Suwa, Australopithecus garhi: a new species of early hominid from Ethiopia. *Science*. **284**, 629–635 (1999), DOI: https://doi.org/10.1126/science.284.5414.629.

120. C. G. I. Turner, C. R. Nichol, G. R. Scott, in *Advances in Dental Anthropology*, M. A. Kelley, C. S. Larsen, Eds. (Wiley-Liss, 1991), pp. 13–31.

121. S. E. Bailey, A morphometric analysis of maxillary molar crowns of Middle-Late Pleistocene hominins. *Journal of Human Evolution*. **47**, 183–198 (2004), DOI: https://doi.org/10.1016/j.jhevol.2004.07.001.

122. S. Molnar, Human tooth wear, tooth function and cultural variability. *American Journal of Physical Anthropology*. **34**, 175–189 (1971), DOI: https://doi.org/10.1002/ajpa.1330340204.

123. R. Quam, S. Bailey, B. Wood, Evolution of M1 crown size and cusp proportions in the genus Homo. *Journal of Anatomy*. **214**, 655–670 (2009), DOI: https://doi.org/10.1111/j.1469-7580.2009.01064.x.

124. A. Ortiz, M. M. Skinner, S. E. Bailey, J.-J. Hublin, Carabelli's trait revisited: An examination of mesiolingual features at the enamel–dentine junction and enamel surface of Pan and Homo sapiens upper molars. *Journal of Human Evolution*. **63**, 586–596 (2012), DOI: https://doi.org/10.1016/j.jhevol.2012.06.003.

125. A. D. Beynon, B. A. Wood, Variations in enamel thickness and structure in East African hominids. *American Journal of Physical Anthropology*. **70**, 177–193 (1986), DOI: https://doi.org/10.1002/ajpa.1330700205.

126. F. E. Grine, R. L. Jacobs, K. E. Reed, J. M. Plavcan, The enigmatic molar from Gondolin, South Africa: implications for Paranthropus paleobiology. *Journal of human evolution*. **63**, 597–609 (2012), DOI: http://dx.doi.org/10.1016/j.jhevol.2012.06.005.

127. T. W. Plummer, P. W. Ditchfield, L. C. Bishop, J. D. Kingston, J. V. Ferraro, D. R. Braun, F. Hertel, R. Potts, Oldest evidence of toolmaking hominins in a grassland-dominated ecosystem. *PLoS One*. **4**, e7199 (2009), DOI: https://doi.org/10.1371/journal.pone.0007199.

128. N. E. Levin, J. Quade, S. W. Simpson, S. Semaw, M. Rogers, Isotopic evidence for Plio–Pleistocene environmental change at Gona, Ethiopia. *Earth and Planetary Science Letters*. **219**, 93–110 (2004), DOI: https://doi.org/10.1016/S0012-821X(03)00707-6.

129. R. L. Quinn, C. J. Lepre, C. S. Feibel, J. D. Wright, R. A. Mortlock, S. Harmand, J.-P. Brugal, H. Roche, Pedogenic carbonate stable isotopic evidence for wooded habitat preference of early Pleistocene tool makers in the Turkana Basin. *Journal of Human Evolution*. **65**, 65–78 (2013), DOI: https://doi.org/10.1016/j.jhevol.2013.04.002.

130. S. Harmand, J. E. Lewis, C. S. Feibel, C. J. Lepre, S. Prat, A. Lenoble, X. Boës, R. L. Quinn, M. Brenet, A. Arroyo, 3.3-million-year-old stone tools from Lomekwi 3, West Turkana, Kenya. *Nature*. **521**, 310–315 (2015), DOI: https://doi.org/10.1038/nature14464.

131. J. D. Kingston, in *Paleontology and geology of Laetoli: Human evolution in context* (Springer, 2011), pp. 293–328.

132. J. G. Wynn, K. E. Reed, M. Sponheimer, W. H. Kimbel, Z. Alemseged, Z. K. Bedaso, C. J. Campisano, Dietary flexibility of Australopithecus afarensis in the face of paleoecological change during the middle Pliocene: Faunal evidence from Hadar, Ethiopia. *Journal of Human Evolution*. **99**, 93–106 (2016), DOI: https://doi.org/10.1016/j.jhevol.2016.08.002.

133. D. B. Patterson, D. R. Braun, K. Allen, W. A. Barr, A. K. Behrensmeyer, M. Biernat, S. B. Lehmann, T. Maddox, F. K. Manthi, S. R. Merritt, Comparative isotopic evidence from East Turkana supports a dietary shift within the genus Homo. *Nature Ecology & Evolution*. **3**, 1048–1056 (2019), DOI: https://doi.org/10.1038/s41559-019-0916-0.

134. E. W. Negash, Z. Alemseged, R. Bobe, F. Grine, M. Sponheimer, J. G. Wynn, Dietary trends in herbivores from the Shungura Formation, southwestern Ethiopia. *Proceedings of the National Academy of Sciences*. **117**, 21921–21927 (2020), DOI: https://doi.org/10.1073/pnas.2006982117.

135. H. T. Bunn, Patterns of skeletal representation and hominid subsistence activities at Olduvai Gorge, Tanzania, and Koobi Fora, Kenya. *Journal of Human Evolution*. **15**, 673–690 (1986), DOI: https://doi.org/10.1016/S0047-2484(86)80004-5.

ACKNOWLEDGEMENTS
The authors thank the National Museums of Kenya and M. Kibunjia, F.K. Manthi, J. Kibii, and E. Ndiema for support and acknowledge Kenya Government permission granted by the Ministry of Sports, Culture and the Arts and by NACOSTI permit P/14/7709/701.We thank Peter Onyango for bringing the Nyayanga exposures to our attention. Nancy Todd assisted with elephant tooth identification.
Funding: Funding from the L.S.B. Leakey Foundation (award # 35805), the National Science Foundation (award # 1327047), the Wenner-Gren Foundation (award # 9428), and the Professional Staff Congress City University of New York Research Award Program (award # 60589-00 48) to TP, and funding from the William H. Donner Foundation and the Peter Buck Fund for Human Origins Research to RP, is gratefully acknowledged.
Author contributions: T.W.P., L.C.B., E.F., J.S.O., B.O., and R.P. contributed to excavation strategy and research design. Magnetostratigraphy sampling was conducted by P.W.D., and analysis of samples and magnetostratigraphic interpretation was undertaken by A.I.R.H. Sampling for (U-Th)/He apatite crystal dates was undertaken by H.H., and (U-Th)/He analysis was carried out by Y.L., T.P.L., S.N., and M.F. provided additional geochronological analysis and contributed to the geochronological framework. Lithostratigraphy and sedimentology was carried out by P.W.D., E.W., and T.H.V. Paleosol carbonates were sampled and analyzed for stable isotopic composition by P.W.D., S.A.B., and P.W.D. interpreted paleosol carbonate results, and S.A.B. sampled and carried out stable isotopic analysis of tooth enamel. B.O., T.W.P., J.S.O., E.M.F., L.C.B., R.L-L., F.L.F., J.L., F.H., and J.A.P. contributed to field direction and data collection during field work. S.A.B., T.W.P., P.W.D., R.N.K., E.W., L.C.B., T.H.V., S.R.F., and R.P. contributed to the paleoenvironmental interpretation. S.E.B. analyzed and described the hominin teeth, and S.R.F. analyzed the monkey fossils. Other taxa were studied by F.H., J.L., E.D.G.E., L.C.B., T.W.P., and J.S.O. Bone identification and surface damage were carried out by J.A.P., J.S.O. and T.W.P. Lithic technology was studied by E.M.F. Additional insights on the lithic technology were provided by D.R.B., J.S.R., C.L., I.C., S.K.B., N.K.R., and E.P.W. C.L. and I.C. carried out use-wear and residue analyses. T.W.P. wrote the article with contributions from J.S.O., E.M.F., P.W.D., L.C.B., C.L., I.C., S.E.B., A.I.R.H., E.W., F.H., and Y.L. All authors contributed editorial comments to the manuscript.
Competing Interests: The authors declare no competing interests.
Data and materials availability: All data supporting the findings of this study are available within the paper and its supplementary information files. All archeological and paleontological collections and field records are archived in the Department of Earth Sciences in the National Museums of Kenya in Nairobi.

SUPPLEMENTARY MATERIALS
Materials and Methods
Figs. S1 to S17
Tables S1 to S21
References (36-135)

Figure captions

Fig. 1. Nyayanga stratigraphy, magnetostratigraphic data, and apatite crystal dating results. (A) Topographic map of the gully system showing the locations of geologic trenches and excavations. (B) Composite stratigraphic column of the Nyayanga Beds showing the stratigraphic placement of Excavations 3 and 5 and the magnetostratigraphic profile. Reversed polarity is shown in white, intermediate normal polarity in gray, and normal polarity in black.

Fig. 2. Oldowan artifact technological analysis. (A) Photos of a dorsal flake (Exc3-1475), ventral flake (Exc3-1413), and core (NY17-128) from Nyayanga next to a principal component analysis based on major technological attributes of Early Stone Age artifact assemblages and a capuchin-derived assemblage (table S4) [material and methods 9, see *(8)*]. Assemblages are plotted according to principal component 1 (x-axis) and principal component 2 (y-axis). The Nyayanga assemblage (NYA) falls within the shaded ellipse that represents the 95% confidence interval for Oldowan sites. A scree plot with eigenvalue percentage of variance for principal components 1 through 11, and a loadings plot showing the contribution of each variable are shown to the right. (B) The frequency of cores in Oldowan assemblages compared with Nyayanga (table S4) and photos of two Nyayanga cores (NY17-54 top, NY17-55 bottom). (C) The frequency of artifacts with percussion damage in Oldowan assemblages compared with Nyayanga (table S4) with photos of a Nyayanga pounded piece (Exc3-195).

Fig. 3. Stone tool-damaged fossilized bones from Bed NY-1. (A) hippopotamid tibia (Exc5-170, proximal end oriented to left) displaying a series of identically oriented cut marks with striae on anterior tibial crest. (B) cut mark on a hippopotamid rib (Exc3-1685) displaying striae

and a concretion filling the middle of the mark. (C) parallel cut marks extending along the spine of size 3 bovid scapula NY17-1. (D) a series of parallel cut marks (upper panel) as well as percussion load points and flake scars created during marrow processing (lower panel) visible on a size 3 bovid long bone shaft fragment (NY15-61).

Fig. 4. *Paranthropus* finds from Nyayanga. (A) *Paranthropus* sp. left upper molar KNM-NG 77315 found on the surface of NY-1. (B) *Paranthropus* sp. left lower molar KNM-NG 77316 found in situ in NY-1 in Excavation 3. (C) Tooth enamel $\delta^{13}C$ of Nyayanga hominins and previously published $\delta^{13}C$ data from eastern African hominins (19, 25–34). Pliocene hominin teeth from Woranso-Mille are identified as "hominini indet (W-M)." Mid-Pliocene hominin teeth from Lomekwi and Lothagam in the Turkana Basin previously attributed to *K. platyops* (28) are identified here as "hominini indet (L-L)," following (35). Hominin teeth from other areas of the Omo-Turkana Basin that cannot be confidently attributed to genus are identified as "hominini indet."

Science
AAAS

Supplementary Materials for

Expanded geographic distribution and dietary strategies of the earliest Oldowan hominins and *Paranthropus*

Thomas W. Plummer*, James S. Oliver, Emma M. Finestone, Peter W. Ditchfield, Laura C. Bishop, Scott A. Blumenthal, Cristina Lemorini, Isabella Caricola, Shara E. Bailey, Andy I.R. Herries, Jennifer A. Parkinson, Elizabeth Whitfield, Fritz Hertel, Rahab N. Kinyanjui, Thomas H. Vincent, Youjuan Li, Julien Louys, Stephen R. Frost, David R. Braun, Jonathan S. Reeves, Emily D.G. Early, Blasto Onyango, Raquel Lamela-Lopez, Frances L. Forrest, Huaiyu He, Timothy P. Lane, Marine Frouin, Sébastien Nomade, Evan P. Wilson, Simion K. Bartilol, Nelson Kiprono Rotich, Richard Potts

Correspondence to: thomas.plummer@qc.cuny.edu

This PDF file includes:

Materials and Methods

1 – Provenance, Excavation and Preparation (TWP, BO, RL-L, FLF, JSO, EMF, LCB, JL, FH, JAP)

Methods

Nyayanga (0° 23.909'S, 34° 27.115'E) was first surveyed by the Homa Peninsula Paleoanthropological Project, a collaboration between researchers at the National Museums of Kenya, the City University of New York, and the Smithsonian Institution, in 2000. Geological observations and surface collections were carried out in brief visits in 2007, 2011, 2012, and 2014. Excavations 1 and 2 were carried out in 2015 but recovered little. Excavations 3-6 were initiated in 2015, and all yielded fossils and stone tools (see material and methods 2-6 for age and authentication of fossils). Sediments were excavated in 5 cm spits in 1 m squares using scratch awls and dental picks, or with a scratch awl struck with a light hammer when sediments were hard. All potentially identifiable remains <2 cm in length and all remains >2 cm in length were individually plotted in three dimensions using a laser theodolite. A unique field number was assigned each specimen and its surrounding geological bed and sediment described. The dip and orientation of all items with a long axis were measured with a Brunton compass. Fragile fossils were coated in butvar and cast in plaster-wrap. Specimens were photographed *in situ*, and were wrapped in toilet paper and placed in labeled bags when collected. Fossil preparation was carried out in the National Museums of Kenya (Nairobi). All fossils and artifacts are curated in the collections of the National Museums of Kenya, Nairobi.

Results

Our research focused on the upper half of bed NY-1. Two hundred and forty-six fossils and 195 artifacts were collected from the surface. Fifteen hundred and eighty fossils and 121 Oldowan artifacts were found in situ in bed NY-1 in Excavation 3. One hundred and ninety-six fossils and 14 Oldowan artifacts were recovered from bed NY-1 in Excavation 5.

2 - Lithostratigraphy and Depositional context (PWD, LW, THV)

Methods

The stratigraphic sequence from Nyayanga was recorded using standard field logging techniques on section profiles from the archeological excavations and from a series of seventeen geological trenches; these observations were supplemented by measurements from natural exposures in the area. In addition, trench locations and heights above the local datum were recorded using EDM surveying techniques. The location of geological trenches and excavations form a roughly NE/SW transect approximately 500 m in length, shown in Figure 1.

Results: Geological setting

The Nyayanga site is exposed in a naturally occurring erosive feature close to the most westerly point of the west coast of the Homa Peninsula. This feature forms an embayment into a broadly northwest to southeast trending paleo-cliff line approximately fifty meters inland of the current Lake Victoria shoreline. The outcrop consists of a bowl-like area of exposures in the SW (referred to as the amphitheater area below) and extends up an incised gully system to the ENE (Fig. 1). This outcrop pattern is heavily influenced by a normal fault trending west to east along

the line of the gully system with a maximum downthrow of 10 m to the southeast. This fault defines the northern margin of a local graben feature, with the southern margin bounded by a second normal fault some 400 m to the south, exposed inland of Akungo Beach.

Results: Lithological sequence

The stratigraphically lowest unit exposed in the local sequence is composed of nonfossiliferous white- and buff-colored fluvial sandstones interbedded with weakly cemented conglomeratic bands and fine-grained carbonate-rich lacustrine silts. These sediments are designated Unit A here and are provisionally correlated to the Homa Formation (*36*), which outcrops at localities north of Homa Mountain with a biostratigraphic age of ca. 4.0 - 3.5 Ma (*13*). Unit A is best exposed in the northern margin of the amphitheater area and forms the foot wall of the fault marking the northern edge of the graben feature. These sediments show a marked lateral facies change to the south where, in the center of the graben, they are represented by more uniform grey clays with occasional light grey indurated carbonate bands that sometimes show stromatolitic structures. These are designated Unit A' and are interpreted as lacustrine deposits that represent a relatively 'offshore' equivalent of the sediments seen in unit A to the north. Unit A is separated from the overlying Nyayanga Bed sequence by a marked angular unconformity. Deformation of Unit A is strongly controlled by the E - W trending normal fault system that bounds the northern side of the graben structure described above.

Stone tools and fauna are eroding from all four Nyayanga Beds, from oldest to youngest NY-1 to NY-4. Nyayanga Bed 1 (NY-1) lies unconformably above Unit A, with a strongly erosive and channelized base (Fig. 1). NY-1 is characterized by a fining upwards sequence of coarse sand with a cobble conglomerate at the base that passes upwards into a grey clayey silt with occasional lenses of yellow grey tuffaceous silts. These sediments are interpreted as a fining upwards channel fill sequence that passes upwards and laterally into related overbank deposits with associated pedogenesis. The base of the channel feature progressively downcuts into unit A to the west and represents a significant, westward flowing paleochannel system coincident with the northern bounding fault of the graben.

Nyayanga Bed 2 (NY-2) consists predominantly of orange and red-brown, often pedogenically altered, clayey silts deposited as overbank deposits of the same fluvial system as NY-1. The base of NY-2 locally shows channelized conglomeratic bodies that are erosive into the upper parts of NY-1 (Fig. 1). The upper part of NY-2 contains a remarkably uniform bed of orange silt that is interpreted as a possible tuff layer, now largely devitrified. This layer forms a prominent marker horizon in many of the geological trenches along the WSW to ENE trending gully system (Fig. 1).

Nyayanga Bed 3 (NY-3) has a weakly erosive contact with NY-2 and consists of pedogenically altered brown clayey silts with high concentrations of coalescing carbonate nodules. This unit represents largely terrestrial deposition in a low energy alluvial environment with episodes of deposition alternating with periods of stability and pedogenesis. Strongly localized tufa deposits, which contain abundant calcified sedge stems and other plant remains, mark the probable location of freshwater springs during NY-3 deposition and perhaps earlier (Fig. 1). The upper part of NY-3 is marked by an erosively based, green, tuffaceous, tabular sandstone up to 30 cm thick.

Nyayanga Bed 4 (NY-4) marks the top of the sequence. It consists of an erosively based, poorly sorted, strongly clast-supported conglomerate that fines upwards to silt grade sediments. The lower part of NY-4 is erosive into the underlying NY-3 with a disconformable contact. NY-

4 often contains large rip-up clasts of the underlying NY-3 tuffaceous sandstone that show minimal rounding or abrasion. It is interpreted as the deposit of a hyperconcentrated flow filling a paleo-gully running down the same fault-controlled axis as the channels seen in the underlying NY-1 to NY-3 sequence.

Nyayanga Beds NY-1 to NY-3 are provisionally correlated to the Rawi Formation outcropping north of Homa Mountain (*36*), which was deposited within the C2An.1n Subchron (3.050-2.595 Ma) within the Gauss Chron (*13, 37*).

3 - Apatite (U-Th)/He dating (Fig. S1; Table S1) (YL, HH)

Methods

Samples for (U-Th)/He dating were collected from two yellow tuffaceous silt lenses, approximately 0.3 m and 0.1 m thick, respectively, bracketing the NY-1 sedimentary sequence investigated in Excavation 3 (WL-9 and WL-10). The (U-Th)/He dating used the single-crystal laser-fusion isotope dilution method at the Institute of Geology, China Earthquake Administration (IGCEA), and follows that of (*38*). Helium analysis was conducted automatically using an Australian Scientific Instruments Alphachron. Inclusion-free euhedral apatite grains with a width of >80 μm and minimal fracturing were handpicked for analysis under a binocular microscope. Individual apatite grains were loaded into Pt foil envelopes and subjected to an 8 A current from a 970 nm diode laser for 5 minutes to extract >99% of the ^{4}He. All samples were subjected to a second heating step to ensure complete ^{4}He extraction. The extracted ^{4}He was then spiked with pure ^{3}He, and the resultant ^{3}He/^{4}He isotopic ratio was measured using a Quadrupole PrismaPlus QMG 220. This was compared with the ^{3}He/^{4}He ratio of a spiked calibrator to yield the ^{4}He content of the samples.

After the helium analysis, the Pt envelopes containing apatite grains were placed in Parrish-style vials (PFA). Following the experimental procedures of (*39*), a spiked solution with 25 μl of mixed 15 ng ml^{-1} ^{235}U and 5 ng ml^{-1} ^{230}Th was added to each vial. Blanks (containing one empty Pt foil envelope) with 25 μl of 7 mol l^{-1} HNO_3, spiked standards (similar empty Pt foil) with 25 μl of the standard with 24.08 ng ml^{-1} U-Th, and 25 μl of the same spike were prepared. The sealed vials were transferred into an ultrasonic bath for 15 minutes and heated to 100 ºC on a hot plate to dissolve the apatite effectively. Finally, the Milli-Q water was added and diluted to a volume of 2.5 ml for the measurements of U and Th using an Agilent 7900 ICP-MS.

Results and rationale for using (U-Th)/He raw dates

The He, U, and Th contents from the analytical experiments and the derived (U-Th)/He raw ages are summarized in Table S1. The (U-Th)/He ages are reported as the arithmetic mean age with 1σ uncertainties. Six single-grain analyses performed on apatite crystals from the WL-9 sample yielded raw ages ranging from 1.96 ± 0.06 Ma to 3.90 ± 0.09 Ma with an average age of 2.87 ± 0.79 Ma (Table S1). The alpha ejection correction factor (Ft) applied to the raw ages derived an arithmetic mean corrected age of 3.65 ± 0.91 Ma (Table S1). Two workable crystals that were inclusion-free, with minimal fracturing, and width > 80 μm were analyzed from sample WL-10. These yielded raw ages of 2.63 ± 0.07 Ma and 3.34 ± 0.09 Ma with an average of 2.98 ± 0.50 Ma, and a corrected age of 3.49 ± 0.60 Ma (Table S1).

The host rocks on Homa Mountain are highly enriched with U and Th (*40–42*). Considering this enrichment, the alpha implantation effect from the surrounding host rock is not

trivial. Therefore, no alpha correction was applied in this study, and we regard the (U–Th)/He raw ages as the depositional ages of sediments. Similar (U-Th)/He dating analyses on other Homa Peninsula deposits (Kanam Formation, Abundu Formation, and Kanjera Formation) indicated the raw ages best approximated ages yielded from other methods (*38*). We therefore regard the (U-Th)/He raw ages of 2.87 ± 0.79 Ma and 2.98 ± 0.50 Ma as the depositional ages of tuffaceous silt layers WL-9 and WL-10, respectively. The two tuffaceous silts are within 1 m of each other, and the numerical ages they yield are indistinguishable within the 1σ uncertainties. Combining the crystals from the two samples yields a best fit age of 2.90 ± 0.70 Ma (Fig. S1).

4 - Magnetostratigraphy (Fig. S2; Table S2) (PWD, AIRH)

Methods

Twenty-one separate layers were sampled from the Excavation 3 slope and in Trenches 9 and 11 (Fig. S2) at Nyayanga; 11 during 2007 (NY01-10) and 10 during 2016 (P.mag A-J). The 2007 set was sampled in individual plastic sample cubes (4 samples per level) and analyzed at the University of Liverpool Geomagnetism Laboratory (ULGL), UK. The 2016 set was taken as block samples within aluminum sample tins and prepared and analyzed at The Australian Archaeomagnetism Laboratory (TAAL) at La Trobe University, Australia. Although the sediments were consolidated enough in the field to cut into sample cubes and blocks, they had to be consolidated further using water glass in the laboratory before they could be analyzed. Water glass was added directly to the plastic cubes for the 2007 samples, and the 2016 samples were consolidated in a water glass solution under a vacuum (*43*). Kostadinova et al. (*44*) showed that the remanence of samples impregnated with water glass are not influenced by this process. Some samples did not survive this treatment and are indicated by an X in Table S2.

Magnetic susceptibility was measured using a Bartington MS2 system at both laboratories. Samples were magnetically cleaned using alternating field (AF) demagnetization. At ULGL an in-house laboratory-built AF demagnetizer equipped with a sample tumbler, Helmholtz coils for minimization of the ambient field, and capable of imparting fields of up to 100 mT was used; at TAAL an AGICO LDA5 AF Demagnetizer was used. The sample's remanence was measured at ULGL using an FIT high temperature SQUID based spinner magnetometer with a minimum sensitivity of $0.002 \times 10^{-6} Am^2 kg^{-1}$ located in a Magnetic Measurements shielded room. At TAAL the samples were measured using an AGICO JR^ spinner magnetometer inside an identical Magnetic Measurements shielded room. Final Characteristic Remanent Magnetization (ChRM) directions were calculated using principal component analysis (*45*) with accepted best-fit components requiring a median angle of deviation (MAD) of < 15°. Mean directions for each sample block were determined using Fisher (*46*) statistics in the ULGL program FISH2 with normal or reversed polarities defined on VGP-latitude directions under the following constraints: Normal: +90°to +65°; Intermediate Normal: +65 to +45°, Intermediate -45° to +45°, Intermediate Reversed -65° to −45°; Reversed: −45°to -90°.

Results

The Nyayanga specimens exhibited low frequency dependence of magnetic susceptibility values <3.3% prior to consolidation with water glass, suggesting a low proportion of ultrafine viscous single domain to superparamagnetic grains. The mean paleomagnetic data from multiple

subsamples (ranging from 3-5) from each layer and their respective Paleolatitude and polarity is outlined in Table S2. In some layers, such as Pmag H, there was simply no consistency between subsamples to provide a consistent mean direction. This is potentially due to these layers being within a reversal (see below). In all the other layers marked with an X data could not be retrieved from due to the samples not surviving the consolidation process. In normal polarity samples, the removal of a strong northerly oriented viscous overprint by ~6mT revealed an underlying normal polarity ChRM that was stable up to fields between 30 and 40mT. These samples had mean angles of deflection of between ~1-8 and are comparable to the behavior seen in other samples from the Homa Peninsula (*11*). Reversed polarity samples exhibited more complex behavior with initial normal polarity overprints that were antiparallel to the reversed polarity ChRM (Fig. S2), a behavior also noted by Ditchfield et al. (*11*) for other areas of the Homa Peninsula. In some of these samples more than one underlying component occurs but both these components were oriented in a southerly field direction. Intermediate directions had a strong viscous overprint oriented in a northerly field direction before the isolation of an underlying intermediate ChRM. In general, these samples had higher MAD values (~9-10). This is to be expected if intermediate directions are true field directions occurring during a magnetic reversal or excursion as the Earth's magnetic field decreases significantly during magnetic reversals, so the stability and strength of magnetizations induced in the samples is often poor. Given that the intermediate magnetic directions in the base of NY-1 occur between underlying reversed polarity in Unit A and overlying normal polarity of NY-2, the behaviors of the intermediate polarity samples could reflect a magnetic reversal. Overall, the Nyayanga sequence shows a change from reversed polarity in Unit A, intermediate to normal polarity in NY-1, normal polarity through NY-2, intermediate normal polarity in the base of NY-3, and reversed polarity in the very top of NY-3. K values were variable throughout the sequence and range from very high values (~420-640) showing little dispersal between subsamples and much lower values (as low as ~2) in other layers. Overall the highest values are for the normal polarity deposits of NY-1 and lower NY-2 with much lower values for intermediate samples and upper NY-2 and NY-3. This does not appear to reflect depositional effects but may show the effects of a low intensity magnetic field during periods close to reversals

This sequence from reversed through intermediate and into normal polarity, along with the (U-Th)/He apatite dates, suggest that the Excavation 3 and 5 deposits are dated to either within or soon after the 3.032 Ma reversal at the beginning of the C2An.1n Gauss Subchron. However, the full reversal is not recorded in the sequence as the change from reversed polarity in Unit A to intermediate and normal polarity in NY-1 is separated by an erosional event at the interface of these two units. Given a biostratigraphic age of 4.0 - 3.5 Ma for Unit A (*13*) this time gap appears to be significant as the reversed polarity may suggest it was deposited in the later part of the Gilbert Chron prior to 3.60 Ma (*14*). Another possibility is that these NY-1 intermediate directions represent the Raiatea magnetic excursion within C2An.1n, at 2.77 ± 0.02 Ma (*47*), but this magnetic excursion remains to be verified and identified elsewhere.

Another reversal appears to occur in NY-3 with a transition from intermediate normal to reversed polarity. It is assumed that this represents the Gauss-Matuyama boundary at 2.595 Ma (*14*). This represents a minimum age for the Excavation 5 and 3 material and a good age for the Excavation 6 material (not described here). It would appear that the Nyayanga sequence records both the beginning (in NY-1) and end (NY-2 to 3) of the C2An.1n Subchron between 3.032 - 2.595 Ma (*14*), taking into account a time gap in deposition due to the erosional contact between NY-1 and 2.

The Nyayanga magnetostratigraphy is similar to the Rawi Fm sequence in the Fish Cliffs Section by Ditchfield et al. (*11*), to which Nyayanga Beds 1-3 have been provisionally correlated. In the Fish Cliffs sequence the Homa Formation recorded both reversed and normal polarity towards the base of the exposed section, in contrast to reversed polarity near the top of the exposure in the current section. Further work would be needed to understand the relationship of these exposures as the nature of the erosional contact between the Homa Formation and overlying deposits is variable across sections in the Homa Peninsula. The majority of the Rawi Formation recorded normal polarity with a single reversed layer at midheight and another slightly higher layer of mixed intermediate directions. The uppermost sample also recorded intermediate directions that was suggested to represent a polarity transition. If both sequences are contemporary then the Nyayanga sequence strengthens this original interpretation of a transition at the top of this sequence and unstable intermediate and reversed directions in the middle of the sequence, perhaps related to the Raiatea excursion at 2.77 ± 0.02 Ma (*47*). If so, then this would provide a minimum age for the NY-1 archeology.

The only other Oldowan occurrence found in the C2An.1n Subchron prior to ~2.6 Ma is the BD 1 site at Ledi-Geraru, Ethiopia (*7*). BD 1 is not older than 2.584 ± 0.034 Ma based on the Ar-Ar dating of the Ali Toyta Tuff below the site. Given the 20 m of sediments at BD 1 were deposited within an unbroken normal polarity period, the sequence must have accumulated very rapidly between 2.595 and 2.618 Ma. The NY-1 Oldowan assemblage is certainly older than BD 1 and as argued above may be closer to ~ 3 Ma.

Paranthropus aethiopicus specimen KNM-WT 17000 derives 3.8 m below the 2.53 ± 0.02 Ma Lokalalei Tuff in the Lomekwi Member of the Nachukui Formation. The holotype of *P. aethiopicus*, Omo 18-18, comes from submember C8 in the upper part of Member C of the Shungura Formation, which is younger than2.595 Ma as the Gauss-Matuyama boundary occurs in the overlying SubMember C9, consistent with a recent estimate of the *age* of submember C8 of 2.55 ± 0.022 Ma calculated using an age model based on stratigraphic height and numeric ages determined by radiometric dating and magnetostratigraphy (*19*). The oldest known *Paranthropus* fossils from the Shungura Formation include a mandibular molar (L62-16) from submember C5, which dates to 2.645 ± 0.031 Ma, and a mandibular fragment (L55-33) from submember C6, which dates to 2.605 ± 0.049 Ma (*19*). A *P. aethiopicus* premaxilla has also been recovered from the Upper Ndolanya Beds at Laetoli (*48*). A tuff 1.5 m above the base of these beds has been dated to 2.660 ± 0.014 Ma (*49*). As such, the NY-1 *Paranthropus* teeth are also likely older than previous published occurrences of this genus.

5 - Dating methods not providing usable results (SN, MF)

Luminescence dating

A series of eight samples was collected for luminescence dating in beds NY-1 (X7343-X7344), NY-2 (X7345-46-47) and NY-4 (X7348, -49, -50). Samples were collected by inserting tubes in the sequence when possible or by carving a sediment block in the sequence. In the luminescence dating laboratory, under orange filtered light conditions, the outer part of the tube or block was used to assess the dose rate. The inner part of the sample was used to measure the equivalent dose (De). The ratio De/Dose rate gives the age of the sample, which corresponds to the last time the mineral grains contained in the sediment were exposed to light.

The Nyayanga site was known to be older than the conventional limit of luminescence dating method, i.e. ~0.5 million years (Ma). However, a recent dating protocol, named Infrared Radiofluorescence (IR-RF, (*50*) is believed to measure luminescence signal from K-feldspar up to 4000 Gy (*51*), which corresponds to an age limit of 2 to 4 Ma, considering a dose rate of 2 to 1 Gy/ka.

IR-RF De's ranging from ~2700 Gy to ~2000 Gy have been obtained for X7344 and X7349, respectively. However, the dose rates range from ~6 to ~3 Gy/ka for these samples. These high dose rate values limit the application of IR-RF in Nyayanga, and only allows to estimate a minimum age of ~0.5 Ma for the Nyayanga sequence.

Ar/Ar dating

A single sample from a tuff near the top of NY-2 was selected in order to determine if datable minerals could be found. After crushing and sieving, about 20 small transparent crystals that look like fresh feldspars were found and handpicked in the 200-300 microns gain size. After a 2h irradiation in the Corvalis TRIGA Tube (CO-01) one by one the crystals were transferred into a copper sample holder into a differential vacuum Cleartran© window. Crystals were individually fused using a Synrad CO2 at 10-15 % nominal power (c.a 25 W). The Ar isotopes were counted using a VG5400 mass spectrometer equipped with a single ion counter (Balzers© SEV 217 SEN), following the procedures outlined in Nomade et al. (*52*). Each Ar isotope measurement consisted of 20 cycles of peak switching of the argon isotopes. Neutron fluence (J) was monitored by co-irradiation of Alder Creek sanidine (ACs-2, 1.189Ma, (*53*) that were placed in the same pit as the sample during irradiation.

Unfortunately, none of the 15 crystals we tried to date give meaningful ages as most of the crystals were very low K bearing plagioclase, or not feldspar but most probably transparent very light-yellow pyroxene.

6 – Biostratigraphy (Table S3) (LB, TWP, JSO, SRF)

Methods

See section 8 Faunal Identification and Taphonomy below.

Results

The NY-1 faunal samples include the suids *Notochoerus* cf. *scotti* (3.36-1.79 Ma) and *Metridiochoerus andrewsi* (3.36-1.7 Ma), the colobine *Paracolobus mutiwa* (2.75-1.9 Ma), the proboscidean *Loxodonta adaurora* (5.0-1.88 Ma), *Eurygnathohippus* sp. (6.5 to less than 1 Ma), and the hominin *Paranthropus* sp. (2.66-1.34 Ma for eastern African *Paranthropus*) (*13, 48, 54–57*) (Table S3). *M. andrewsi* teeth from Nyayanga are less derived than those found at Kanjera South dated to ca. 2 Ma, but similar to *M. andrewsi* teeth from the Rawi Fm, also deposited during the C2An.1n Subcron (*37*) and to which Nyayanga Beds 1-3 have been provisionally correlated. *Paracolobus mutiwa* is among the most readily recognized colobines due to its large size and distinctive morphology (*58, 59*). Outside of Nyayanga *P. mutiwa* is only recognized from the Turkana Basin where diagnostic material ranges from Members C through G of the Shungura Formation, the uppermost Lomekwi Member of the Nachukui Formation, and the Upper Burgi Member of the Koobi Fora Formation, yielding an age range of 2.75 - 1.9 Ma. Less diagnostic, large, isolated teeth could extend its range back to Member A (3.6 Ma) of the Shungura Formation (*58, 59*). The equid sample at Nyayanga consists exclusively of hipparionin

(*Eurygnathohippus* sp.) fossils, consistent with a date prior to the dispersal of *Equus* across Africa at ca. 2.3 Ma (*15*). *Equus* fossils are absent from Homa Peninsula deposits known to predate 2.3 Ma (e.g., the Kanam, Homa, and Rawi Formations), but are common in sediments postdating 2.3 Ma (e.g., the Kanjera, Kasibos, Luanda, and Apoko Formations) (*11–13*). *Equus* fossils are also present in NY-4, which sits disconformably above the other Nyayanga beds, and has other biostratigraphic indications of a younger age, including the suid *Metridiochoerus modestus* (2.2 -0.7 Ma) and proboscidean *Elephas recki* (4 -0.5 Ma; (*54*, *56*).

7 – Lithic Technology (Fig. S3; Table S4) (EMF)

Methods

Analysis pooled artifacts recovered from Excavations 3 and 5 and artifacts collected from the surface of the upper half of NY-1. All artifact raw materials were attributed to lithological groups through visual inspection with a 10x hand lens by EF and PD. Technological features of the assemblage were then recorded by EF.

Artifacts were divided into four categories: detached pieces (DP, i.e., debitage), pounded pieces (PP, i.e., hammerstones), flaked pieces (FP, i.e., cores), or manuports. Detached pieces were classified further into debitage types (whole flakes, snapped flakes, split flakes, split and snapped flakes, or angular fragments). Mass and maximum dimension were recorded for each specimen. Maximum dimension was measured in millimeters as the longest distance across an artifact. Mass was measured with a digital scale to 0.1 g.

Methods: Flake Attributes

In addition to maximum dimension, the length, width, maximum width and thickness were measured with digital calipers in millimeters. Technological length was defined as the distance between the point of initiation to the distal end of the flake on the ventral surface in the direction of percussion. Width was measured as the distance across the ventral surface of the flake at the midpoint, perpendicular to the axis of length. Maximum width was measured at the widest point across the ventral flake at a 90-degree angle to the axis of length. Thickness was measured at the point where width and length measurements intersected. The type of fracture termination (i.e., feather, step, hinge, or overshoot) was noted. We also recorded the number of dorsal flake scars with a maximum dimension greater than 10 mm and estimated the percentage of cortex on the dorsal surface.

We determined the number of platform facets and estimated platform cortex within 10% (e.g., 0, 1-10%, 10-20%, etc.). Platform thickness and length were measured in millimeters. Platform thickness was defined as the distance across the platform between the ventral and the dorsal margin at the point of initiation of percussion. Platform length was defined as the perpendicular distance at the midpoint of platform thickness. Finally, external platform angle (the angle between the ventral surface and platform surface) was measured using a goniometer.

Using these measurements, flakes were divided into one of six Technological Flake Categories based on the presence or absence of cortex on the dorsal surface and platform (*60*). Type I contains cortical platforms and completely cortical dorsal surfaces. Type II flakes have cortical platforms and partial cortex on the dorsal surface. Type III flakes have cortical platforms but lack cortex on the dorsal surface. Type IV flakes contain non-cortical platforms but complete cortex on the dorsal surface. Type V flakes have partial dorsal cortex and no platform cortex.

Finally, Type VI flakes have no cortex on any surface. Prevalence of flake Types I-III are associated with early stage flaking and are often indicative of unifacial reduction whereas later stage Technological Flake Types IV-VI represent a higher degree of reduction intensity and bifacial reduction (*61*, *62*).

The ratio of Edge Length to Mass (EL/M) provides a measure of flake utility and an estimate of the amount of cutting edge present on a given quantity of stone (*63–65*). Mackay (*65*) demonstrated that edge length can be estimated by adding together the maximum width, technological length and maximum dimension of a flake. The estimated edge length of Nyayanga flakes was then compared with mass to provide a proxy for the efficiency with which mass is converted to cutting edge (Fig. S3).

Methods: Core Attributes

The maximum length, width, and thickness of each core was measured in mm using a digital caliper. Core length was defined as the longest axis. Core width was measured perpendicular to the axis of maximum length. Core thickness was defined as the maximum dimension perpendicular to the axis of length and the axis of width. Core percent cortex (an estimate of the proportion of the whole piece covered by cortex) was estimated within 10%. Negative flake scars greater than 20 mm on the surface of the core were considered. Scar patterns were recorded using the typology developed by de la Torre et al. (*66*). Cores were classified as unifacial, bifacial, or multifacial, and unidirectional based on the location of flake removals.

Methods: Comparison to other Assemblages

Principal component analysis (PCA) on technological attributes useful in distinguishing among industries was used to compare Nyayanga artifacts to other Early Stone Age assemblages (*7*). Published values that underwent principal components analysis in Braun et al., (*7*) and Mercader et al., (*67*) were compiled alongside values calculated for the Nyayanga assemblage (Table S4). The dataset included Acheulean, Lomekwian, and SCNP capuchin-produced assemblages. The technological variables included were: the percentage of unifacial cores, percentage of bipolar percussion, percentage of cores in the assemblage, percentage of angular fragments in the assemblage, average core maximum dimension, the ratio of average flake size to average core size, average flake scar count, the ratio of flake scar count to the log of mean core size, average flake maximum dimension, average flake thickness, and the percentage of the assemblage that had evidence of percussion damage. These technological variables were defined and calculated according to Braun et al., (7). Assemblages with missing data were omitted from the analysis. The resulting dataset underwent a PCA based on a correlation matrix in the statistical software R (version 4.2.2, The R Foundation for Statistical Computing) using the FactoMineR package.

Results: Assemblage Composition

In total, 330 artifacts were recovered from the upper half of unit NY-1 through excavation and surface surveys. This included 121 artifacts from Excavation 3, 14 artifacts from Excavation 5, and 195 artifacts from the surface of NY-1. Artifacts generally exhibit excellent surface preservation with relatively fresh and well-preserved edges. The majority of the sample (86.2%) showed no or minimal edge-rounding macroscopically. This is consistent with the observations of surface preservation assessed microscopically for use-wear analysis and reported

in Section 9. The majority of stones from Excavations 3 and 5 were recovered from fine-grained sedimentary layers primarily composed of silts, and less frequently sandy-silts and fine sands. Together this evidence is consistent with rapid burial by fluvial sediments.

The upper NY-1 assemblage is composed of cores (20.6%, n=68), whole flakes (31.2%, n=103), broken flakes (6.1%, n=20), angular fragments (39.1%, n=129), hammerstones (2.1%, n=7), and manuports (0.9%, n=3). Flakes were sometimes snapped (n=11), split (n=6), or both (n=3). Most flake terminations were feather (84.5%, n=87), although the frequency of step (9.7%, n=10) and hinge (5.8%. n=6) terminations were moderate. Cores make up a notable portion of the assemblage, although the assemblage also contains very small, detached pieces (n=16 under 20 mm).

Results: Reduction Strategy

Ninety-eight flakes could be classified into a Technological Flake Category. Five were unassigned because their platforms were crushed or broken. Technological Flake Categories for many flakes in the Nyayanga assemblage indicate late-stage reduction. However, early-stage reduction is also evidenced by the presence of Type I flakes and flakes at all stages of the reduction sequence are present (Type I: 7.1%, Type II: 14.3%, Type III: 2.0%, Type IV: 8.2%, Type V: 53.1%, Type VI: 15.3%). The overall distribution of Technological Flake Categories closely approximates what is observed in unconstrained experimental assemblages in terms of possessing all flaking stages and containing a high percentage of Type V flakes (*61*).

Cores and flakes at Nyayanga indicate a high degree of bifacial reduction. Nyayanga core reduction has a higher bifacial component than other early Oldowan sites, except for OGS-7 at Gona South (*62*). Roughly half of the cores at Nyayanga were bifacial (38.1%) or multifacial (11.1%) which is similar to frequencies at the early Pleistocene sites of Douglas Korongo (DK) and FLK-Zinj, Olduvai Gorge.

The distribution of Technological Flake Categories also resembles what is seen in Oldowan assemblages with strong bifacial components (OGS7, (*62*); and replications of reduction at FxJj1 and FxJj10, (*61*). Technological Categories V and VI are associated with bifacial reduction and these flake types account for 68.4% of flakes at Nyayanga. Non-cortical platforms are also indicative of bifacial flaking, and Nyayanga possesses a high percentage of non-cortical platforms (73.8%; n=76), similar to what is observed at OGS-7 (66%, (*62*). Of the preserved platforms (n=107), 7.5% were bifaceted (n=7) or multifaceted (n=1).

Despite the site's antiquity, hominins at Nyayanga were able to remove flakes while efficiently preserving core volume. Nyayanga toolmakers were proficient at maximizing cutting edge, minimizing flake mass, and controlling and minimizing platform depth (Fig. S3). The average platform depth (9.04 mm +/- 4.94) is comparable to other Oldowan assemblages (*7*). The relationship of edge length to mass suggests controlled platform management and flaking efficiency (Fig. S3). Flakes and cores preserve relatively few mistakes and most flake terminations are feathered.

Results: Affinity to Other Oldowan Assemblages

A principal component analysis (PCA) based on major technological attributes of artifact assemblages from various Early Stone Age and capuchin-derived assemblages (Table S4, Fig. 2) revealed similarity in Oldowan assemblage characteristics. PC1 drives much of the variation (50.2%) between Early Stone Age assemblages, the Lomekwian, and the SCNP capuchin-produced assemblages. The first 2 principal components s together explained 73.5% of the

variance. We considered the scores for PC 1 and PC 2 because they represented the majority of variance. The variables that load most heavily on PC1 are the frequency of cores, the frequency of percussion and the frequency of bipolar percussion. The variables that load most heavily on PC2 are the average flake thickness, flake size, and number of flake scars. Nyayanga possessed the highest frequency of cores (20.6%, Figure 2b) and among the highest frequency of percussion (7.0%, figure 2c) in the Oldowan sample. However, Nyayanga still falls within the 95% confidence interval of Oldowan sites in the plot of PC1 and PC2 (Fig. 2). The NY-1 samples and the rest of the Oldowan assemblages were distinct from the two Acheulean samples (FxJj63 and FxJj37), the Lomewkian (LOM3) and the capuchin-derived assemblage (SCNP) (Fig. 2). The assemblages most similar to Nyayanga on PC1 and PC2 are Ewass Oldupa (EO) and Fejej, suggesting that early Oldowan (>2 Ma) and later Oldowan (<2 Ma) samples do not differ dramatically in their technological attributes.

8 - Faunal Identification and Taphonomy (Figs. S4-S7, Tables S5-S7) (TWP, LCB, FH, JSO, JAP, JL, FF)

Methods

Element and taxonomic identifications were made at the National Museum of Kenya using the NMK Paleontology collections and the Zoology Department's comparative material as references. Element portion and completeness were recorded. Age estimates based on epiphyseal fusion and tooth wear and eruption were made when possible. Following Sahnouni et. al (*22*) we categorized mammals according to size groups modified from Bunn (*68*): 1) very small size (<20 kg); 2) small size (20 – 100 kg); 3) medium size (100 – 300 kg); 4) large size (300 – 1000 kg); and 5) very large size (> 1000 kg).

All fossils from Excavations 3 and 5 were examined for weathering, deformation, cracking, exfoliation, corrosion, rounding, dry fractures, excavator and preparation marks, root, insect, rodent, carnivore, and tool damage. All carnivore and tool damages (cut marks, percussion marks, and percussion fractures) were identified using microscope illuminators and microscopes at 5-20x magnifications, and checked by three analysts (TP, JSO, JP). Modification types and, when appropriate, modification location, dimensions, and orientation were recorded.

Butchery behavior was identified by the presence of cut marks, percussion marks, and percussion fracture damages such as incipient flakes, flake scars, and hammerstone notches (*69–76*). Carnivore activity was identified by the presence of tooth scores, pits, furrows, and punctures (*77–79*).

Results

A list of all taxa recovered from excavations and surface collection at Nyayanga is shown in Table S3. Taxa recovered from Excavation 3 and Excavation 5 are presented in Figure S4. Excavation 3 and Excavation 5 mammalian taxon element frequencies and percentage of taxon NISP by anatomical region are given in Tables S5 and S6, respectively. Figures S5 and S6 show the 3-dimensional distributions of artifacts and select taxa recovered in situ from Excavation 3 and Excavation 5, respectively.

Damage frequencies observed on Excavation 3 and Excavation 5 fossils are shown in Figure S7. The frequencies of Excavation 3 and Excavation 5 fossils that display cut marks (CM)

and/or percussion damage (PD) are provided in Table S7. Examples of fossils with tool marks are provided in Figure 3.

Bone surface preservation was highly variable. Trampling, root damage, and rodent gnawing are rare, but cracking, exfoliation, deformation, and corrosion are common, particularly at Excavation 3 (Fig. S7). These alterations were likely the result of alternating post-depositional waterlogging and drying of overbank sediments while the paleochannel was active. More than 85% of the sample in both excavations showed no or minimal weathering, consistent with rapid burial by fluvial sediments.

Carnivores were present, but the frequency of carnivore-damaged bones is low, so little can be said about the mode of carnivore acquisition of fauna. Similarly, the low frequency of tool-damaged bones prevents any assessment of hominin scavenging or hunting behavior (Table S7).

Cut marked hippopotamid bones from both Excavation 3 and Excavation 5 document the butchery of two hippos in two separate butchery events. The next oldest examples of butchered megafaunal carcasses are from 2-1.8 Ma in eastern and northern Africa (*80*). The Nyayanga data pushes hominin butchery of megafauna back at least 800 - 600 Ka to the earliest inception of the Oldowan.

The presence of NY-1 bones from multiple size classes that exhibit definitive cut marks and percussion damage indicates that Nyayanga hominins processed animal carcasses on multiple occasions. Hominin processing of animal carcasses based on tool-damaged bones is supported by use-wear analysis (see section 9, Use-Wear Analysis, below).

9 - Use-Wear Analysis (Figs. S8-S12; Tables S8-S12) (CL, IC)

Methods: Experimental protocols for reference collections

Two reference collections were used for the analysis of Nyayanga lithic stone tools:
a) Use-wear analysis of Nyayanga tools with well-preserved cutting edges was carried out using the quartz and quartzite experimental sample used to interpret the function of artifacts from the nearby Oldowan locality of Kanjera South (*81*, *82*).
b) A dedicated percussive stone tool (*16*) reference collection was created using quartz and quartzite cobbles from Homa Peninsula conglomerates that are the same raw material, size, and shape as Nyayanga tools (Table S8). Experiments were designed to identify use-wear from four categories of materials: 1) tubers and roots (cassava, yam, horseradish), 2) fruits (passion fruit, custard apple), 3) wood (hazel bark), and 4) animal tissues (sheep bone with adherent soft tissue).

Percussive stone tools use-wear was examined in relation to physical and chemical properties (e.g., hardness, moisture, and fiber content) of plant foods: a) soft and juicy (i.e., passion fruit, *Passiflora edulis*, and custard apple, *Annona cherimoya*), b) pulpy/fibrous (i.e., cassava, *Manihot esculenta*), or c) woody/fibrous (i.e., horseradish, *Armoracia rusticana)*. Tubers and roots were processed using crushing actions. Larger tubers (>50 cm length) were initially struck to break them open and then crushed. Our wood reference collection was created by pounding bark from hazel (*Corylus*) tree branches. Carcass processing reference PPs were generated by fracturing fresh sheep (*Ovis aries*) femora and ribs. Some flesh and tendons were present on the pounded bones; thus, the tools contacted this soft material as well.

Experimental lithic stone tools were examined using a RH-2000 Hirox digital microscope with magnifications up to 2000X and a Hitachi Tabletop TM3000 SEM with magnifications up to 5000X and accelerating voltage 15kV at the LTFAPA Laboratory of Sapienza University of Rome. A Nikon Eclipse metallographic microscope equipped with a reflected light with a range of magnification from 50x to 200x, was used to observe use-wear developed on the experimental tools. For the use-wear analysis of the flakes, a stereomicroscope Nikon SMZ equipped with a reflected light with a range of magnifications from 0,75X to 7,5X was used with the metallographic microscope to observe, respectively, macro and micro-traces.

Methods: Archeological use-wear

Three hundred thirty tools were recovered from Exc3 (n=121), Exc5 (n=14), and the surface of NY-1 (n=195). The NY-1 assemblage is currently under ongoing analysis for use-wear. Preliminary sampling and observations of use-wear reported here were undertaken at the National Museums of Kenya in Nairobi. First, a sample of artifacts with potentially functional morphology (*80*) suggestive of cutting edge activities (n=125) and percussive activities (n=23) were examined to determine their potential for preserving use-wear. The state of preservation was documented using a stereomicroscope. Next, a subset of these artifacts was selected for further examination to determine tool function using macro-wear and micro-wear analysis (n=30). This sample included 7 cutting edge tools and 23 pounding tools (Table S9).

Macro-wear analysis of the archaeological tools was carried out at the Nairobi National Museum. Macro-pits, striations, negatives of scars, fractures, and grain morphology were observed using a RH-Hirox digital microscope with magnification from 10x to 90x and a stereomicroscope Nikon SMZ-U with magnifications ranging from 0.67X to 6.7X (*81–84*). Then, these artifacts were analyzed at higher magnification (metallographic, digital microscopes and SEM) to detect micro-traces of use carried out on silicone molds at LTFAPA laboratory following the protocol described in Lemorini (*81*, *82*). Micro-wear (polishes, micro-striations, micro-pits, and micro-cracks) was observed using higher magnifications under a metallographic Nikon Eclipse microscope with a range of magnification from 50x to 200x in reflected light and a Hitachi Tabletop TM3000 SEM (magnification range up to 5000x and accelerating voltage 15kV) at the LTFAPA laboratory (*85–89*). The observations were made on gold-coated epoxy resin casts (Araldite® LY 554 and HY 956) from silicon molds (Provil Novo Light Fast Heraeus®). The samples were washed with ultra-pure water prior to observation.

Results: Experiments

Use-wear of percussive activities (Fig. S8) visible under the metallographic microscope (Fig. S9) and under SEM (Fig. S10) include polishes that form levelled areas on the grains, abrasions, cracks on grains, micro-pits, and striations (Table S10). Processing of pulpy/fibrous roots created a distinctive very smooth, flat polish (cassava and yams; Fig. S9A, B). Yam processing resulted in short, polished, chaotic striations while cassava processing created irregular pits and cratering and short, polished, and chaotic striations (Fig. S9B).

Tools used to process hazel wood bark resulted in rough, domed polish and short, parallel, and tapering micro-striations (Fig. S9C; S10A, B, F). Horseradish processing presents a polish with round and well-defined micro-pits associated with unpolished long striations (Fig. S9D) and cracks (Fig. S10C, D, E).

A distinctive polish, deep leveling, and long, deep, parallel, and polished striae were observed on tools used to process bone (Fig. S9E, F). Processing of soft, juicy fruits created

rough and domed polish extent on the top and edges of the crystals (Fig. S9G, H). No leveled topography was observed.

Results: Preservation of archeological use-wear

Three types of non-use related surface alteration were recognized in the lithic sample: 1) generalized rounding of the surface, 2) edge breakage or crumbling, and 3) widespread glossy/bright appearance of the raw material matrix. Generalized rounding and widespread glossy appearance can be caused by sedimentary abrasion during transport, pedogenic processes following deposition, or postdepositional chemical alteration (*90–92*). Edge crumbling is caused by pressure, from trampling or sedimentary load, which results in micro-fracturing of the more fragile portions of the artifact edges (*93*, *94*).

Of the lithic tools examined for potential cutting activities (n=125; DPs n=111; FPs n=14), stereomicroscope analysis generally documented excellent preservation. Only 23% (n=29) of the sample exhibited alterations (heavy rounding or surface degradation) preventing macro- and micro-trace observations. This rounding likely reflects in situ chemical alteration, as has been noted in the in situ fossil assemblages from Excavations 3 and 5. The remaining 77% (n=96) show a well-preserved surface or a moderate glossy appearance that does not prevent the use-wear analysis (Tab.S9). Of the 23 FPs and PPs analyzed for pounding damage, 52% (n=12) displayed well-preserved surfaces unaltered by diagenetic processes. The stereomicroscope analysis shows a light glossy appearance on 35% of the sample (n=8) that does not obscure the preservation of macro and micro-traces. Five specimens (22%) had adhering concretions, but none were present on the functional areas.

Results: Archeological use-wear

Use-wear analysis of the Nyayanga assemblage is ongoing. Thirty artifacts from NY-1 that preserve macro-wear and micro-wear have thus far been analyzed (Table S9). Both surface-collected and excavated PPs, FPs, and DPs preserve use-wear. Surface collected pieces eroded out of NY-1 between annual field seasons, and so were exposed for a limited amount of time (days to months) on the outcrops. Initial inspection revealed that 6 PPs show use-wear on one or both ends (e.g., manuports or hammerstones), and 18 FPs (i.e., cores) and 6 DPs display preserved macro- and micro-wear related to various activities. Analyses and interpretations of 4 percussive stone tools (NY15-33, NY15-135, Exc3-103, Exc3-485) and 7 tools with cutting edge wear (Exc3-104, NY16-147, Exc3-352, Exc3-1188, Exc3-1379, Exc3-1633, Exc5-90) are presented as examples of use-wear that indicate Nyayanga hominins processed plant and animal tissues (Fig. S11 and S12; Tables S11 and S12).

Use-wear indicates that several artifacts were used to process plants. The smooth, cratered, and extensive polish occurring on grains observed on FP NY15-33 (Fig. S11 A-C, Table S11) are like the traces observed on the experimental pounding replicas used in the processing of vegetal organic materials with a pulpy consistency (Fig. S9A, B). Well-developed abrasion, furrow striae, edge rounding, and smooth polish noted on experimental lithic tools used to cut and scrape USOs (see Lemorini et al., (*81*, *82*) for the description of the use-wear and the experimental reference collection) are similar to that observed on Nyayanga Exc3-1379 and DP Exc3-104 (Fig. S12A-D, Table S12). Traces such as micro-pits and polishes with rough to smooth texture and polished micro-striae on another Nyayanga PP Exc3-485 (Fig. S11D-F) are similar to those created on replicas used to pound woody roots and tubers (i.e., horseradish and yams; Fig. S9B, D). Some specimens have puncture-like macro-pits associated with bands of

macro-striations of mixed orientations suggestive of close crushing of the worked substance (NY15-33; Fig. S11A). Localized and well developed abrasion, furrow striae, and smooth domed to flat polish created on experimental flakes used for woodworking (*81, 82*) are like those observed on Nyayanga Exc3-1633 (Table 12). Taken together, these results suggest that Oldowan hominins were cutting, scraping, and pounding USOs, wood, and likely other plant tissues (Tables S11 and S12).

Processing of animal tissue is indicated by the use-wear on several PPs, FPs, and DPs. One core, Exc3-135, displays micro-traces that include smooth and flat polish, leveling, and long parallel striations (Fig. S11K, L; Table S11) like those observed on experimental PPs used to break bone (Fig. S9E, F; Table 10). Several specimens display deep flake removal scars (e.g., NY15-135) (Fig. S11J) suggesting that considerable force (such as striking from a distance) was used in fracturing material during processing. Experimental animal butchery by cutting and scraping creates distinctive macro- and micro-traces, including edge rounding, pits and short sleek striae, abrasion and smooth and melting polish on a flat to domed topography (*81, 82*) like that observed on Nyayanga NY16-147, Exc3-352, Exc3-1379, Exc3-1188 and Exc5-90 (Fig. S12, Table S12). The traces of butchery activities on flakes are characteristic of intensive contact with bone as well as with meat, suggesting that hominins exploited the remains of fleshy tissues attached to carcasses.

Many percussive tools from Nyayanga appear heavily used, showing deep pits, well-developed polishes, and striations at low and high magnifications (Figs. S8 and S11). Comparison with experimental replicas allows us to hypothesize that several hours of use are required to produce comparable use-wear. In summary, macro-traces, micro-traces observed on Nyayanga PPs, FPS, and DPs indicate that hominins used cutting, scraping, crushing, and pounding actions to process a variety of plants and animal tissues.

10 - Stable isotopic analysis of paleosol carbonates (Fig. S13; Table S13) (PWD, SAB)

Methods

Paleosol carbonate nodules for isotopic analysis were collected from paleosol sections exposed in excavation and geological trenches. Five soil carbonate nodule bearing horizons were identified from the Nyayanga sequence, located in the middle and upper parts of NY-1, the middle and upper parts of NY-2, and the upper part of NY-4 (Fig. 1). Only nodules from greater than 30 cm below the top of each paleosol horizons were analyzed to avoid the possibility of atmospheric CO_2 effects (*95*). Samples were cleaned of any adhering sediment, washed in deionized water, dried, then ground using an agate pestle and mortar and homogenized. Subsamples of 100 mg were treated with 0.5 ml of a 3% sodium hypochlorite (NaOCl) solution in 1.5 ml centrifuge tubes for 24 hours to oxidize any organic matter, then rinsed 5 times in deionized water and dried in a 60 °C oven.

Oxygen and carbon stable isotopic results were obtained in Oxford, U.K. using a Thermo delta V isotope ratio mass spectrometer (IRMS) coupled to a Thermo Gasbench. Each sample was reacted with purified phosphoric acid (H_3PO_4) at 90^{o}C with the liberated CO_2 being frozen into a liquid nitrogen cooled 'cold finger' apparatus prior to admission to the mass spectrometer.

Both oxygen and carbon isotopic ratios are reported in per mil (‰) notation relative to Vienna Pee Dee Belemnite (V-PDB). Calibration was against multiple aliquots of IAEA CO-1 and IAEA CO-8 carbonate standards, run in the same batch as the samples. Replicate analyses of

in-house NOCZ Carrara Marble standard were also made alongside the samples as a quality control check. These gave a reproducibility of better than 0.1 ‰ for both $\delta^{13}C$ and $\delta^{18}O$.

Results

Carbon and oxygen stable isotopic results are shown in Table S13 and Fig. S13. Stable carbon isotopic analysis of pedogenic carbonates from the Excavation 3 slope, (approximately 40 m away from the paleochannel), suggest 40-60% C_3 vegetation through the NY-1 and NY-2 sequence (Table S13). Following Cerling et al. (*96*), the predicted fraction of woody cover (~20-50%) suggests that wooded grassland and grassy woodland/bushland/shrubland were the dominant vegetation structure categories near the channel during NY-1 carbonate formation, similar to the habitats of site formation of other late Pliocene archeological occurrences (Fig. S13b).

Carbonates from NY-2 indicate wooded grasslands to grasslands (~5-30% woody cover), and the decrease in woody cover continues from NY-2 to NY-4. Support for this paleoenvironmental context is also provided by the reconstruction of fossil mammalian herbivore diet from NY-1 using tooth enamel carbon isotopes (n = 98) (see section 11, Stable isotopic analysis of fossil mammalian tooth enamel, below; Figs. S14 and S15; Table S14).

11 - Stable isotopic analysis of fossil mammalian tooth enamel (Figs. S14 and S15; Table S14) (SAB)

Methods

Fossil teeth analyzed here were recovered during field expeditions between 2007 and 2017, including surface collected and excavated material and are housed in the Paleontology collections of the Nairobi National Museum. Tooth enamel was sampled from specimens (n = 128) identifiable to genus, tribe, or family using a rotary drill with diamond tipped burr. This collection includes representatives of Artiodactyla, Perissodactyla, Proboscidea, Primates, and Carnivora (Table S14). Prior to sampling, teeth were cleaned with ethanol. Approximately 2-4 mg of enamel powder was removed from non- diagnostic parts of each tooth, avoiding contaminating enamel powder samples with dentin, cementum, or matrix. All samples were pretreated using 0.1 M buffered acetic acid for 30 minutes to remove secondary exogenous carbonates. Carbon and oxygen isotope ratios of enamel carbonate were measured by digestion with 100% phosphoric acid with the resulting CO_2 analyzed on an isotope ratio mass spectrometer. We report our results in per mil (‰) notation, $\delta^{13}C = (R_{sample}/R_{standard}-1) * 1000$, where R_{sample} and $R_{standard}$ are the $^{13}C/^{12}C$ ratios of the sample and standard, respectively; the standard being Vienna Pee Dee Belemnite (V-PDB). Reproducibility ($\pm 1\sigma$ ratios of reference materials) was 0.1‰ for and 0.2‰ for $\delta^{18}O$.

The carbon isotopic composition of tooth enamel reflects diet and, among African mammals, can readily distinguish between consumers of C_3 (mostly dicots) and C_4 (mostly monocots) biomass, based on the isotopic composition of modern C_3 and C_4 vegetation in Africa, corrected for the estimated carbon isotopic composition of preindustrial (ca. 1750) atmospheric CO_2 and assuming a diet-enamel enrichment of 14‰ (*97–99*). Body size has been reported to predict enamel-diet enrichment ($\varepsilon_{apatite\text{-}diet}$) across mammals (*100*), but available data on relevant taxa (Artiodactyla, Perissodactyla, Proboscidea) used in the same study shows no relationship ($p > 0.05$) between $\varepsilon_{apatite\text{-}diet}$ and body mass. Further, considerable intra-specific variation $\varepsilon_{apatite\text{-}diet}$

has been observed (*101*), suggesting that future isotopic analyses of enamel (or breath) from animals with controlled diets, such as zoo animals, is needed to clarify relationships with body mass and/or digestive physiology. Therefore, we use the conventional diet-enamel enrichment of 14‰. We do not correct $\delta^{13}C$ values from fossil teeth for changes in the carbon isotopic composition of atmospheric CO_2 because this value remained relatively constant throughout the Pliocene and Pleistocene and was similar to the preindustrial value (*99, 102*).

Among large mammalian herbivores, we consider that C_4 grazers consume predominately C_4 biomass (> ~75% C_4), corresponding to $\delta^{13}C_{enamel}$ > -1‰. C_3 browsers consume predominately C_3 biomass (> ~75% C_3), corresponding to $\delta^{13}C_{enamel}$ < -8‰. Mixed feeders consume intermediate amounts of C_3 and C_4 biomass and have $\delta^{13}C_{enamel}$ between -8‰ and -1‰. Proportions of C_4 grazers (G), C_3- C_4 mixed feeders (M), and C_3 browsers (B), are expressed as G:M:B, calculated using a predominate mode of feeding defined by the average $\delta^{13}C$ value of each taxon within a fossil collection (*99*). For characterizing the diet variation of individuals within a single taxon, we calculate G:M:B as a fraction of individuals that are C_4 grazers, C_3-C_4 mixed feeders, and C_3 browsers. Differences in the proportion of these diet classes (G:M:B) can be used to address ecosystem change on the scale of large mammal ranging (10s of km^2) and time span of fossil preservation.

The oxygen isotopic composition of tooth enamel reflects body water, which in turn relates to oxygen in food, drinking water, and inspired air (*103*). Oxygen isotopic variation among some mammal taxa more closely tracks meteoric water, whereas in others it tracks evaporative enrichment (*104*, *105*). Among African ungulate species, the oxygen isotopic enrichment of enamel over meteoric water ($\varepsilon_{enamel\text{-}mw}$) is negatively correlated with dung moisture content (*106*) and reflects differences in water requirements (*105, 107*). Mammalian taxa where $\varepsilon_{enamel\text{-}mw}$ are highly invariant with increasing annual water deficit (a measure of aridity) are considered evaporation insensitive (EI), likely reflecting consistently high dependence on water (*104*, *105*). Mammalian taxa where $\varepsilon_{enamel\text{-}mw}$ increases with water deficit are considered evaporation sensitive (ES), likely reflecting decreasing dependence on drinking water and water loss, and increasing reliance on food water with increasing aridity. The oxygen isotopic enrichment between ES and EI taxa ($\varepsilon_{ES\text{-}EI}$) correlates with water deficit. We calculate paleoaridity using $\varepsilon_{ES\text{-}EI}$ values from Nyayanga Bed 1 fossils using Hippopotamidae, Elephantidae, and Rhinocerotidae as EI taxa and Tragelaphini as the ES taxon following (*105*). For ES-EI comparisons, we include fossils excavated from NY-1 in Excavations 3 and 5, which are separated stratigraphically by ~1 m of sedimentation and a constrained period of deposition. We exclude surface fossil collections to reduce potential bias in climate variability associated with time averaging.

We also address paleoclimate using intratooth $\delta^{18}O_{enamel}$ variability in equids. Equids are water-dependent, such that $\delta^{18}O$ variation of body water, and thus also tooth enamel $\delta^{18}O$, relates to local environmental waters. The intratooth oxygen isotope range correlates with the intra-annual range of the oxygen isotopic composition of precipitation so isotopic variation within fossil equid teeth provides an indication of the isotopic seasonality of past precipitation (*108*). Since the isotopic signal can be blurred by amelogenesis, we correct the measured intra-tooth isotopic range to infer the $\delta^{18}O_{precipitation}$ intra-annual range from the undamped $\delta^{18}O_{enamel}$ intra-tooth range (*108*). Here we present results from a single *Eurygnathohippus* upper third molar for preliminary comparison to results from similar analyses of Early Pleistocene equid teeth from the Homa Peninsula and Olduvai Gorge (*108, 109*).

Results: Nyayanga Bed NY-1: $\delta^{13}C_{enamel}$

Artiodactyla – Bovidae: Bovidae are well represented in the Nyayanga fossil collection (Fig. S14, Table S7). The Alcelaphini (n = 11) are all C_4 grazers with a $\delta^{13}C$ range from 0.1‰ to 3.2‰ (G:M:B = 100:0:0). The Antilopini (n = 7) have a $\delta^{13}C$ range from -3.3‰ to 3.0‰ indicating C_4-dominated diets (G:M:B = 86:14:0). A single bovini specimen was analyzed, showing a C_4 dominated diet ($\delta^{13}C$ = 2.9‰). The Reduncini (n = 3) are all C_4 grazers with a $\delta^{13}C$ range from 1.0‰ to 3.5‰ (G:M:B = 100:0:0). The Tragelaphini (n = 8) range from -12.2‰ to 0.3‰ and are predominately mixed feeders (G:M:B = 25:50:25). We also analyzed 9 bovid specimens that were no identified to the tribe, which have a $\delta^{13}C$ range from -13.7‰ to 3.4‰ (G:M:B of 67:22:11), consistent with the abundance of C_4-grazers among the bovids at Nyayanga.

Artiodactyla – Giraffidae: We analyzed a single giraffid specimen and it had a C_3 dominated diet ($\delta^{13}C$ = -10.5‰). For comparisons with other fossil collections, we informally recognise the browsing "Giraffid B" and mixed feeding and grazing "Giraffid MG" group, based on the consistent difference between the mixed feeding and grazing *Sivatherium* lineage and browsing *Giraffa* lineage in eastern Africa during the Plio-Pleistocene (*110*).

Artiodactyla – Hippopotamidae: The Hippopotamidae are represented by 19 individuals, which have a $\delta^{13}C$ range from -11.4‰ to 2.6‰ and are predominately C_4 grazers (G:M:B = 63:32:5).

Artiodactyla – Suidae: Two genera of Suidae were analyzed. *Metridiochoerus* (n = 3) specimens are all C_4 grazers, with a $\delta^{13}C$ range from 0.9‰ to 1.3‰ (G:M:B = 100:0:0). *Kolpochoerus* (n = 1) is a mixed feeder ($\delta^{13}C$ = -1.2‰).

Perissodactyla – Rhinocerotidae: The Rhinocerotidae are represented by 16 specimens that have a $\delta^{13}C$ range from -11.1‰ and 2.0‰. Although these specimens are too fragmentary for identification to genus, following Cerling and colleagues (*99*) we informally recognize grazing "Rhino G" ($\delta^{13}C$ > -1‰) and browsing "Rhino B" ($\delta^{13}C$< -8‰) groups based on the consistent dietary difference between the two rhinocerotid lineages leading to extant *Ceratotherium* and *Diceros* (*110*). As members of both lineages during the Pliocene were mixed feeders ($\delta^{13}C$ > -8‰ and < -1‰) (*110*), mixed feeding individuals are not included in either group. This approach differs from (*99*), where mixed feeding individuals were included in the "Rhino G" and "Rhino B" groups based on $\delta^{13}C$ higher and lower than -5‰, respectively. Among fossil rhinocerotids analyzed here, the "Rhino G" group has an average $\delta^{13}C$ value of 0.6 ± 0.8‰ (n = 10; G:M:B = 100:0:0) and the "Rhino B" group has $\delta^{13}C$ range from -11.1‰ to -9.6‰ (n = 2). Specimens (n = 5) identified as "Rhinocerotidae gen. sp. indet" are mixed feeders, with a $\delta^{13}C$ range from -6.1‰ to -1.3‰.

Perissodactyla – Equidae: The Equidae are represented by two *Eurygnathohippus* specimens, which are both C_4 grazers with a $\delta^{13}C$ range from -0.3‰ to 3.5‰ (G:M:B = 100:0:0). Seven equid specimens that were not identified to genus have a $\delta^{13}C$ range from -0.3‰ to 1.8‰ (G:M:B = 100:0:0).

Proboscidea – Deinotheriidae: The Deinotheriidae (n = 2) are C_3 browsers, with a $\delta^{13}C$ range from -13.5‰ to -11.7‰ (G:M:B = 0:0:100).

Proboscidea – Elephantidae: The elephantids are represented by two genera. *Elephas* (n = 2) has an average $\delta^{13}C$ value of -0.2 ± 1.8‰ and is predominately a C_4 grazer. *Loxodonta* (n = 2) has an average $\delta^{13}C$ value of -1.2 ± 2.7‰ and is predominately a mixed feeder. Two additional specimens of elephantids not identified to genus had $\delta^{13}C$ values ranging from -3.0‰ to -0.4‰, consistent with the presence of C_4 grazing and mixed feeding elephantids.

Proboscidea gen. sp. indet.: One proboscidean fossil not identified to family is a C_4 grazer ($\delta^{13}C$ = -0.9‰).

Primates – Hominidae: We analyzed two hominin specimens, both attributed to *Paranthropus*, with $\delta^{13}C$ values -1.0‰ and -0.4‰, indicating a C_4 dominated diet. The notion that dietary (i.e. increased consumption of C_4-based foods) and morphological changes (i.e. increased tooth size) are linked is consistent with previous taxon-level relationships between diet and morphology among early hominins (*29*). The Nyayanga data add to the evidence that the dietary strategies of early *Paranthropus* were flexible. The diets of Omo-Turkana basin *P. aethiopicus* individuals range from mostly C_3 foods to mostly C_4 foods ($\delta^{13}C_{enamel}$ values range from -10.8‰ to -0.3‰) (*19*, *28*). Among *P. boisei*, a small number of individuals from the Shungura Formation in Ethiopia (n = 2) and the Chiwondo Beds in Malawi (n = 1) relied on substantial amounts of C_3 foods ($\delta^{13}C_{enamel}$ < -4.0), whereas most individuals consumed a C_4-dominated diet (*19*, *25*, *27*, *32*).

Primates – Cercopithecidae: One single Colobini specimen ($\delta^{13}C$ = -15.3‰) and a papionini tooth ($\delta^{13}C$ = -11.6‰), both have C_3 dominated diets.

Results: Nyayanga Bed NY-2: $\delta^{13}C_{enamel}$

Carnivora – Felidae: We analyzed a single fossil felid specimen (*Megantereon*), with a $\delta^{13}C$ value of -2.7‰, suggesting a reliance on prey consuming a mixture of C_3 and C_4 biomass.

Results: Nyayanga Bed NY-3: $\delta^{13}C_{enamel}$

Artiodactyla – Bovidae: One Hippotragini specimen is a C_4 grazer (1.4‰) and one Tragelaphini specimen is a mixed feeder (-6.7‰). We also analyzed 3 bovid specimens not identified to tribe, which have an average $\delta^{13}C$ value of 0.9‰ indicating the presence of additional grazers among the bovids.

Artiodactyla – Suidae: A single specimen attributed to *Metridiocheorus* is a C_4 grazer (-0.9‰).

Perissodactyla – Rhinocerotidae: Two Rhinocerotidae specimens are both C_4 grazers ($\delta^{13}C$ = -0.4‰ and 2.4‰) and are included in the "Rhino G" group.

Results: Nyayanga Bed NY-4: $\delta^{13}C_{enamel}$

Artiodactyla – Bovidae: We analyzed a single Alcelaphini specimen, which is a C_4 grazer (0.9‰), and a single Antilopini specimen, which is a C_4 grazer (2.0‰). One bovid specimen that is not identified to tribe is also a C_4 grazer (1.4‰).

Artiodactyla – Hippopotamidae: One hippo specimen from Bed 4 is a C_3 browser with a $\delta^{13}C$ value (-8.4‰) within the range of the larger sample of Nyayanga Bed 1 hippopotamids.

Artiodactyla – Suidae: One *Metridiocheorus* specimen, which is a C_4 grazer (1.7‰), and two specimens not identified to genus are also C_4 grazers ($\delta^{13}C$ = 0.7‰ and 1.7‰).

Results: Nyayanga Surface collections: $\delta^{13}C_{enamel}$

Artiodactyla – Bovidae: The Bovids are represented by two specimens, which are not identified to tribe and both are C_4 grazers ($\delta^{13}C$ = -0.9‰ and 3.9‰).

Artiodactyla – Suidae: A single specimen attributed to *Metridiochoerus modestus* is a C_4 grazer ($\delta^{13}C$ = 1.2‰). One specimen not identified to genus is also a C_4 grazer (- 0.2‰).

Perissodactyla – Equidae: Two equid specimens are not identified to genus and are both C_4 grazers ($\delta^{13}C$ = 1.4‰ and 1.7‰).

Proboscidea gen. sp. indet.: We analyzed one proboscidean fossil, which is not identified to family and is a C_4 grazer ($\delta^{13}C = 0.0‰$).

Results: All samples: $\delta^{18}O_{enamel}$

Oxygen isotope results for all taxa are presented in Table S14 but are not discussed further except for aridity index and equid sampling results.

To address paleoaridity, we used tooth enamel oxygen isotope data from NY-1 fossils. We calculated $\varepsilon_{ES\text{-}EI}$ for taxon pairs Tragelaphini-Hippopotamidae ($\varepsilon_{Tragelaphini\text{-}Hippo} = 1.9‰$), Tragelaphini-Elephantidae ($\varepsilon_{Tragelaphini\text{-}Eleph} = -1.2‰$), and Tragelaphini- Rhinocerotidae ($\varepsilon_{Tragelaphini\text{-}Eleph} = -1.0‰$). The estimated mean water deficit is -414 ± 326 mm/y, indicative of moderately mesic climatic conditions within the range of previously analyzed Pliocene-Pleistocene fossil collections on the Homa Peninsula (Kanjera South KS-2) and the Turkana Basin (*105*).

To address paleoseasonality, we measured the intra-tooth oxygen isotope range of an equid tooth (1.8‰), yielding a corrected intra-tooth range of 3.9 ± 0.5‰ that indicates paleo-precipitation isotopic seasonality within the range estimated from previous analyses of Early Pleistocene fossil equids from the Homa Peninsula and northern Tanzania (Fig. S15) (*108*).

Synthesis

The non-hominin primates (papionini and the very large colobine *P. mutiwa* with C_3-dominated diets, and Galagidae), as well as browsing mammalian herbivore taxa such as the proboscidean *Deinotherium* sp., the rhinocerotid *Diceros* sp., and a giraffid, are consistent with the presence of C_3 woody and herbaceous vegetation near the paleochannel. Other environmental proxies are consistent with mosaic ecosystems dominated by grassy and herbaceous flora with limited woody cover over the broader landscape (see section 12, Bovid tribal representation and dietary analysis of APP taxa, below; Fig. S16 and S17). Oxygen isotopic analysis of fossil tooth enamel of ES and EI taxa preserved at Nyayanga indicates local conditions were relatively mesic, within the range of paleo-water deficit estimations from Kanjera South at ~2.0 Ma and various Pliocene-Pleistocene fossil collections from the Turkana Basin (Fig. S15).

These results indicate that the Nyayanga archeological sites were deposited in a well-watered habitat with some trees, similar to the habitats of site formation of other late Pliocene archeological occurrences (Fig. S13b; (*112*).

12 - Bovid tribal representation and dietary analysis of APP taxa (Figs. S16 and S17) (TWP)

Methods

See section 8, Faunal Identification and Taphonomy, and section 11, Stable isotopic analysis of fossil mammalian tooth enamel, above.

Results

Bovid tribal representation and proportions of C_4 grazers, C_3-C_4 mixed feeders, and C_3 browsers (G:M:B) among Artiodactyla-Perissodactyla-Proboscidea (APP) taxa are consistent with predominantly grassy and herbaceous flora with limited woody cover over the broader landscape near Nyayanga. The frequencies of bovid tribes preferring open, dry grasslands (Antilopini and Alcelaphini), versus those favoring dry woodland or bushland (Tragelaphini and

Aepycerotini), or seasonally flooded edaphic grasslands (Reduncini and Bovini) (*113*, *114*) vary considerably between modern game reserves, and permit some general characterizations of the environment. Nyayanga has a high frequency of antilopin and alcelaphin bovids (63%), similar to those found in modern grass-dominated ecosystems, as well as those from comparably aged samples from Ledi-Geraru (Gurumaha, Lee Adotya) (Fig. S16) and Mille-Logya from the Afar Triangle in Ethiopia (*18, 115*). These latter localities have both yielded fossils of early *Homo*, and are more grazer dominated than paleocommunities in the Hadar Formation that immediately precede them in time. The moderate frequency of reduncin bovids (20%) at Nyayanga likely indicates areas with wet grass seasonally flooded by the stream or near the freshwater spring, and the tragelaphins (17%) were likely sheltering in bushland/woodland near the stream and spring.

Tooth enamel $\delta^{13}C$ values show that the diets of APP taxa are dominated by C_4 grazers (>50%), with lower representation of mixed feeders and browsers (Fig. S17). The Nyayanga samples resemble those drawn from modern C_4 grazer-dominated mosaic ecosystems that include a mix of grasslands, wooded grasslands, and grassy woodlands (*99*). *Paranthropus* fossils at Nyayanga demonstrate that early members of this genus, as well as early *Homo*, were found in settings that were more C_4 rich than *Australopithecus afarensis*. Nyayanga *Paranthropus* $\delta^{13}C$ values indicate a strong dietary reliance on the tropical grass and/or C_4 herbaceous resources that were common in the vicinity of the locality.

13 - Hominin Description (Tables S15-S21) (SEB)

Methods

Two hominin molars were recovered from Nyayanga, KNM-NG 77315 and NY17-Exc3-1600 (Fig. 3). The bulk of our comparative data (metrics and morphology) come from Wood and colleagues (*116–118*). Data from *Australopithecus garhi* come from (*119*), *Au. afarensis* are from SEB's dataset (Table S15, S16), and Ledi-Geraru is from (*21*). Our sample is provided in Tables S17-S21. Non-metric traits are scored according to the ASUDAS (*120*). Cusp areas and crown base areas not taken from Wood and colleagues were measured following Bailey (*121*).

Results; Hominin molar KNM-NG 77315

Left upper molar KNM-NG 77315 is the largest hominin molar currently known, measuring 18.1 mm buccolingually and >17.1 mm mesiodistally (up to 0.7 mm of the mesial enamel is missing due to interproximal wear) (Table S17). The measured crown area (278-282 mm) is well above the range of all *Paranthropous boisei* and *P. robustus* upper molars (Table S18). The crown is completely formed, and a portion of the root is preserved just below the cementoenamel junction. A small piece of enamel is missing from the buccal aspect of the inferior part of the paracone. The mesial aspect possesses a large (6.7 x 5.2 mm) interproximal wear facet. A smaller distal (3.9 x 8.1 mm) interproximal facet is also present. The crown wear is moderate (*122*) (wear stage 4), and quite flat. The lingual cusps are more worn than the buccal cusps, as is typical of hominin upper molars. The protocone possesses a large, exposed area of dentine, while the metacone and paracone possess medium and small dentine patches, respectively. On the lingual aspect there is a deep vertical crack along the protocone midline and thinner vertical cracks on the hypocone. The buccal aspect also possesses thin vertical cracks along the paracone and metacone midlines. The lingual groove separating the hypocone and protocone is short and weakly expressed, whereas the buccal groove separating the paracone and

metacone is slightly deeper and longer, being moderately expressed. Mesial wear prevents assessment of mesial marginal morphology (e.g., mesial marginal ridge, mesial accessory cusps, epicrista, or anterior fovea). The distal portion is less worn and better preserves morphology (see below).

KNM-NG 77315 is best identified as M^2. Based on the distal interproximal facet, we can eliminate the M^3 as a possible molar position. The crown's exceptionally large size favors an M^2 position, as M^1 tends to be smaller than M^2 in Pliocene hominins. This molar possesses four major cusps: protocone, metacone, paracone, hypocone. The crown shape is a slightly skewed rhombus. Although worn, the major fissure separating metacone and paracone, as well as that separating metacone and hypocone, are intact. The fissures separating protocone from hypocone and metacone from protocone are less complete, requiring some extrapolation regarding their position. Estimates of cusp areas (Table S18) indicate PROT>HYP>PAR>MET. Relative cusp areas also favor an M^2 attribution. In this crown, the metacone is smaller than the paracone. (*123*) found that the upper M^1 of *Australopithecus, Paranthropus* and most early *Homo* possess a larger metacone than paracone. This relationship appears to be reversed on the M^2, based on average values for various Plio-Pleistocene hominins (*118*): the metacone is smaller than the paracone in all Plio-Pleistocene taxa. The large size, the relatively smaller metacone, and the presence of a distal interproximal wear facet all point to M^2 as its most probable position. On the mesial aspect of the protocone there is a small enamel pit (grade 2 Carabelli's feature in Ortiz (*124*) (Table S19). It is possible that this feature was larger in the unworn crown. There is a thick distal marginal ridge, portions of which are contributed to by the metacone and hypocone. The enamel is thick (3.2 mm estimated from protocone). The lingual enamel line is straight.

The crown shape and occlusal morphology, including the thick distal marginal ridge, are typical of *Paranthropus* specimens. Carabelli's feature tends to be present but weakly expressed (groove, pit, or Y) in all Pliocene hominins. A similar expression of Carabelli's feature is observed on the KNM-WT 17400 M^2. The thick enamel is also consistent with *Paranthropus* attribution (*125*). The rhomboid shape of the Nyayanga molar is somewhat unusual for *P. boisei* M^2, which tend to be narrower distally than mesially.

The crown size and morphological characters suggest that this tooth is best accommodated within *Paranthropus* rather than *Australopithecus* or *Homo*. Both the *Au. garhi* upper M^1 and M^2 are smaller, especially in MD length, than the Nyayanga M^2. Likewise, both *Au. garhi* and Mille-Logya M^2s are narrower distally, compared to the Nyayanga M^2. We hesitate to assign this molar to a definite species because the relatively poor comparative sample of eastern African *Paranthropus* molars makes it impossible to confidently differentiate between *P. boisei* and *P. aethiopicus* based on crown size and trait expression at the enamel surface. Moreover, it is very possible that we do not know the full size range of either species due to biases in preservation (see (*126*). The Nyayanga molar differs from the single *P. aethiopicus* M^2 in the latter's series of vertical fingerlike extensions on the mesiolingual aspect where Carabelli's feature is typically found. There are only two M^2s attributed to *P. boisei* and both have a weak Carabelli's feature (groove/pit) as is observed in the Nyayanga molar.

Results: Hominin molar KNM-NG 77316

KNM-NG 77316, a minimally worn fragment of a lower left M_1 or M_2 preserves most of the metaconid and entoconid, as well as lingual portions of the protoconid and hypoconid (Fig. 4). No root is present and tapering of the enamel on the preserved mesial aspect suggests that the

crown was broken just above the cervix, preserving most of the crown height (8.6 mm from the lingual aspect).

The KNM-NG 77316 molar is most likely an M_1. The tooth is unlikely to be an M_3 based on its lobate lingual border, presence of a lingual fissure, and unreduced, non-tapering entoconid. Morphology and cusp proportions of the preserved cusps do not discriminate well between M_1 and M_2; however, the estimated crown size suggests that the crown is most likely an M_1. The fragment measures 9.0 mm BL and 13.0 mm MD. Based on a near-exact match in the fissures, outline shape and morphology between the Nyayanga molar and *P. boisei* molar KNM-WT 15930 (14.6x15.5 mm) M_1, we suggest that KNM-NG 77316 was slightly smaller, with an estimated crown area between 200 - 226 mm^2 (Table S20). The estimated crown area is above the range of all eastern African *Homo* lower molars in Wood and Abbot's (*116*) sample and falls within the *P. boisei* M_1 range (there are no *P. aethiopicus* teeth for comparison; see Table S6). Measured cusp areas are provided in Table S20. The relative size of the entoconid to the metaconid falls closest to Wood et al.'s (*117*) eastern African "robust" sample (Table S20). The measured enamel thickness of the Nyayanga molar ranges between 3.0 and 3.3 mm. This is most similar to Beynon and Wood's (*125*) East African "robust" group (Occlusal 3.1 mm; Cuspal 3.3 mm; Lateral 2.4 mm) and substantially thicker than their East African *Homo* group (Occlusal 1.4 mm; Cuspal 1.6 mm; Lateral 1.6 mm).

The KNM-NG 77316 molar almost certainly possessed a Cusp 6 based on the mesial position of the entoconid; Cusp 7 is absent (Table S21). Approximately half (n=10) of *P. boisei* M_1s and nearly all (8/9) M_2s possess a Cusp 6 and none has a Cusp 7. None of the early eastern African *Homo* M_1s and 67% (2/3) of M_2s have a Cusp 6. In contrast to *Paranthropus*, most (2/3) of the early East African *Homo* M_1s have a Cusp 7 and all (2/2) of the M_2s possess this accessory cusp. The Ledi-Geraru M1 and M2 are considerably smaller than the KNM-NG 77316 molar and possess a Cusp 7. Thus, the likely presence of a Cusp 6 and the absence of a Cusp 7 in KNM-NG 77316, a pattern characteristic of eastern African *Paranthropus*, supports our diagnosis (Table S21).

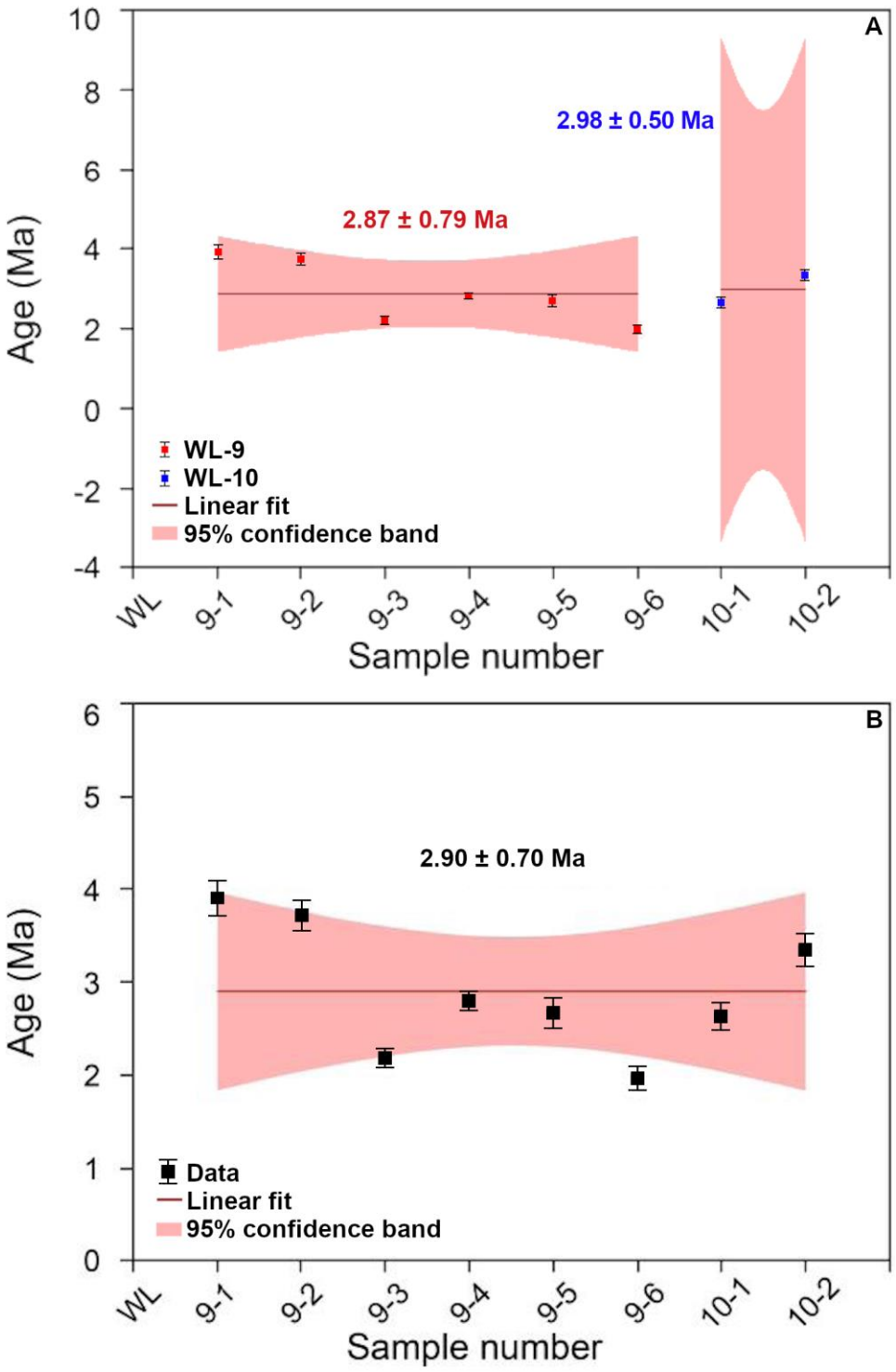

Fig. S1.

Raw (U-Th)/He results for apatite crystals from the WL-9 and WL-10 samples. Ages considered separately (A) and combined (B).

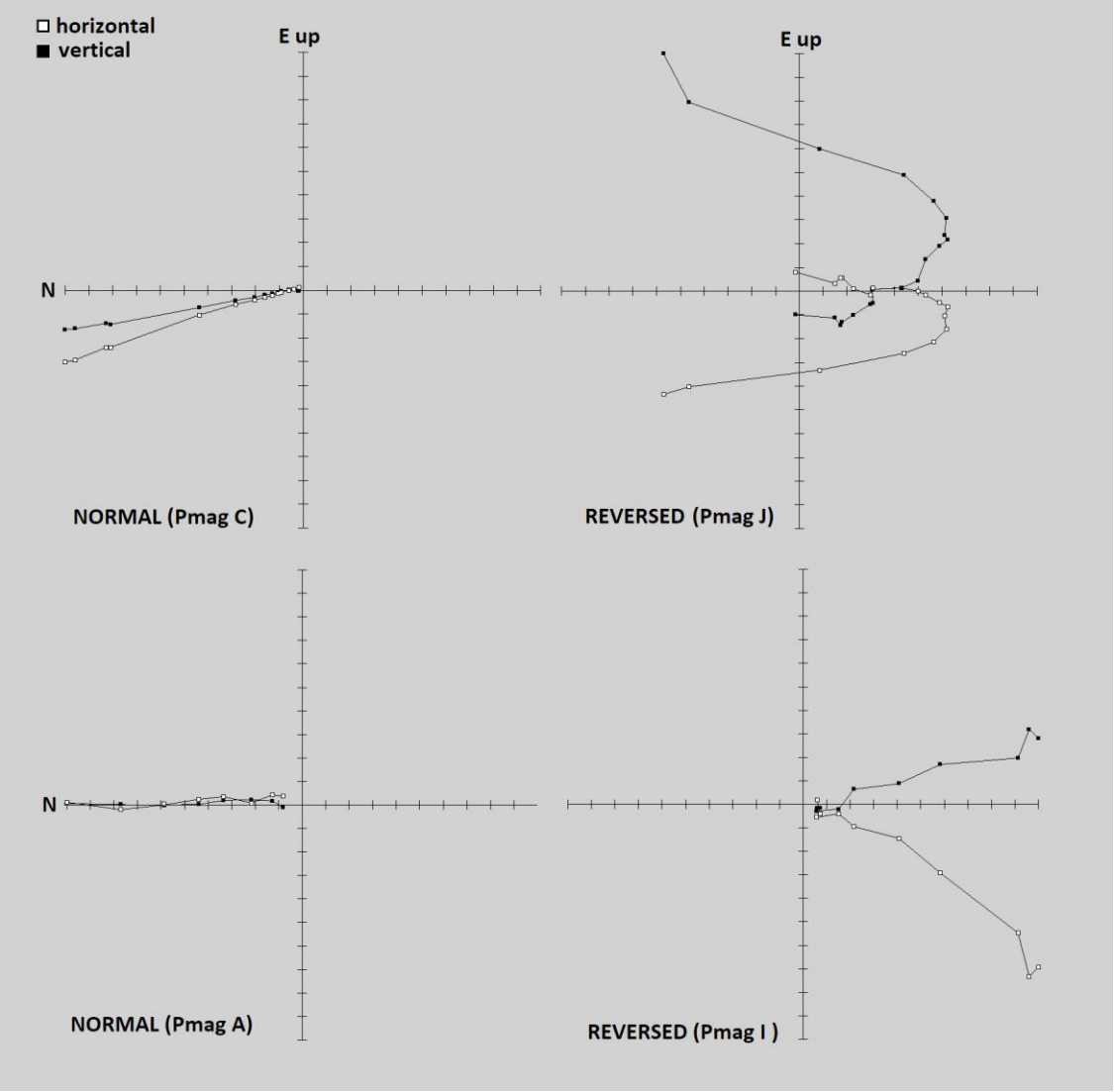

Fig. S2.

Alternating Field Zijderveld plots for (A) normal and (B) reversed polarity samples from the Nyayanga sequence.

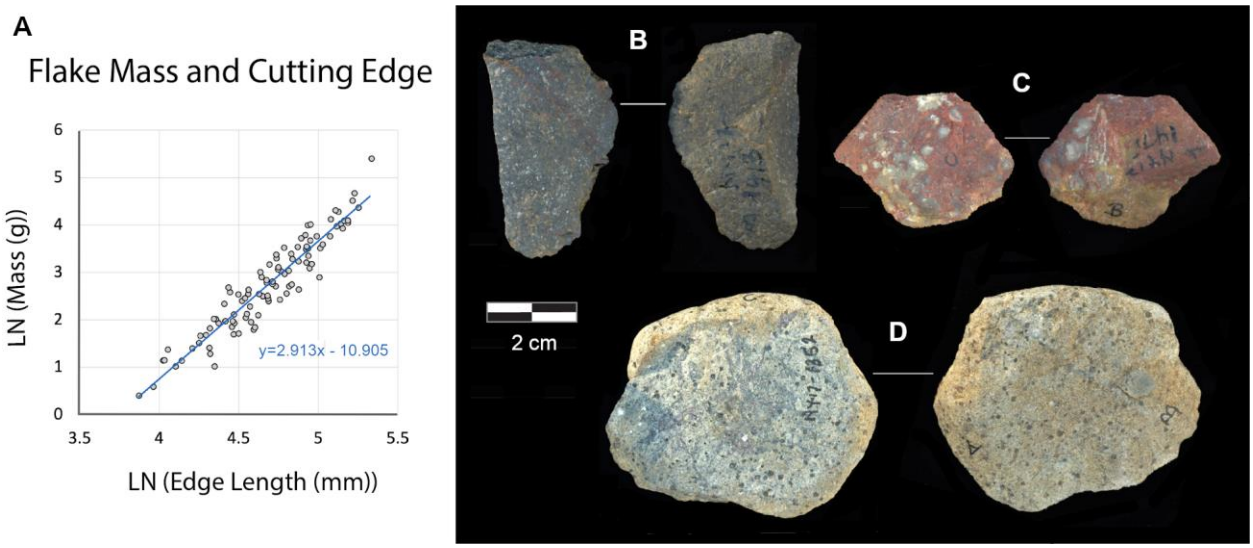

Fig. S3.

Nyayanga flake morphology. (A) the relationship between the natural log of flake mass (y-axis) and the natural log of estimated edge length (x-axis). Each point represents a single flake. The linear trend line and equation is shown. (B-D) selected flakes from Excavation 3. The ventral and dorsal surfaces are shown. (B) Exc3-1413. (C) Exc3-1475. (D) Exc3-1352.

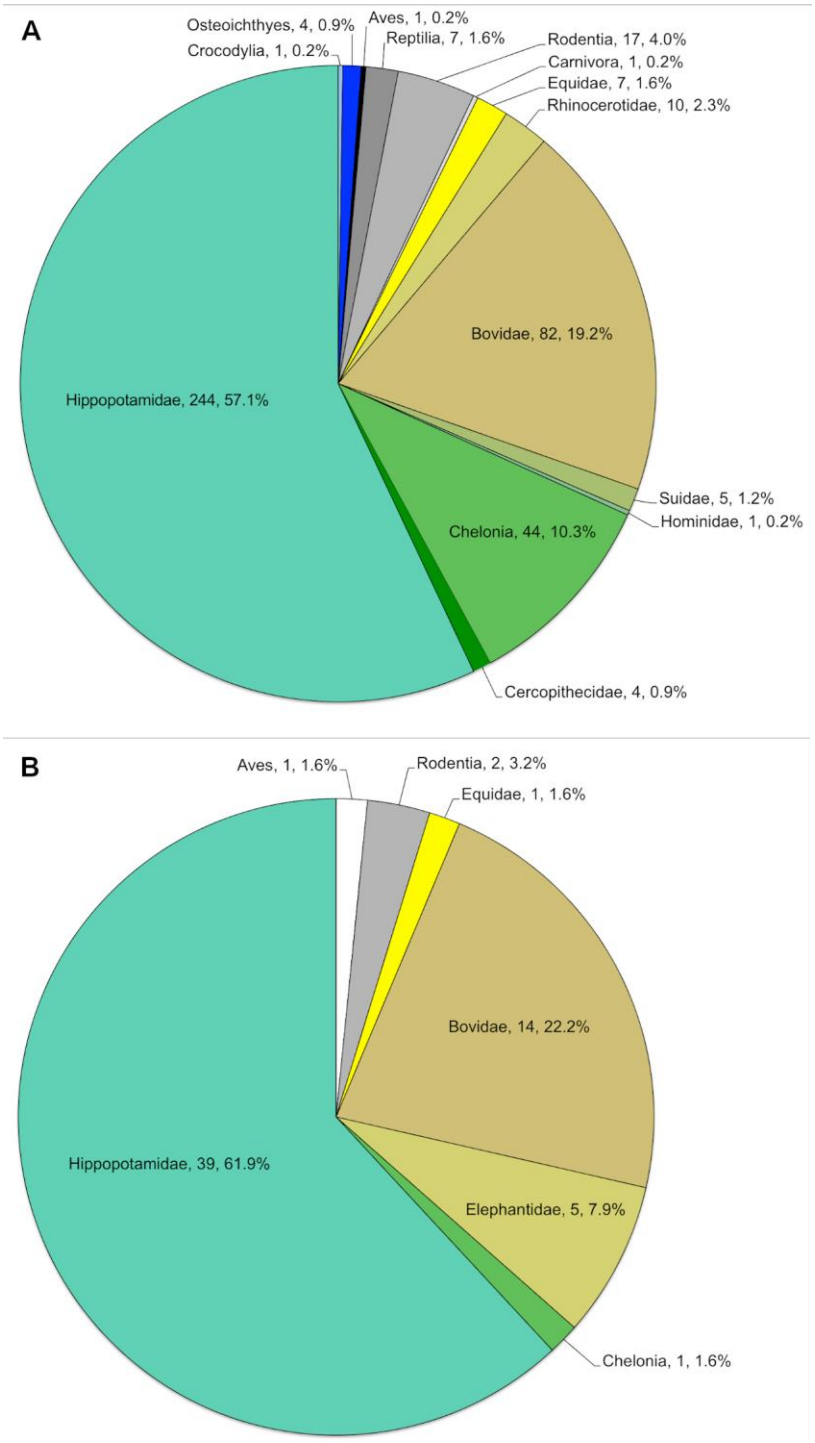

Fig. S4.
Relative proportions of NY-1 fossil taxa from Excavations 3 (A) and 5 (B).

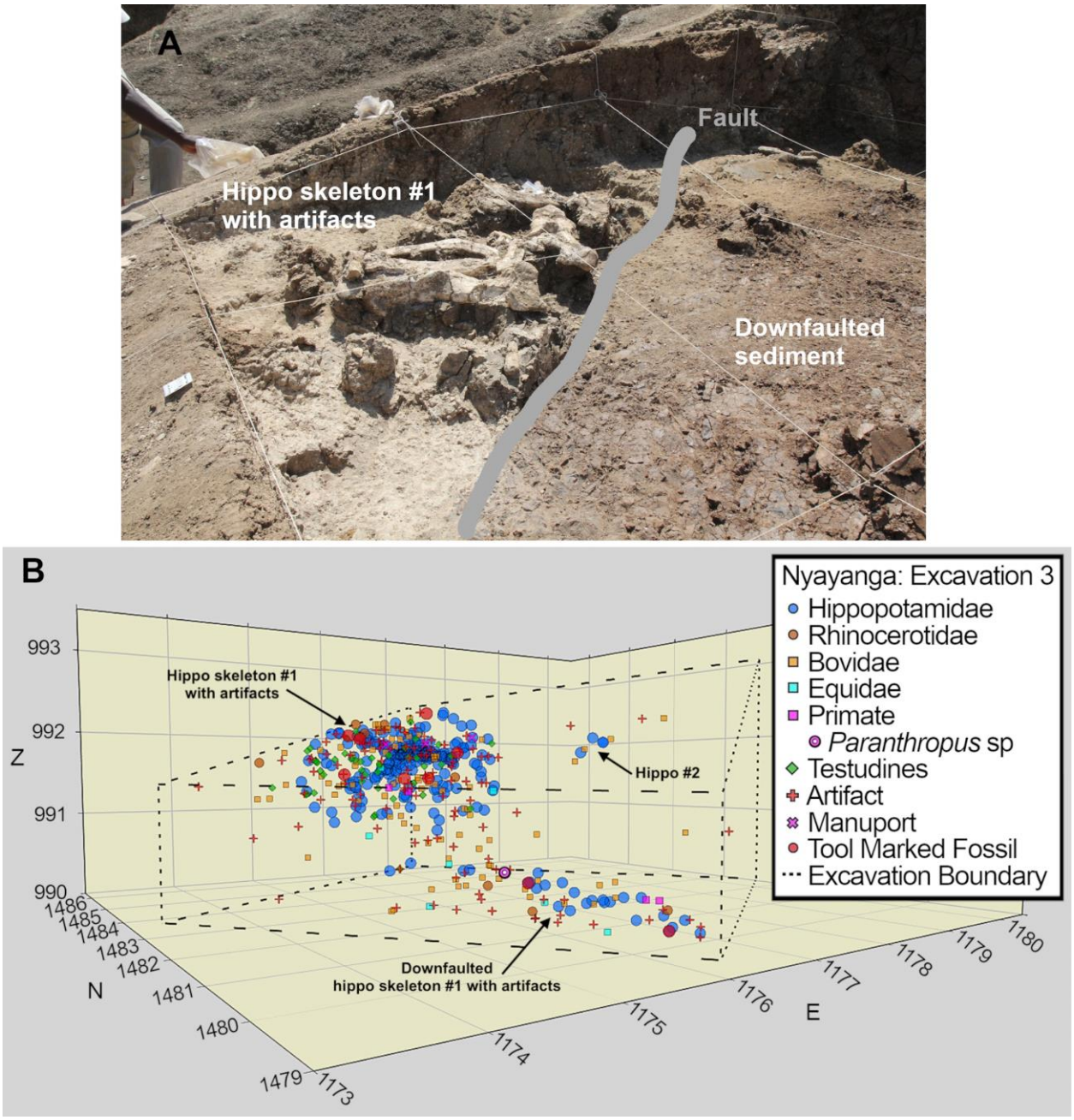

Fig. S5.

Excavation 3 showing hippopotamid skeleton and associated artifacts in NY-1. (A) The skeleton during excavation, part of which was downfaulted two meters. (B) Three-dimensional plot of select taxa and artifacts, showing the downfaulted portion of the hippopotamid was reached and the find location of *Paranthropus* KNM-NG 77316.

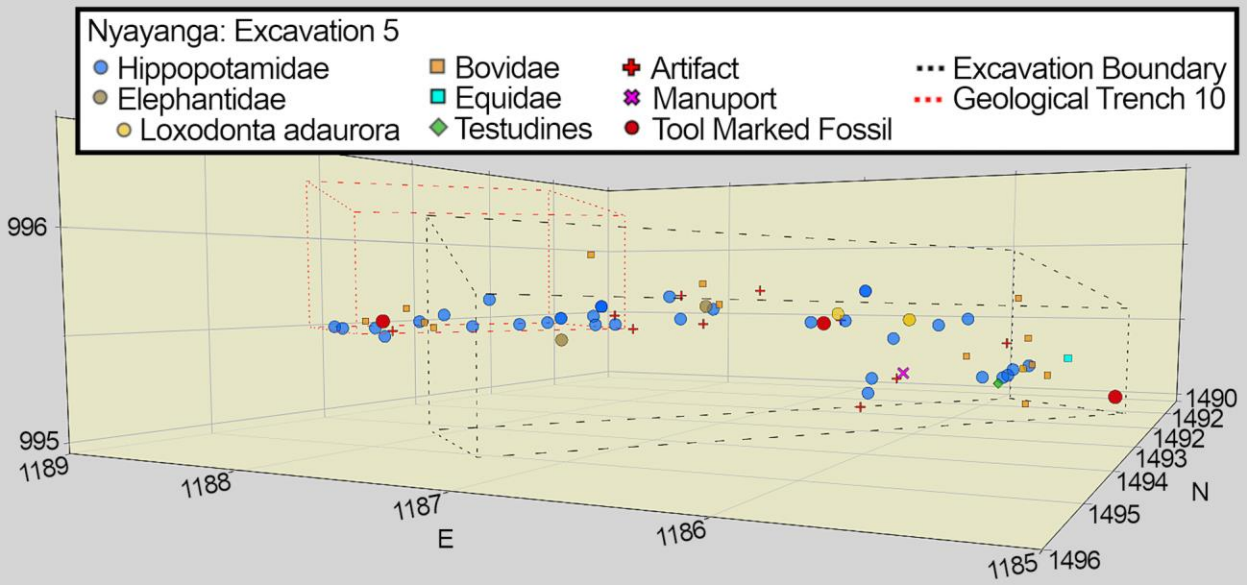

Fig. S6.

Excavation 5 showing 3-dimensional distribution of select taxa and artifacts from NY-1.

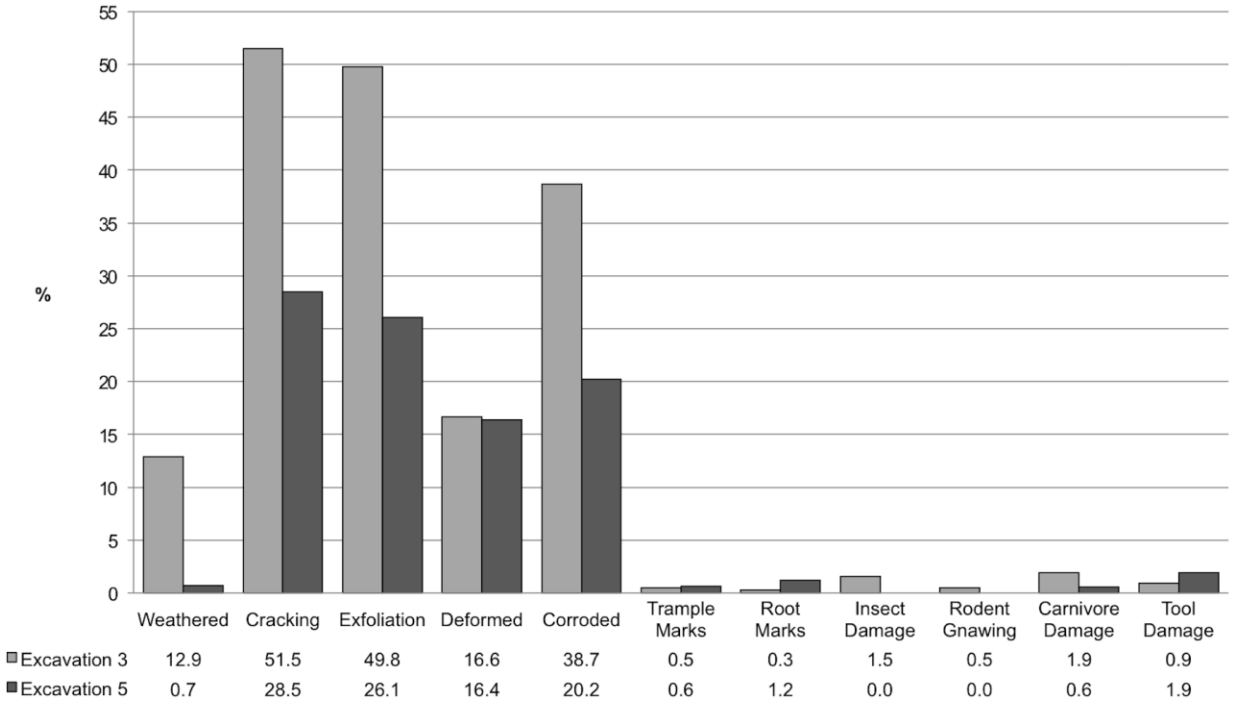

Fig. S7.

Relative frequencies of surface damages observed on Excavation 3 and Excavation 5 fossils. Weathered bones exhibit alterations consistent with weathering greater than stage 1. Cracking refers to post-depositional fissures within the specimen. Exfoliation refers to fossils in which some portion of surficial bone layer(s) have flaked off. Fossils geometrically altered from their natural appearance are deformed. Corroded fossils exhibit a partial or complete loss of surficial bone leaving a granular to slightly rounded appearance. The overall lack of rounding of edges indicates that observed corrosion is related to biogenic and chemical processes, not mechanical processes. Exfoliation, cracking, deformation, and corrosion are all post-depositional and likely related to alternating periods of wet and drying sediment. Trample marks typically have a curvilinear appearance indicating different trajectories, mark entrance and exit may display shallow striae, auxiliary striae outside of the main groove, and a flat to rounded base. Carnivore damage includes tooth pits, scores, and punctures. Tool marks include cut marks, percussion marks, and various percussion fracture features including large, oblong impact notches, incipient flakes, flake scars, and cones. Cut marks are v-shaped grooves that exhibit a consistent trajectory, display striae, and are found parallel to or perpendicular to the long axis of a diaphysis. All but the tool damage percentages are calculated using the total NISP for each excavation (Excavation 3 NISP = 1368: very large = 336, large = 77, medium = 48, small = 96, very small = 40, and indeterminate animal size = 872; Excavation 5 NISP = 172: very large = 43, large = 20, medium = 8, small = 15, very small = 6, and indeterminate animal size = 80). Percentages of bones showing tool damage are based on the number of specimens with good surface preservation (see Table S7). Table S1.

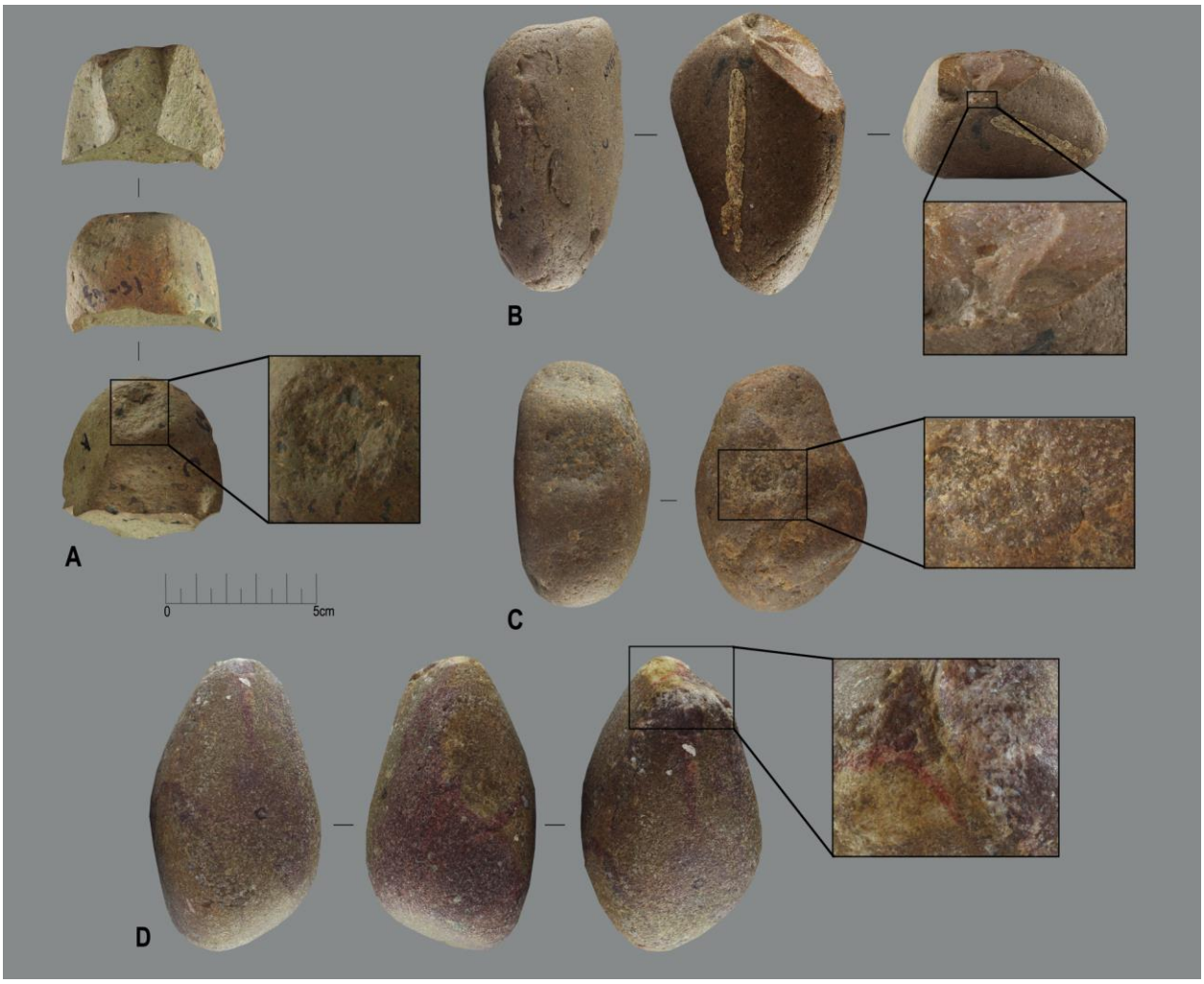

Fig. S8.

Examples of percussive stone tools from Nyayanga with the macroscopic details (in the square) of the functional areas examined. (A) Detached piece, NY15-33. (B) Pounded piece, NY15-135. (C) Pounded piece, Exc3-103. (D) Pounded piece, Exc3-485.

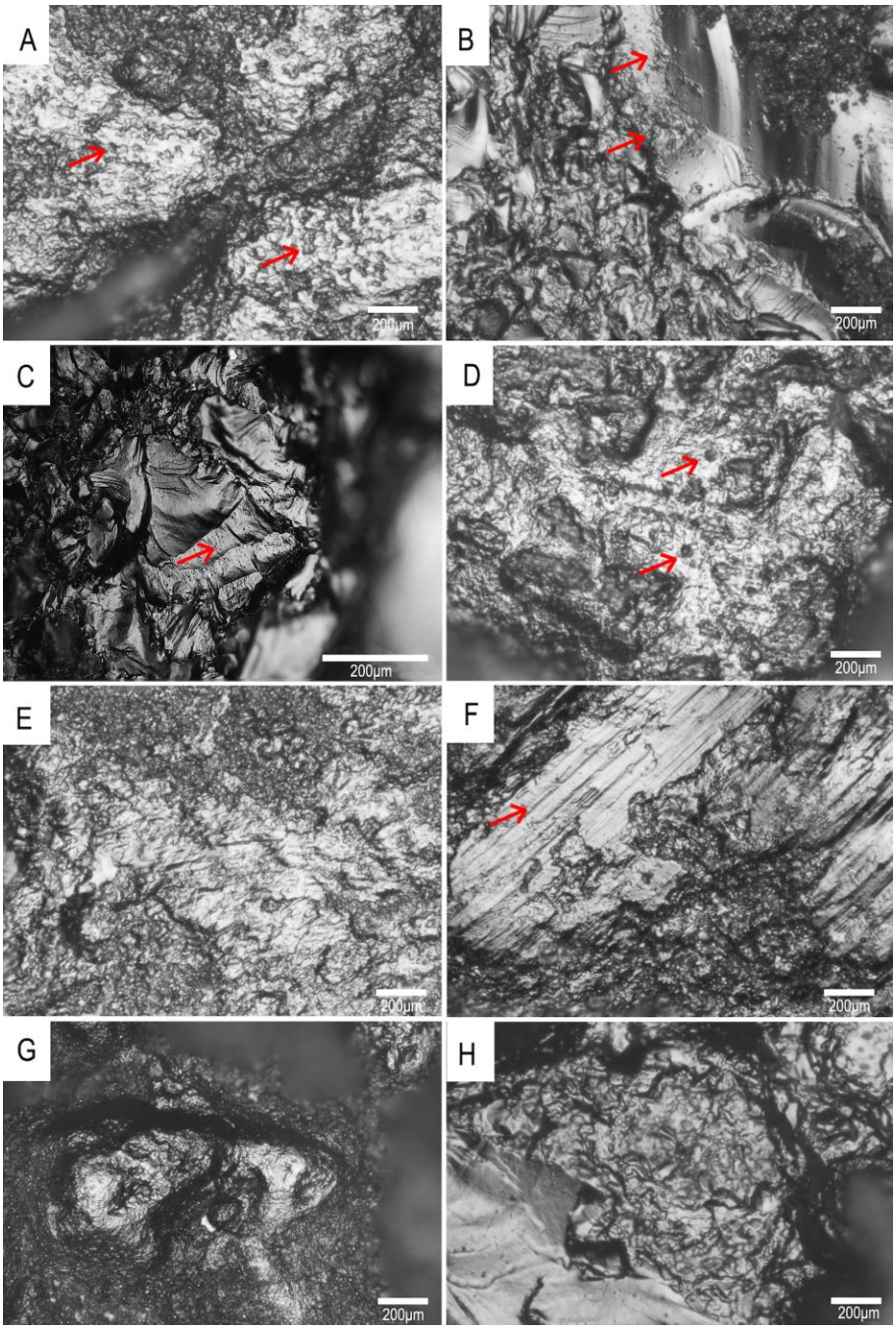

Fig. S9.

Micro-traces observed on experimental replicas. (A) irregular pitted and cratered polishes formed by processing *Manihot esculenta* (manioc or cassava). (B) polishes, pits, and cracks on artifact grains resulting from *Dioscorea* (yam) processing. (C) dotted micro-striations and polish from processing wood. (D) polish from processing *Armoracia rusticana* (horse radish) characterized by rounded, pitted and long unpolished striae. (E-F) polish and long, deep, polished striae (F) from processing bone with detail of texture and topography (E). (G-H) polishes of *Passiflora edulis* (passion fruit) on the top and edges of the crystals.

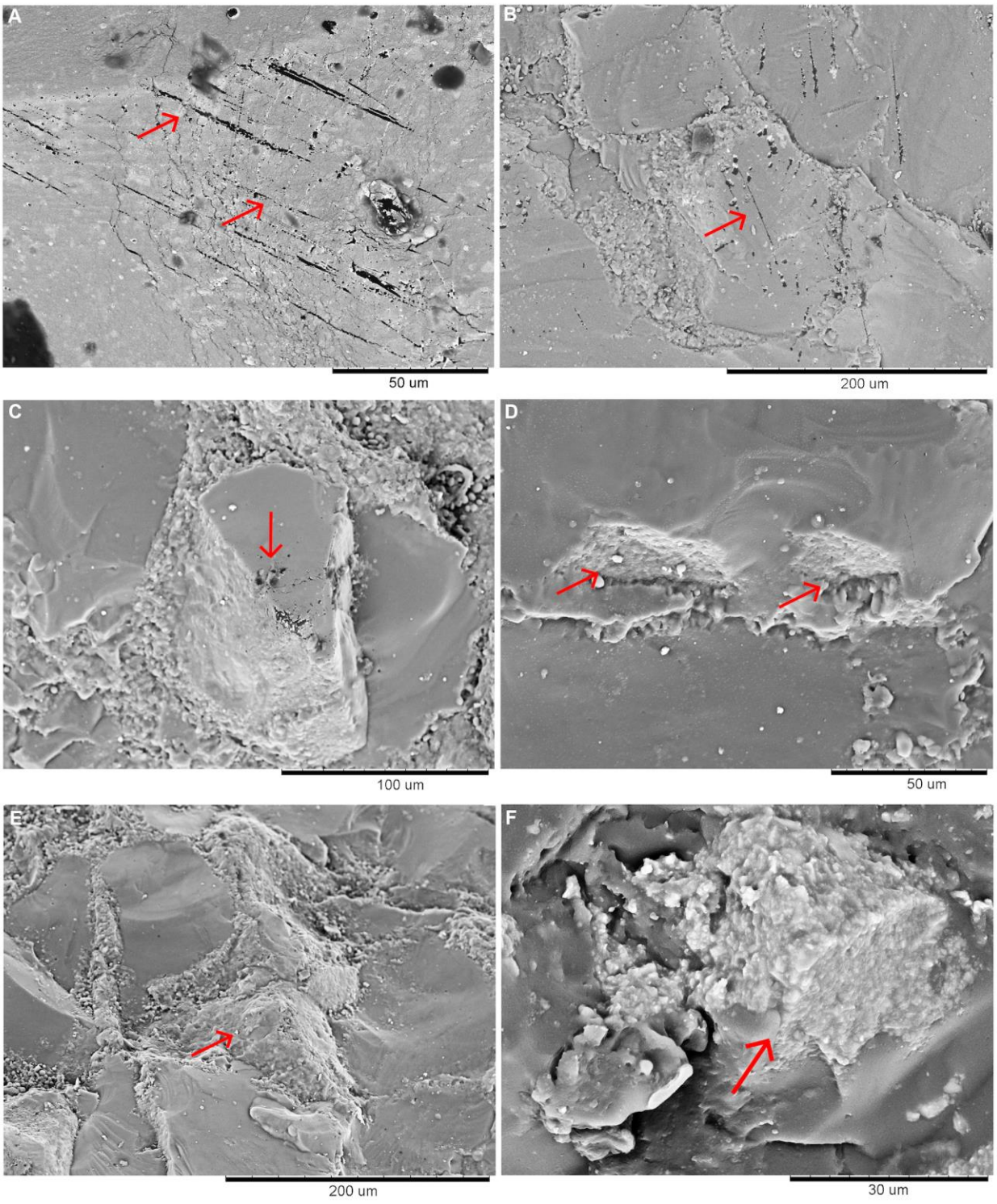

Fig. S10.

Experimental traces observed using a Scanning Electron Microscope. Striations (A) and (B) created by percussion of hazel tree; Pits and fractured grain (C) flake scars (D), and polish (E) formed by processing horseradish; Polish created in processing hazel tree bark (F).

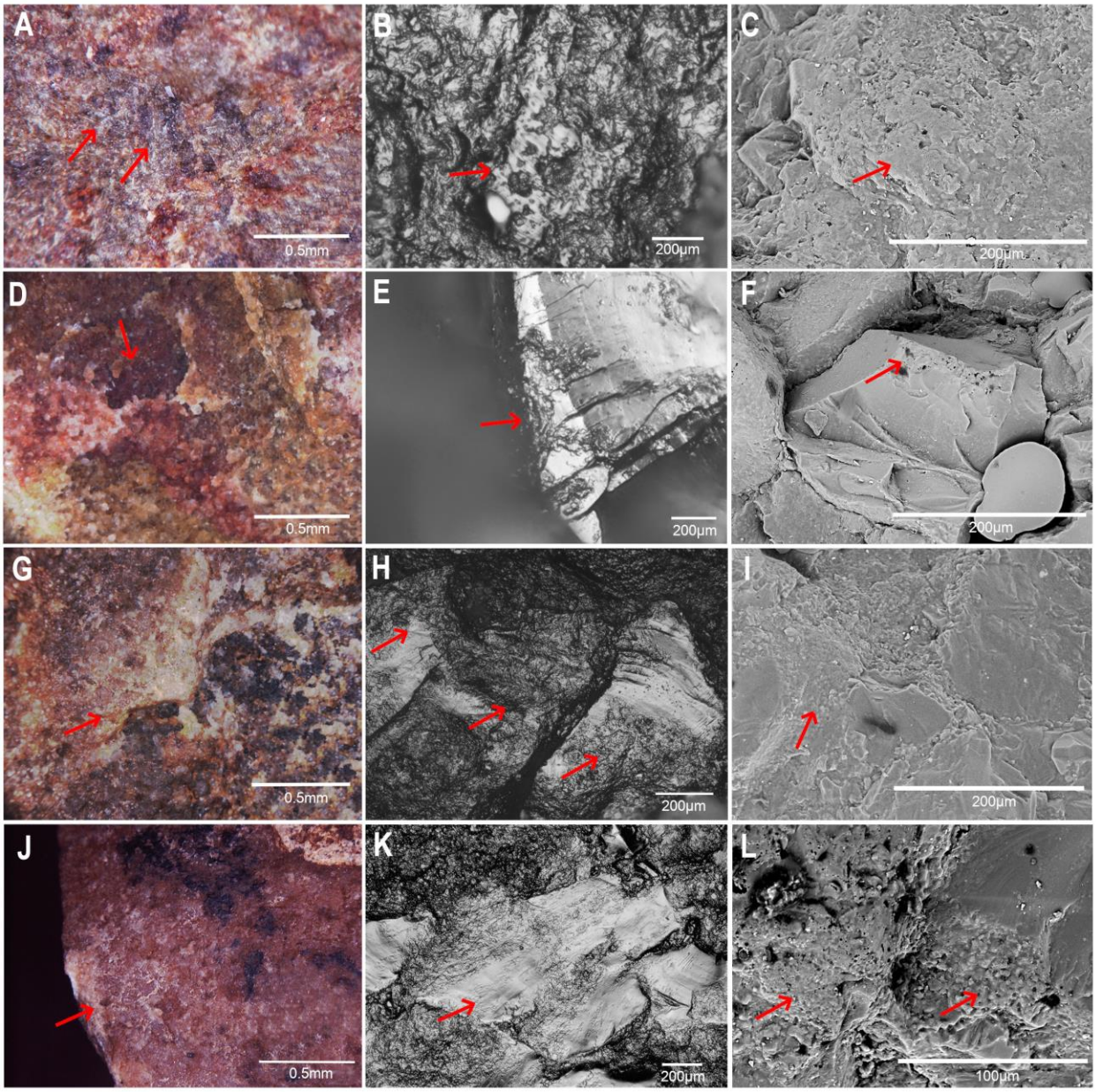

Fig. S11.

Use-wear observed on percussive tools from Nyayanga inferred to have been used to process soft, pulpy plant tissue (NY15-33; A-C), woody plant parts (Exc3-485; D-F), both plant and animal tissue (Exc3-103; G-I) and break bones (NY-135; J-L). NY15-33 exhibiting macro-pits associated with bands of macro-striations of mixed orientations (A). NY15-33, smooth-cratered polish (B). NY15-33, detail of the cratered polish (show in image B) observed at the SEM (C). Exc3-485 macro-traces, grains removal and pits (D). Exc3-485, pits on the crystal and polish (E). Exc3-485, polish localized on the top of the crystal observed at the SEM (F). Exc3-103, macro-traces, pits and grains morphology (G). Exc3-103, oriented polish (H) observed also at the SEM (I). NY15-135, negative of scar (J). NY15-135, polishes, levelling, and oriented long striations (K). NY15-135, detail of the oriented polish (K) observed at the SEM (L).

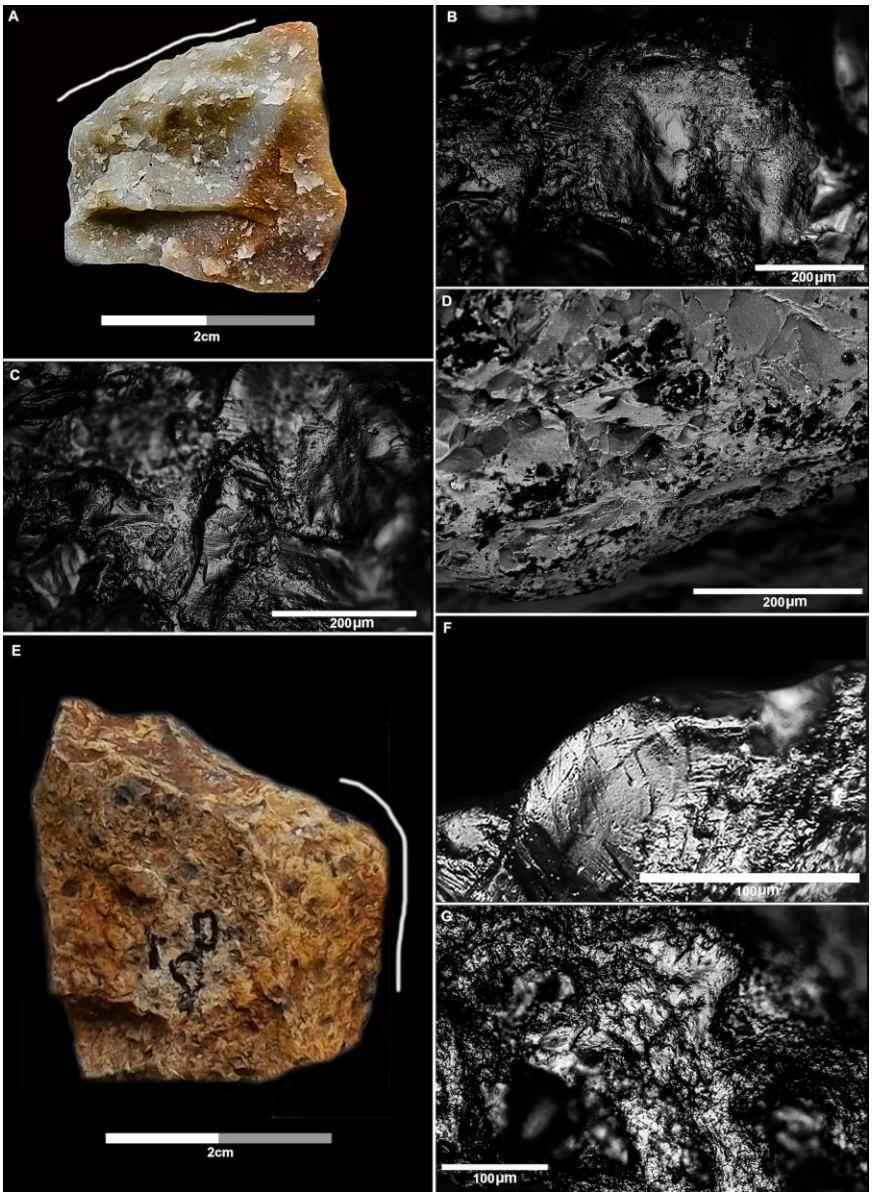

Fig. S12.

Use-wear observed on Nyayanga detached pieces; white line adjacent to working edge documented by the use-wear pictures; Exc3-104, quartz flake inferred to have been used to process USOs; DLM (A). Localized well developed abrasion and furrow striae on Exc3-104; OLM (B-C). Edge-rounding on protruding points, smooth polish with domed to flat topography SEM (D). Exc5-90, rhyolite flake inferred to have been used to process animal material; DM (E). Pitted melting polish with domed to flat topography and few sleek striae on crystal (inferred contact with bone) on Exc5-90; OLM (F). Rough polish (inferred contact with soft animal material) and smooth polish with a flat topography (bone contact) on matrix on Exc5-90 (G). Digital Microscope (DM); Optical Light Microscopes (OLM); Electron Scanning Microscope (SEM).

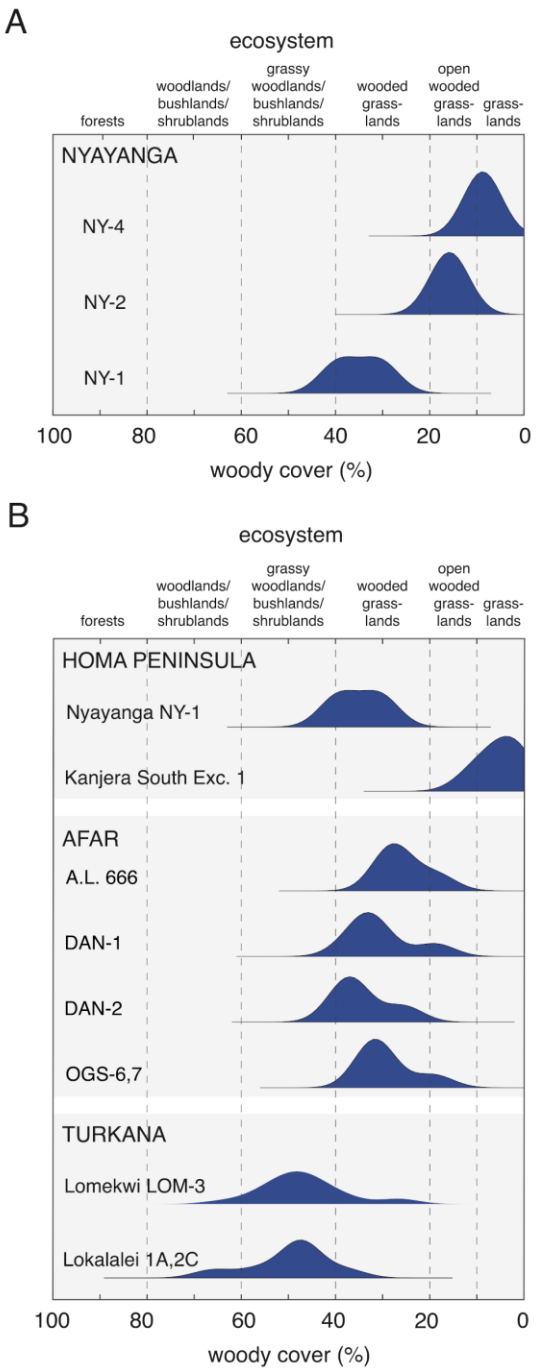

Fig. S13.

Normalised probability density functions of predicted fraction woody cover. (A) Results determined using the carbon isotopic composition of pedogenic carbonates from Nyayanga NY-1, NY-2, and NY-4 following the approach described by Cerling et al. (*96*). (B) Predicted woody cover determined for early lithic sites in eastern Africa (~3.4-2.0 Ma) using previously published isotopic data from pedogenic carbonates collected within or in close proximity to archeological sites (*96*, *127–130*).

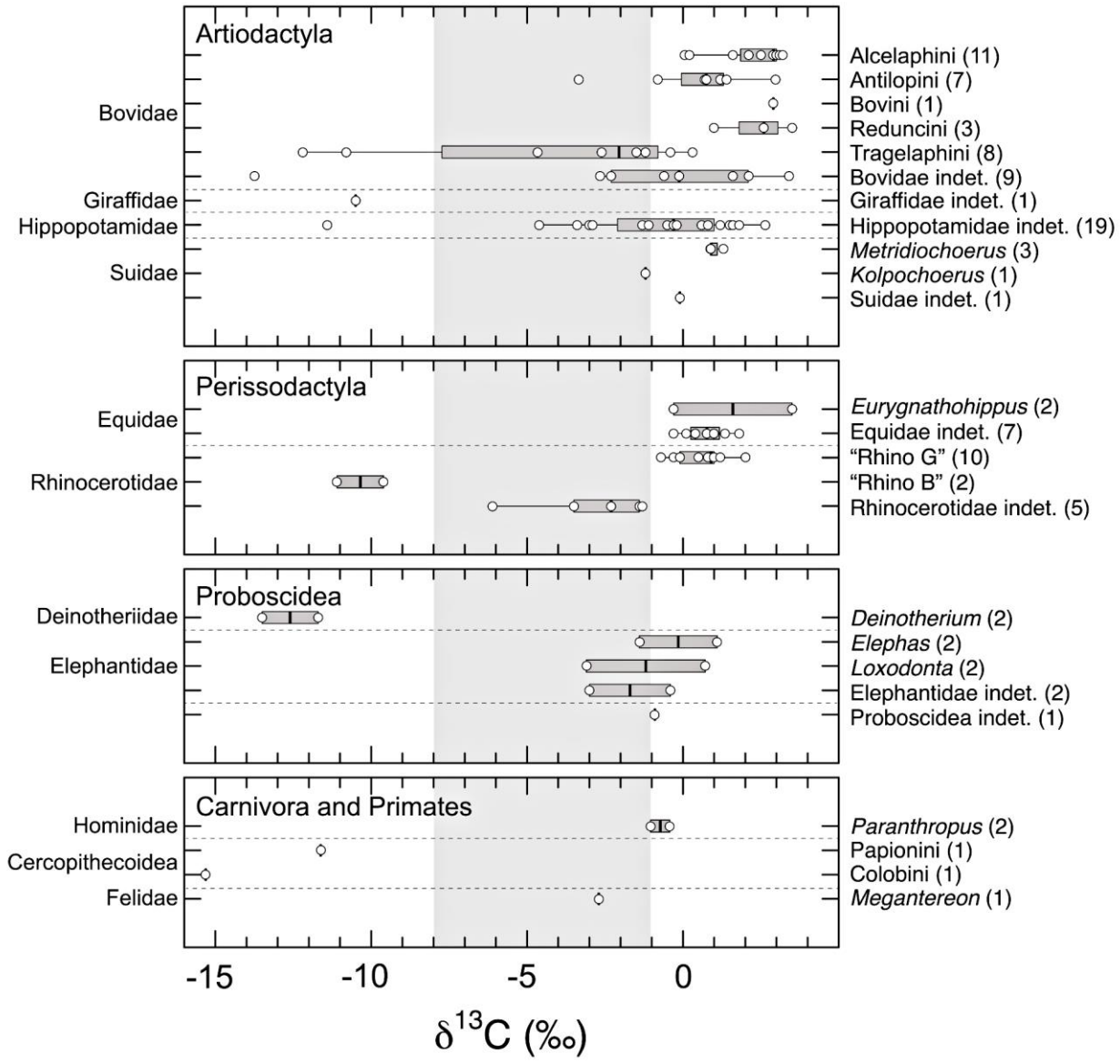

Fig. S14.

Boxplots showing $\delta^{13}C$ of tooth enamel of Artiodactyla, Perissodactyla, Proboscidea, Carnivora, and Primates from NY-1 (Table S14). One felid tooth from NY-2 is included for comparison. Within each box, the vertical black line represents the median, the boxes indicate the 1st and 3rd quartiles, and the lines indicate the range, except for outliers. All $\delta^{13}C$ are plotted as white circles. Order and Family are noted on the left side of the plot and individual taxonomic groups (family, tribe, or genus) are noted on the right side of the plot with sample size noted in parenthesis. The gray shaded region in the middle of the plot represents the isotopic range corresponding to mixed C_3-C_4 diet.

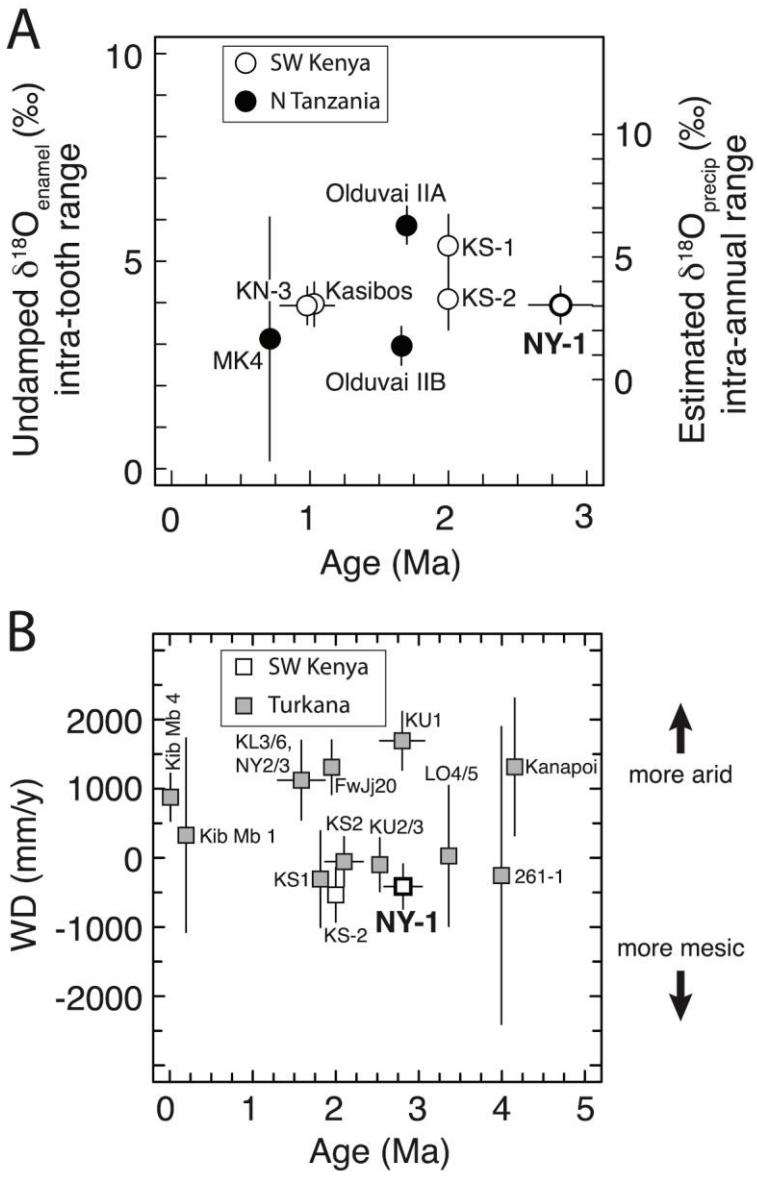

Fig. S15.

Stable isotopic analysis of fossil mammalian tooth enamel. (A) Intra-tooth range in $\delta^{18}O$ of fossil equid cheek teeth and estimated $\delta^{18}O_{precip}$ intra-annual range for Nyayanga equids and previously published $\delta^{18}O$ data from fossil equid teeth collected from Kanjera North (KN-3), Kanjera South (KS-1 and KS-2), Kanam East (Kasibos Fm), Olduvai Gorge Bed IIA (between Tuff IIA and Tuff IIB) and IIB (between Tuff IIB and Tuff IIC), and the Manyara Beds (MK4) in the Makuyuni area in northern Tanzania. Uncertainty represents the propagated error of estimated $\delta^{18}O_{precip}$ intra-annual range. (B) Paleoaridity (WD) estimates for Nyayanga and previously published eastern African fossil collections (*105*), with error bars indicating age uncertainty and propagated SE of mean WD estimates using all available combinations of evaporation sensitive (ES) and evaporation insensitive (EI) taxa.

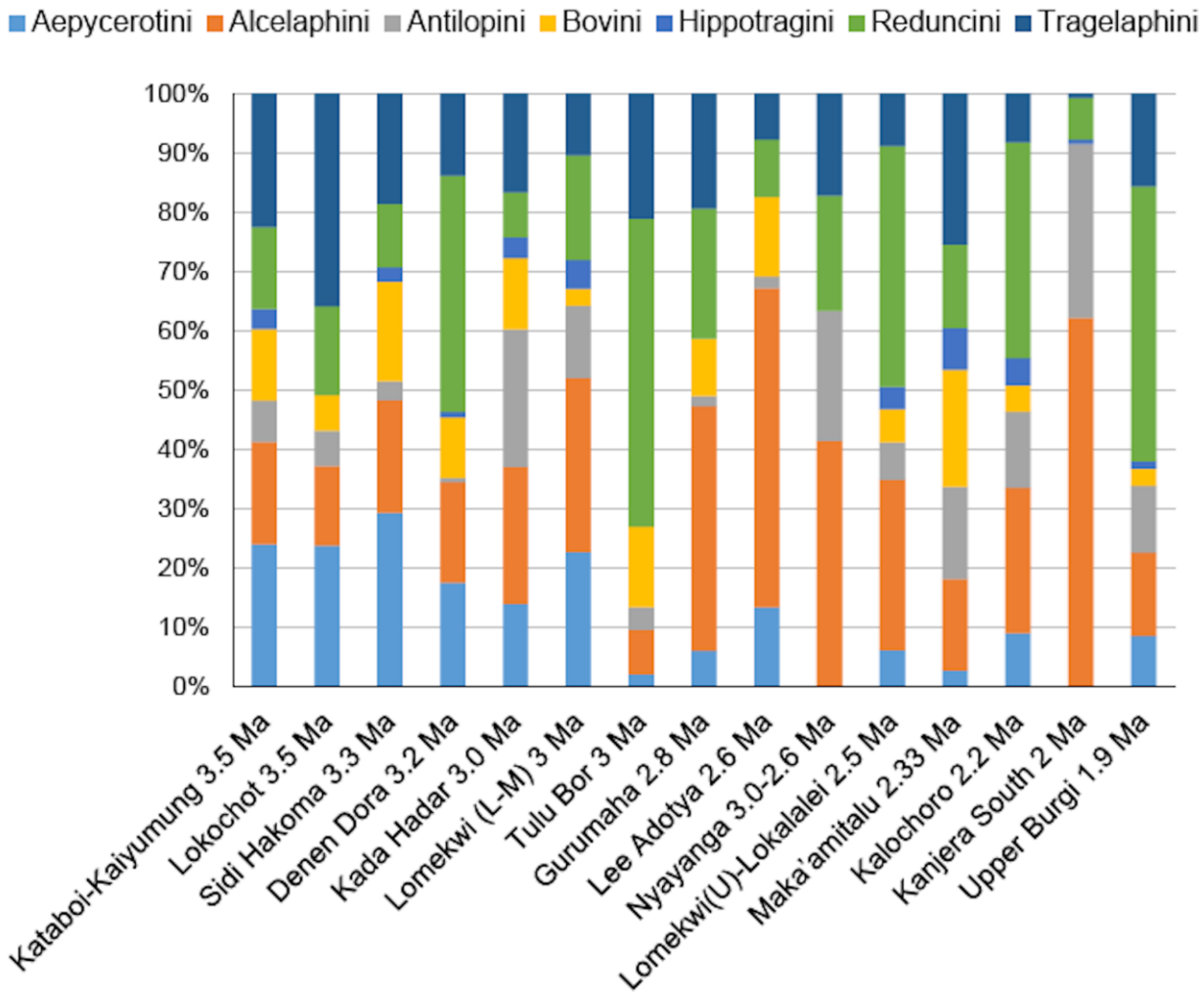

Fig. S16.
Tribal abundance at select middle Pliocene to early Pleistocene localities in East Africa.

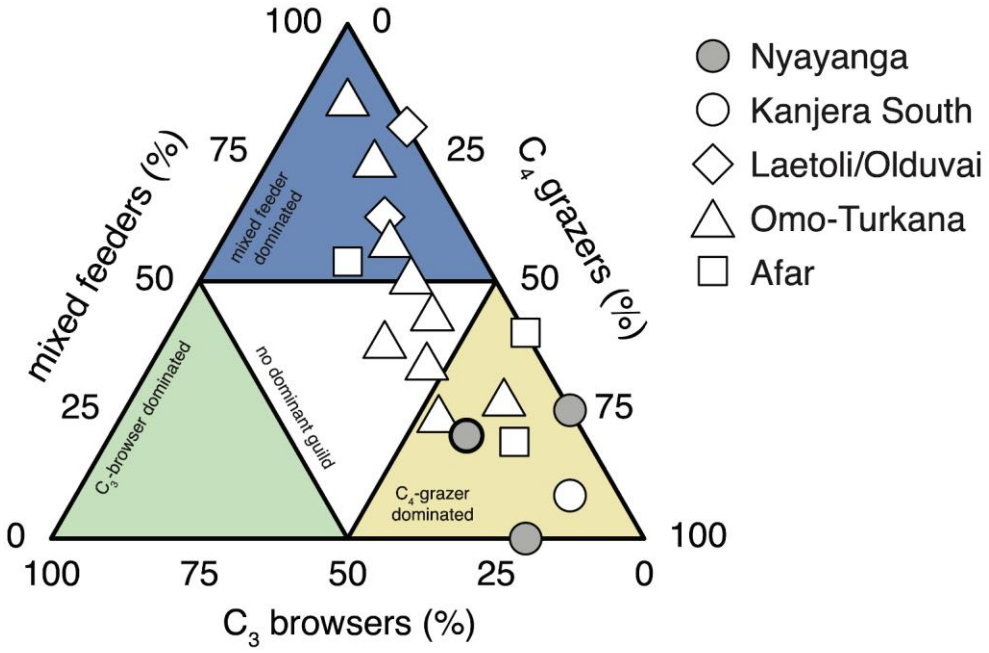

Fig. S17.

Ternary diagram showing proportions of C_4 grazers, C_3-C_4 mixed feeders, and C_3 browsers (G:M:B) among Artiodactyla-Perrissodactyla-Proboscidea (APP) taxa. Each symbol represents the G:M:B proportions from a fossil collection. Yellow, blue, and green regions represent areas where the fossil collection is dominated (>50%) by C_4 grazers, mixed feeders, and C_3 browsers, respectively. The open area in the middle represents mixed ecosystems, where no dietary guild is dominant. The grey circles represent Nyayanga fossil collections (Table S14), and the largest of these (NY-1) is highlighted. The Nyayanga fossil assemblages all fall within the area dominated by grazing species. We also present G:M:B calculated using previously published fossil tooth enamel $\delta^{13}C$ data from the Homa Peninsula, Laetoli/Olduvai, Omo-Turkana, and Afar (*31*, *67*, *99*, *127*, *131–134*).

Sample No.	238U (ppm)	±1sd (ppm)	232Th (ppm)	±1sd (ppm)	He (ppm)	±1sd (ppm)	Th/U	Raw age (Ma)	±1sd (Ma)	FT	Corrected Age (Ma)	±1sd (Ma)
WL-9												
WL-9-1	0.57	0.038	15.21	0.302	3.52E-04	4.76E-06	26.83	3.90	0.09	0.8064	4.84	0.11
WL-9-2	2.03	0.105	32.97	0.612	7.90E-04	8.95E-06	16.21	3.71	0.08	0.8023	4.62	0.10
WL-9-3	2.16	0.110	65.86	1.193	8.35E-04	1.07E-05	30.55	2.18	0.05	0.7761	2.80	0.06
WL-9-4	5.42	0.164	57.92	0.938	1.16E-03	1.23E-05	10.69	2.80	0.05	0.8166	3.43	0.06
WL-9-5	3.76	0.206	59.14	1.860	1.02E-03	1.49E-05	15.72	2.66	0.08	0.7510	3.54	0.11
WL-9-6	2.94	0.171	74.42	2.386	8.74E-04	1.28E-05	25.27	1.96	0.06	0.7410	2.65	0.09
						WL-9	**Age**	**2.87**	**0.79**		3.65	0.91
WL-10												
WL-10-1	2.17	0.086	31.88	0.978	5.53E-04	6.34E-06	14.68	2.63	0.07	0.8569	3.07	0.09
WL-10-2	2.71	0.094	26.03	0.787	6.41E-04	7.26E-06	9.62	3.34	0.09	0.8530	3.91	0.10
						WL-10	**Age**	**2.98**	**0.50**		3.49	0.60
			Combined WL-9 and WL-10 samples				**Age**	**2.90**	**0.70**		3.61	0.80

Table S1.

Results of apatite (U-Th)/He dating for NY-1 tuffaceous silt samples WL-9 and WL-10, and for their combined samples. Uncorrected age averages in bold.

Specimen	Bed	Declination	Inclination	Paleolatitude	K	Polarity
Pmag I	NY-3	187.9	-12.5	-79.6	8.3	R
Pmag H	NY-3	x	x	x	x	x
Pmag F	NY-3	29.5	-21.1	58.9	60.5	IN
NY10	NY-2	x	x	x	x	x
Pmag G	NY-2	12.5	14.2	75.4	22.2	N
Pmag E	NY-2	14.9	31.8	67	12.8	N
NY09	NY-2	2.4	-9.5	85	760	N
NY08	NY-2	1.1	1.8	76.5	540	N
Pmag A	NY-2	357.6	3	86.9	637.4	N
NY07	NY-1	233.5	-35.8	-33.9	25.8	I
Pmag B	NY-1	x	x	x	x	x
NY06	NY-1	x	x	x	x	x
NY05	NY-1	335.9	-11.1	65.4	173.4	N
Pmag C	NY-1	356.2	1.7	86	417.9	N
NY04	NY-1	64.6	-14.2	25.2	197.8	I
NY03	NY-1	38.3	-23.7	50.2	48.1	IN
Pmag D	NY-1	x	x	x	x	x
NY02	NY-1	36.3	-10.6	53.4	410.7	IN
NY01	NY-1	87.8	-11.8	19	2.2	I
Pmag J	Unit A	190.6	3.8	-79.3	17.8	R

Table S2.

Paleomagnetic data for Nyayanga, in stratigraphic order from highest to lowest. See also sample positions in Fig. 1b and Fig. S2.

		NY-1	NY-1/2	NY-2	NY-2/3	NY-3	NY-3/4	NY-4
Primate indet.		X						
Galagidae	*Galago* cf. *crassicaudatus*		X					
Cercopithecidae	Cercopithecidae indet	X		X				
	Papionini gen. et sp. indet.	X						
	Paracolobus cf. *mutiwa*	X						
Hominidae	*Paranthropus* sp.	X						
Carnivora	Carnivora indet.			X				
	Megantereon sp.			X				
	Felidae, size 3	X				X		
	Hyaenidae						X	
Suidae	*Metridiochoerus* sp.	X				X		
	Metridiochoerus andrewsi	X						
	Metridiochoerus modestus							X
	Kolpochoerus sp.	X						X
	Kolpochoerus cf. *heseloni*	X				X		
	Notochoerus sp.	X						
	Notochoerus cf. *scotti*	X						
Hippopotamidae	Hippopotamidae	X		X	X	X		X
Giraffidae	Giraffidae indet.	X		X				
Bovidae	Bovidae size 1, 2, 3. 4/5	X		X		X		X
	Tragelaphini size 1, 2, 3	X						
	Alcelaphini, size 3	X		X				
	Reduncini, size 2, 3	X						
	Bovini cf. *Pelorovis/Syncerus*							X
	Pelorovis sp.						X	
	Antilopini, size 1, 2, indet.	X	X			X		
Equidae	Equidae indet.	X		X		X		X
Hipparionini	*Eurygnathohippus* sp.	X		X				
Equini	*Equus* sp.							X
Rhinocerotidae	Rhinocerotidae indet.	X			X	X		
	Diceros sp.	X						
Proboscoidea	Proboscidea indet.	X				X		
	Deinotherium sp.	X		X		X		
	Paleoloxodon recki	X						X
	Loxodonta sp.	X						
	Loxodonta adaurora	X						
Rodentia	Rodentia indet	X				X		X
	Hystricidae	X				X		
	Thryonomys sp.	X						
Leporidae	Leporidae indet.	X						
Aves	Aves indet.	X						
Reptilia	Testudines	X				X		
	Crocodylia	X		X		X		
Gastropoda	*Limocolaria* sp.					X		
Osteichthyes		X						

Table S3.

Nyayanga in situ and surface collected fauna attributable to bed.

Locality	Age	Industry	% Unifacial cores	% Bipolar	% Cores	% Angular fragments	Average core size (mm)	Ratio of mean flake size to mean core size ratio	Average flake scar count	Ratio of flake scar count to Log (mean core size)	Average flake maximum dimension (mm)	Average flake thickness (mm)	% Assemblage associated with percussive activities
EFHR	1.4	Acheulean	12.5	0	22.6	39.5	94.9	0.61	10.2	5.16	58		0.9
FxJj63	1.5	Acheulean	6.94	0	6.65	37.92	108.88	0.55	7.02	3.44	60.01	10.18	0.28
FxJj37	1.5	Acheulean	26.79	0	8.86	26.66	84.56	0.78	7.13	3.7	66.01	15.21	4.37
FxJj20Main	1.5	Oldowan	31.4	0	1.96	63.71	50.5	0.52	7.14	4.19	26.01	6.46	0.14
FxJj18IHS	1.6	Oldowan	37.72	0	3.49	55.13	52.88	0.7	9.14	5.3	37.01	8.31	0.18
GarbalV	1.7	Oldowan	23.53	0	15.32	38.38	61.97	0.71			44.13	19.02	0
DK	1.8	Oldowan	37.5	0	16.1	40.1	67.93	0.59	7.2	3.93	40.18	11.89	3
FLKZinj	1.8	Oldowan	50.9	1.1	3.4	56.5	76.35	0.48	5.8	3.08	36.78	11.51	1.2
FxJj1	1.8	Oldowan	20	0	13.83	46.7	54.41	0.72	5.4	3.11	38.98	11.3	0.63
FxJj10	1.8	Oldowan	8	0	6.29	48.43	58.55	0.69	5.32	3.01	40.38	11.93	0.19
Omo57	2.3	Oldowan		0	1.4	35.9	37.4	0.66	3.2	2.03	24.7	7.7	0.6
Omo123	2.3	Oldowan		15.38	1.2	41.36	30.5	0.58	3.2	2.16	17.7	6.4	0.2
KJS	2	Oldowan	10.1	0	11.21	50.4	56.28	0.58	5.4	3.09	32.6	9.9	0.07
Fejej	1.9	Oldowan	59.8	0	3.52	35.95	58.3	0.63	5.1	2.89	36.9	10.7	7.01
EO	2	Oldowan	34.48	5.17	10.3	18.76	70.9	0.43	6.3	3.4	30.37	12.47	2.83
LA2C	2.3	Oldowan	82	0	2.4	23.18	66	0.58			38	11	0.7
Al894	2.3	Oldowan			0.79	16.9	75.01	0.48	6.88	3.67	35.9	10.46	0
OGS7	2.6	Oldowan	14	0	3.78	44.94	44.14	0.89	5.43	3.3	39.1	11.8	1.08
EG10	2.6	Oldowan	75	0	5.61	57.25	83.33	0.43	7.25	3.77	36.1	13.6	0
EG12	2.6	Oldowan	78	0	1.5	41.32	74.45	0.46	5.38	2.87	34.6	12.8	0
BD1	2.6	Oldowan	76	0	13	23.37	58.03	0.56	2.9	1.64	32.36	9.35	1.33
NYA	2.6	Oldowan	50.79	0	20.61	39.09	72.65	0.59	5.02	2.7	43.07	13.9	6.97
LOM3	3.3	Lomekwian	100	36.14	55.7	20	147.8	0.72	4.7	2.17	120	43.9	9.4
SCNP	-	Capuchin	100	100	21	28.26	71.73	0.44	1	0.54	44.34	13.2	25.2

Table S4.

Values for technological attributes for Lomekwian, Oldowan, and Acheulean sites compiled in Braun et al. (*7*). Nyayanga (NYA) lithic characteristics from this study and Ewass Oldupa (EO) (*67*) are added. Sites with missing data were omitted from the principal components analysis in Figure 2A. All Oldowan assemblages were included in Figure 2B and 2C and all other industries were omitted.

Element	Carnivora	Rodentia	Primate	Suidae	Equidae	Bovidae, very small	Bovidae, small	Bovidae, medium	Bovidae, large	Bovidae, size indeterminate	Bovidae Total	Hippopotamidae	Rhinocerotidae	Total
Crania												14		**14**
Horn Core								3		1	4			**4**
Maxilla												1		**1**
Mandible		1	1			2	1	1			4	5		**11**
Gnathic Indet.												2		**2**
Incisor	1	3	1	1	2					1	1	6		**15**
Canine				1								9		**10**
Premolar			1			1	4	1		2	8	7		**16**
Molar		3	1	2	4		6	9		3	18	7	9	**44**
Tooth Indet.					1	1				3	4	3	1	**9**
Axis								1			1			**1**
Thoracic							1	1			2	1		**3**
Indet. Vert.		1								1	1	21		**23**
Rib									3		3	90		**93**
Innominate							4				4	6		**10**
Scapula						1	2				3	2		**5**
Humerus			1				2	2			4	4		**9**
Radius-ulna										1	1	2		**3**
Radius							2	2			4	1		**5**
Ulna								1			1			**1**
Pisiform												2		**2**
Scaphoid												2		**2**
Semi Lunate												2		**2**
Unciform												2		**2**
Metacarpal												3		**3**
Femur						1	2				3	4		**7**
Tibia		1					1				1			**2**
Fibula												1		**1**
Calcaneum				1					1		1	2		**4**
Cuboid												2		**2**
Navicular							1	1			2	1		**3**
Cuneiform												1		**1**
Metatarsal						2	1	2			5	3		**8**
Phalange		1				1		2			3	9		**13**
Metapodial												7		**7**
Sesamoid								1	1		2	3		**5**
Podial Indet.												8		**8**
LBSF						1		1			2	11		**13**
Total	**1**	**10**	**5**	**5**	**7**	**10**	**27**	**28**	**5**	**12**	**82**	**244**	**10**	**364**
Cranial	100.0	70.0	80.0	80.0	100.0	40.0	40.7	50.0	0.0	83.3	47.6	22.1	100.0	**34.6**
Axial	0.0	10.0	0.0	0.0	0.0	0.0	3.7	7.1	60.0	8.3	8.5	45.9	0.0	**33.0**
Girdle	0.0	0.0	0.0	0.0	0.0	10.0	22.2	0.0	0.0	0.0	8.5	3.3	0.0	**4.1**
Limb	0.0	20.0	20.0	20.0	0.0	50.0	33.3	42.9	40.0	8.3	35.4	28.7	0.0	**28.3**

Table S5.

Excavation 3 mammalian taxon element frequencies and percentage of taxon NISP by anatomical region.

Element		Rodentia	Equidae	Bovidae			Elephantidae	Hippopotamidae	Total
				small	size indeterminate	Total Bovidae			
Crania								3	**3**
Horn Core				2	1	3			**3**
Incisor		1							**1**
Canine								4	**4**
Molar		1		1	1	2	5		**8**
Tooth Indet.			1		2	2		1	**4**
Thoracic				1		1			**1**
Indet. Vert.								3	**3**
Rib					1	1		11	**12**
Innominate								2	**2**
Sacrum								1	**1**
Scapula								1	**1**
Humerus								2	**2**
Radius				1		1			**1**
Pisiform								2	**2**
Unciform								1	**1**
Magnum								1	**1**
Femur				3		3			**3**
Tibia								1	**1**
Calcaneum								2	**2**
Phalange				1		1		1	**2**
Metapodial								1	**1**
Podial Indet.								1	**1**
LBSF								1	**1**
	Total	2	**1**	**9**	**5**	**14**	**5**	**39**	**61**
	Cranial	100.0	100.0	33.3	80.0	50.0	100.0	20.5	37.7
	Axial	0.0	0.0	11.1	20.0	14.3	0.0	35.9	26.2
	Girdle	0.0	0.0	0.0	0.0	0.0	0.0	10.3	6.6
	Limb	0.0	0.0	55.6	0.0	35.7	0.0	33.3	29.5

Table S6.

Excavation 5 mammalian taxon element frequencies and percentage of taxon NISP by anatomical region.

Excavation Taxon/Size Category	NISP	Tool Mark	% NISP
Excavation 3			
Size Class 5: very large mammal			
Hippopotamidae	145	2[a]	1.4
Mammal, size class 5	48	0	0.0
Unidentifiable, size class 5	8	0	0.0
Total size class 5: very large mammal	201	2	1.0
Size Class 4 & 4-5: large mammal			
Bovidae, size class 4	2	0	0.0
Bovidae, size class 4-5	3	0	0.0
Mammal, size class 4	2	0	0.0
Mammal, size class 4/5	41	0	0.0
Total Size Class 4 & 4-5: large mammal	48	0	0.0
Size Class 3 & 3-4: medium mammal			
Suidae	1	0	0.0
Tragelaphini, size class 3	1	0	0.0
Bovidae, size class 3	14	0	0.0
Bovidae, size class 3-4	1	0	0.0
Mammal, size class 3	8	0	0.0
Mammal, size class 3-4	15	0	0.0
Total Size Class 3 & 3-4: medium mammal	40	0	0.0
Size Class 2 & 2-3: small mammal			
Bovidae, size class 2	8	0	0.0
Bovidae, size class 2-3	5	0	0.0
Mammal, size class 2	25	1[b]	4.0
Mammal, size class 2-3	32	3[c]	9.4
Total Size Class 2 & 2-3: small mammal	70	4	5.7
Size Class 1 & 1-2: very small mammal			
Bovidae, size class 1	5	0	0.0
Bovidae, size class 1-2	3	0	0.0
Mammal, size class 1	7	0	0.0
Mammal, size class 1-2	17	1[d]	5.9
Total Size Class 1 & 1-2: very small mammal	32	1	3.1
Size Class indeterminate			
Bovidae, size class indet.	3	0	0.0
Mammal, size class indet.	212	1[e]	0.5
Non-identifiable, size class indet.	391	1[f]	0.3
Total Size Class indet.	606	2	0.3
Total Excavation 3	997	9	0.9
Excavation 5			
Size Class 5: very large mammal			
Hippopotamidae	34	1[g]	2.9

Mammal, size class 5	6	1[h]	16.7
Total size class 5: very large mammal	40	2	5.0
Size Class 4 & 4-5: large mammal			
Mammal, size class 4-5	19	0	0.0
Total Size Class 4 & 4-5: large mammal	19	0	0.0
Size Class 3 & 3-4: medium mammal			
Mammal, size class 3	1	0	0.0
Mammal, size class 3-4	7	1[i]	14.3
Total Size Class 3 & 3-4: medium mammal	8	1	12.5
Size Class 2 & 2-3: small mammal			
Tragelaphini, size class 2-3	1	0	0.0
Bovidae, size class 2	5	0	0.0
Mammal, size class 2	3	0	0.0
Mammal, size class 2-3	3	0	0.0
Total Size Class 2 & 2-3: small mammal	12	0	0.0
Size Class 1 & 1-2: very small mammal			
Mammal, size class 1-2	6	0	0.0
Total Size Class 1 & 1-2: very small mammal	6	0	0.0
Size Class indeterminate			
Bovidae, size class indet.	2	0	0.0
Mammal, size class indet.	51	0	0.0
Non-identifiable, size class indet.	19	0	0.0
Total Size Class indet.	72	0	0.0
Total Excavation 5	157	3	1.9
Total Excavation 3 & Excavation 5 (NY1)	1154	12	1.0

Table S7.

Frequency of Excavation 3 and Excavation 5 fossils, excluding those with poor surface preservation, that display cut marks (CM) and/or percussion damage (PD) by taxon and mammal size group. Mammal size groups are modified after Bunn (*68*, *135*): very small = <20 kg); small = 20 - 100kg; medium = 100-300 kg; large = 300 – 1000 kg; and very large = > 1000kg.

a) Exc3-1685, rib, CM; Exc3-1604, long bone shaft fragment (lbsf), PD

b) Exc3-88, lbsf, PD

c) Exc3-696, lbsf, CM; Exc3-635, femur/humerus shaft, PD; Exc3-529, femur/humerus shaft, PD

d) Exc3-615, radius shaft, PD

e) Exc3-660, lbsf, PD

f) Exc3-246, indeterminate, CM

g) Exc5-170, proximal tibia, CM

h) Exc5-87, lbsf/mandible, CM

i) Exc5-61, rib neck, CM

Experiment	Raw Material	Worked Material	Dimensions (mm)			Wt (g)
			Length	Width	Thickness	
1	Quartz	Cassava	62	55	56	500
2	Quartzite	Cassava	120	95	55	714
3	Quartz	Cassava	73	61	48	459
4	Quartzite	Horseradish	97	101	74	1028
5	Quartzite	Bone	125	80	115	1521
6	Quartz	Cassava	450	610	500	419
7	Quartz	Wood	60	45	50	440
34	Quartzite	Custard apple	58	39	54	389
35	Quartzite	Passion fruit	67	46	51	460
36	Quartzite	Yam	110	130	70	1250

Table S8.

Experiments performed using pounded piece replicas. Dimensions (length, width, thickness) and weight (Wt) of each pounded piece provided. Duration of each experiment was 90 minutes.

Specimen #	Isaac Type	Length	Width	Thickness	Wght (g)	Raw Material	Edge Preservation
Exc3-104	Detached Piece	34.4	29.0	9.4	9	Quartz	Preserved
Exc3-1188	Detached Piece	55.0	35.6	21.6	26	Quartz	Preserved
Exc3-1379	Detached Piece	28.5	19.2	12.7	7	Quartz	Preserved
NY16-147	Detached Piece	28.6	40.0	11.9	11	Quartz	Preserved
Exc3-1633	Detached Piece	14.71	18.1	6.8	4	Quartz	Preserved
Exc3-352	Detached Piece	24.9	26.6	15.3	15	Quartz	Glossy appearance (light)
Exc5-90	Flaked Piece	30.4	17.6	20.4	7	Rhyolite	Preserved
Exc3-166	Flaked Piece	95.7	88.7	74.1	750	Quartzite	Preserved
Exc5-16	Flaked Piece	111.7	96.6	71.9	933	Quartzite	Glossy appearance (light)
NY12-58	Flaked Piece	113.5	85.7	88.4	1269	Quartzite	Preserved
NY12-79	Flaked Piece	77.2	64.9	46.5	273	Quartz	Glossy appearance (light)
NY12-84	Flaked Piece	96.9	68.0	56.2	476	Quartz	Preserved
NY15-104	Flaked Piece	86.0	79.7	58.9	483	Rhyolite	Preserved
NY15-111	Flaked Piece	92.0	81.7	65.6	656	Quartzite	Preserved
NY15-134	Flaked Piece	118.6	87.8	68.1	956	Quartzite	Crystal abrasion alteration
NY15-135	Flaked Piece	126.7	87.6	60.4	877	Rhyolite	Preserved
NY15-33	Flaked Piece	61.3	49.5	40.5	177	Rhyolite	Preserved
NY15-55	Flaked Piece	82.2	49.3	48.1	327	Quartzite	Preserved
NY15-66	Flaked Piece	92.7	71.1	49.8	389	Quartzite	Preserved
NY16-52	Flaked Piece	111.6	84.1	80.7	930	Quartzite	Glossy appearance (light)
NY17-16	Flaked Piece	69.1	52.9	55.2	238	Granite	Preserved
NY17-32	Flaked Piece	98.4	83.6	59.6	561	Quartz	Crystal abrasion alteration
NY17-8	Flaked Piece	90.0	72.9	51.9	448	Quartz	Glossy appearance (light)
NY18-12	Flaked Piece	109.4	76.5	65.9	636	Granite	Glossy appearance (light)
Exc3-103	Pounded Piece	107.0	85.5	61.9	686	Quartzite	Glossy appearance (light)
Exc3-164	Pounded Piece	88.9	68.2	47.3	379	Quartzite	Preserved
Exc3-37	Pounded Piece	106.4	69.8	53.5	566	Quartzite	Glossy appearance (light)
Exc3-485	Pounded Piece	131.6	91.1	75.4	1195	Quartzite	Preserved
NY16-92	Pounded Piece	92.6	76.1	41.8	371	Quartzite	Crystal abrasion alteration
NY18-15	Pounded Piece	111.2	77.6	45.2	601	Carbonatite	Glossy appearance (light)

Table S9.

Dimensions and raw materials of the Nyayanga stone tool sample from NY-1 with use-wear discussed here. Artifacts with prefix “Exc” were recovered *in situ* from the excavations. Those with the “NY” prefix were found eroding from, or on the surface of, Bed NY-1.

Experiment	Percussive Stone Tool Raw Material	Macro Traces	Micro Traces							
			Polish							
			Texture	Topography	Extent	Levelling	Abrasion	Striations	Micro-Pits	Cracks
Manihot esculenta (cassava)	Quartzite	Detachment of micro-flakes associated with irregular pits	Smooth	Flat+Cratered and pitted	On the top and edges of the crystals	Yes	None	Long, Parallel, not-polished	Yes	On quartz grains
Corylus (hazel tree)	Quartz	Slight rounding of the grains	Rough	Domed	Along the ridges of the crystals	None	Yes	Furrow Short, Parallel	None	None
Armoracia rusticana (horseradish)	Quartzite	Overlapping, sub-circular pits	Rough to Smooth	Flat+Pitted	On the top and edges of the crystals	Yes	Yes	Parallel, Long, not-polished	None	On quartz grains; quartz removals
Dioscorea (yam)	Quartzite	Cracks on the grains and micro-flakes	Smooth	Flat	On the top and bottom of crystals	Yes	Yes	Short, Polished, +Chaotic	Sub-triangular and sub-circular pits	On quartz grains
Passiflora edulis (passion fruit)	Quartzite	Slight rounding of the grains	Rough	Domed	On the top and edges of the crystals	None	None	None	None	None
Annona cherimoya (custard apple)	Quartzite	Slight rounding of the grains	Rough	Domed	On the top and edges of the crystals	None	None	None	None	None
Ovis aries (sheep femora, ribs with attached flesh and tendons)	Quartzite	Detachment of 1 Macro-flake; cracks on the grains	Smooth	Flat	On the top of the crystals	Yes	Yes	Long, Deep, Parallel, Polished	None	On quartz grains

Table S10.

Experimental pounded pieces. Use-wear observed using low (macro-traces) and high (micro-traces) magnification.

Specimen	Raw Material	Type	Macro-Traces	Micro-Traces	Action	Interpretation of use
NY15-33	Rhyolite	FP	Overlapping pits, which create a depression on the surface of use, associated with bundles of long striations having different orientations	Smooth and flat cratered/ pitted polish; rounded grains; polish extends to the top and bottom of the crystals	Percussion and crushing	Used in the processing of vegetal organic materials with a pulpy consistency
NY15-135	Quartzite	FP	negative scar and a residual surface with pits	Smooth and flat polish; long, deep, parallel, polished striations; abrasions; levelling; cracking of the grains; micro-pits; polish extends to the top of the crystals	Percussion	Used for breaking bone
Exc3-103	Quartzite	PP	Overlapping pits with “flake” morphology	Smooth and flat, pitted, polish; abrasion on the crystals; polish extension on the top and bottom of the grains	Percussion	Processing of mixed organic materials (probably of animal and vegetable origin)
Exc3-485	Quartzite	PP	Overlapping pits with “flake” morphology	Cracking on the top of crystals; abrasions; rough and domed polish; extends along the ridges of the crystals	Percussion	Processing of woody plant parts

Table S11.

Archeological pounded pieces (PP) and flaked pieces (FP) from Nyayanga Bed NY-1 with use-wear and interpretation.

Specimen	Raw Material	Type	Macroscopic Traces (OLM)	Microscopic Traces (OLM and SEM)	Edge Angle	Action	Material Processed
Exc3-104	Quartz	DP	Light-medium edge-rounding	Localized well-dev. abrasion, furrow striae (OLM); edge-rounding on prot. points, smooth polish, domed to flat topography (SEM)	45°	Mixed	USOs
NY16-147	Quartz	DP	High edge-rounding, large scars with hinge-termination	Lightly dev. abrasion, pitted melting polish, few sleek striae on domed to flat topography (OLM); edge-rounding on prot. points, smooth polish with a flat topography and few sleeks striae (SEM)	70°	Cutting	Meat+Bone (Butchering)
Exc3-352	Quartz	DP	Medium edge-rounding	Abrasion, pitted melting polish, few sleek striae on domed to flat topography (OLM); edge-rounding on prot. points, smooth polish with a flat topography and few sleeks striae (SEM)	90°	Mixed	Meat+Bone (Butchering)
Exc3-1188	Quartz	DP	Medium edge-rounding scars with step termination	Lightly dev. abrasion, pitted smooth polish, sleek striae on domed to flat topography (OLM); edge-rounding on prot. points, smooth polish with a flat topography and few sleeks striae (SEM)	55°	Scraping	Meat+Bone (Butchering)
Exc3-1379	Quartz	DP	Localized medium edge-rounding	Localized well-dev. abrasion, furrow striae (OLM); edge-rounding, smooth polish, domed to flat topography (SEM)	56°	Scraping	USOs
Exc3-1633	Quartz	DP	Medium edge-rounding, small scars with step termination	Localized well-dev. abrasion, smooth polish with domed topography, furrow striae (OLM); edge-rounding on prot. points, smooth polish with a domed topography and sleeks striae (SEM)	70°	Scraping	Wood
Exc5-90	Rhyolite	FP	Medium edge-rounding, small scars with feather termination	Rough and smooth topography on matrix; pitted melting polish, few sleek striae on domed to flat topography (OLM)	78°	Mixed	Meat+Bone (Butchering)

Table S12.

Archeological detached pieces (DP) and flaked piece (FP) used for cutting edge activities from Nyayanga Bed NY-1 with artifact type, traces and interpretation. OLM indicates traces seen under Optical Light Microscope; SEM indicates traces seen under Scanning Electron Microscope.

Sample	Bed	$\delta^{13}C$ VPDB	$\delta^{18}O$ VPDB	Approximate % C3
PWD 070608/5	NY-4	-2.0	-2.3	30%
PWD 070608/4	NY-2 (upper)	-3.4	-3.6	40%
PWD 070608/3	NY-2 (middle)	-3.2	-2.2	40%
PWD 070608/2	NY-1 (upper)	-6.4	-3.2	60%
PWD 070608/1	NY-1 (middle)	-5.4	-2.1	50%

Table S13.

Average carbon and oxygen isotope composition of pedogenic carbonates by Nyayanga bed.

Order	Family	Tribe	Genus species	Field ID	Collection	Bed	Tooth	$\delta^{13}C$ (‰, VPDB)	$\delta^{18}O$ (‰, VPDB)
Artiodactyla	Bovidae	Alcelaphini		NYA 2017 #1274	Exc 3	NY-1	M3 frag	0.1	-1.8
Artiodactyla	Bovidae	Alcelaphini		NY15-18	surface	NY-1	M1	0.2	-1.7
Artiodactyla	Bovidae	Alcelaphini		NY15-38	surface	NY-1	M	1.6	-0.2
Artiodactyla	Bovidae	Alcelaphini		2007-9s	surface	NY-1	UM	2.1	-1.1
Artiodactyla	Bovidae	Alcelaphini		NY15-83	surface	NY-1	M	2.5	-0.7
Artiodactyla	Bovidae	Alcelaphini		NY12FOS-78	surface	NY-1	M3	2.9	-2.4
Artiodactyla	Bovidae	Alcelaphini		NYA09-2	surface	NY-1	LM3	3.0	0.1
Artiodactyla	Bovidae	Alcelaphini		NY12FOS-19	surface	NY-1	M	3.0	-0.2
Artiodactyla	Bovidae	Alcelaphini		NY12FOS-48	surface	NY-1	UM3	3.0	-1.3
Artiodactyla	Bovidae	Alcelaphini		NY12FOS-42	surface	NY-1	UM	3.1	-1.7
Artiodactyla	Bovidae	Alcelaphini			surface	NY-1	PM	3.2	0.4
Artiodactyla	Bovidae	Antilopini		NYA 2017 #1132	Exc 3	NY-1	UM	-3.3	-0.2
Artiodactyla	Bovidae	Antilopini		NY15-48	surface	NY-1	M3	-0.8	-1.9
Artiodactyla	Bovidae	Antilopini		NY15-37	surface	NY-1	M3	0.7	0.7
Artiodactyla	Bovidae	c.f. Antilopini		NY12FOS-44	surface	NY-1	M	0.8	-1.4
Artiodactyla	Bovidae	Antilopini		NY15-58	surface	NY-1	M	1.2	0.1
Artiodactyla	Bovidae	Antilopini		2007-2j	surface	NY-1	LM3	1.4	-1.6
Artiodactyla	Bovidae	Antilopini		NYA 2016 #162	Exc 5	NY-1	M	3.0	-0.2
Artiodactyla	Bovidae			NYA 2017 #518	Exc 3	NY-1	M frag	-13.7	-5.6
Artiodactyla	Bovidae			NYA 2017 #1133	Exc 3	NY-1	M	-2.6	4.0
Artiodactyla	Bovidae			2007-9	surface	NY-1	PM/M	-2.3	-2.4
Artiodactyla	Bovidae			KB 07-4d	surface	NY-1	PM/M	-0.6	1.0
Artiodactyla	Bovidae			NYA 2017 #1288	Exc 3	NY-1	M	-0.1	-1.1
Artiodactyla	Bovidae			NYA 2017 #1249	Exc 3	NY-1	M	1.6	3.2
Artiodactyla	Bovidae			2007-2g	surface	NY-1	PM/M	2.1	-1.7
Artiodactyla	Bovidae			KB 07-4b	surface	NY-1	PM/M	2.1	-0.6
Artiodactyla	Bovidae			KB 07-4e	surface	NY-1	PM/M	3.4	0.4
Artiodactyla	Bovidae	Bovini		2007-2k	surface	NY-1	UPM	2.9	-0.6
Artiodactyla	Bovidae	Reduncini		NY12FOS-14	surface	NY-1	M1/2	1.0	-0.6
Artiodactyla	Bovidae	Reduncini		2007-2A	surface	NY-1	M1/2	2.6	0.3
Artiodactyla	Bovidae	Reduncini		NY12FOS-49	surface	NY-1	UM	3.5	-0.2
Artiodactyla	Bovidae	Tragelaphini		2007-5	surface	NY-1	M	-12.2	-2.6
Artiodactyla	Bovidae	Tragelaphini		NY12FOS-77	surface	NY-1	M3	-10.8	-3.9
Artiodactyla	Bovidae	Tragelaphini		NYA 2016 #440	Exc 3	NY-1	M	-4.7	-1.6
Artiodactyla	Bovidae	Tragelaphini		2007-2m	surface	NY-1	M	-2.6	-2.8
Artiodactyla	Bovidae	Tragelaphini		NY15-96	surface	NY-1	M	-1.5	-1.0
Artiodactyla	Bovidae	Tragelaphini		2007-2k	surface	NY-1	UM	-1.2	-2.4
Artiodactyla	Bovidae	Tragelaphini		NY11FOS5c	surface	NY-1	UM	-0.4	0.5
Artiodactyla	Bovidae	Tragelaphini		NY12FOS-16	surface	NY-1	M	0.3	-1.1
Artiodactyla	Giraffidae				surface	NY-1	M	-10.5	0.5
Artiodactyla	Hippopotamidae			NY12FOS-43	surface	NY-1	TTH	-11.4	-3.4
Artiodactyla	Hippopotamidae			NYA 2017 #62	Exc 3	NY-1	M	-4.6	-3.5
Artiodactyla	Hippopotamidae				surface	NY-1	TTH	-3.4	-0.4
Artiodactyla	Hippopotamidae			NY12FOS-27	surface	NY-1	TTH	-3.0	-1.7
Artiodactyla	Hippopotamidae			NY12FOS-27	surface	NY-1	TTH	-2.9	-1.5
Artiodactyla	Hippopotamidae			NY12FOS-47	surface	NY-1	M	-1.3	-4.8
Artiodactyla	Hippopotamidae			NY15-7	surface	NY-1	TTH	-1.1	-3.6
Artiodactyla	Hippopotamidae			NY15-12	surface	NY-1	PM	-0.5	-4.1

Order	Family	Tribe	Genus species	Field ID	Collection	Bed	Tooth	$\delta^{13}C$ (‰, VPDB)	$\delta^{18}O$ (‰, VPDB)
Artiodactyla	Hippopotamidae			NY14-4	surface	NY-1	TTH	-0.3	-3.8
Artiodactyla	Hippopotamidae			NY15-53	surface	NY-1	C	-0.3	-2.7
Artiodactyla	Hippopotamidae			NY15-91	surface	NY-1	C	-0.2	-4.1
Artiodactyla	Hippopotamidae			NY12FOS-18	surface	NY-1	M	0.6	-5.5
Artiodactyla	Hippopotamidae			NY12FOS-15	surface	NY-1	C	0.6	-4.8
Artiodactyla	Hippopotamidae			NY12FOS-29	surface	NY-1	C	0.8	-3.7
Artiodactyla	Hippopotamidae			NYA 2017 #148	Exc 5	NY-1	tusk	1.2	-4.1
Artiodactyla	Hippopotamidae			NY12FOS-50	surface	NY-1	C	1.5	-4.1
Artiodactyla	Hippopotamidae			NY12FOS-43	surface	NY-1	TTH	1.6	-2.5
Artiodactyla	Hippopotamidae			NYA 2017 #106	Exc 5	NY-1	tusk	1.8	-5.7
Artiodactyla	Hippopotamidae			NYA 2017 #1555	Exc 3	NY-1	PM	2.6	-0.6
Artiodactyla	Suidae		c.f. *Metridiochoerus*	NYA 2017 #1466	Exc 3	NY-1	M	0.9	1.8
Artiodactyla	Suidae		*Metridiochoerus* sp.	NY12FOS-3	surface	NY-1	M	0.9	-2.4
Artiodactyla	Suidae		*Metridiochoerus* sp.	NY12FOS-21	surface	NY-1	TTH	1.3	-2.3
Artiodactyla	Suidae		*Kolpochoerus* sp.	NY12FOS-22	surface	NY-1	M	-1.2	-2.4
Artiodactyla	Suidae			NY14-1	surface	NY-1	M3	-0.1	-1.1
Perissodactyla	Equidae			NY15-77B	surface	NY-1	PM/M	-0.3	-2.0
Perissodactyla	Equidae			NY14-9	surface	NY-1	PM/M	0.1	0.2
Perissodactyla	Equidae			NY15-68	surface	NY-1	TTH	0.4	-2.3
Perissodactyla	Equidae			NYA 2017 #1637	Exc 3	NY-1	M	0.8	-2.4
Perissodactyla	Equidae			NY14-9	surface	NY-1	PM/M	1.0	-0.8
Perissodactyla	Equidae			NYA 2017 #1615	Exc 3	NY-1	PM/M	1.3	1.3
Perissodactyla	Equidae			NY12FOS-41	surface	NY-1	LM	1.8	-3.9
Perissodactyla	Equidae		*Eurygnathohippus*	NYA 2017 #1177	Exc 3	NY-1	M	3.5	1.9
Perissodactyla	Equidae		*Eurygnathohippus*		surface	NY-1	UM3	-0.3	-0.3
Perissodactyla	Rhinocerotidae		"Rhino G"	NY14-7	surface	NY-1	M	-0.7	-1.9
Perissodactyla	Rhinocerotidae		"Rhino G"	NYA09-1	surface	NY-1	TTH	-0.3	-2.1
Perissodactyla	Rhinocerotidae		"Rhino G"	KB07-3	surface	NY-1	TTH	-0.1	-2.9
Perissodactyla	Rhinocerotidae		"Rhino G"	NYA 2016 #474	Exc 3	NY-1	M	0.5	-0.8
Perissodactyla	Rhinocerotidae		"Rhino G"	NYA 2016 #455	Exc 3	NY-1	M	0.8	-
Perissodactyla	Rhinocerotidae		"Rhino G"	NYA 2016 #620	Exc 3	NY-1	M	1.0	-0.7
Perissodactyla	Rhinocerotidae		"Rhino G"	NY15-60	surface	NY-1	TTH	1.0	-3.0
Perissodactyla	Rhinocerotidae		"Rhino G"	NY12FOS-45	surface	NY-1	LM	1.2	-2.7
Perissodactyla	Rhinocerotidae		"Rhino G"	NYA 2017 #1540	Exc 3	NY-1	M	2.0	-0.1
Perissodactyla	Rhinocerotidae		"Rhino B"	NY15-10	surface	NY-1	TTH	-11.1	-2.0
Perissodactyla	c.f. Rhinocerotidae		"Rhino B"	NY15-26	surface	NY-1	M	-9.6	-2.7
Perissodactyla	Rhinocerotidae			NY14-5	surface	NY-1	TTH	-6.1	-2.4
Perissodactyla	Rhinocerotidae			NY15-13	surface	NY-1	M	-3.5	-2.6
Perissodactyla	Rhinocerotidae			NYA 2016 #340	Exc 3	NY-1	M	-2.3	-0.7
Perissodactyla	Rhinocerotidae			NY11FOS4	surface	NY-1	M	-1.4	-3.0
Perissodactyla	Rhinocerotidae			KB 07-4a	surface	NY-1	PM	-1.3	-2.2
Primates	Cercopithecoidea	Colobini		NYA 2016 #27	surface	NY-1	M1	-15.3	0.1
Primates	Cercopithecoidea	Papionini		NYA 2017 #815	Exc 3	NY-1	P4	-11.6	-1.1
Primates	Hominidae	Hominini	*Paranthropus* sp.	KNM-NG 77316	Exc 3	NY-1	LM1/2	-1.0	-
Primates	Hominidae	Hominini	*Paranthropus* sp.	KNM-NG 77315	surface	NY-1	UM2	-0.4	-2.7
Proboscidea	Deinotheriidae		*Deinotherium* sp.	NY12FOS-2	surface	NY-1	M1	-13.5	-3.6
Proboscidea	Deinotheriidae		*Deinotherium* sp.	NY15-159	surface	NY-1	TTH	-11.7	-3.7
Proboscidea	Elephantidae			NY14-3	surface	NY-1	TTH, decid?	-3.0	-4.2

Order	Family	Tribe	Genus species	Field ID	Collection	Bed	Tooth	$\delta^{13}C$ (‰, VPDB)	$\delta^{18}O$ (‰, VPDB)
Proboscidea	Elephantidae			NY15-89	surface	NY-1	TTH	-0.4	0.2
Proboscidea	Elephantidae		*Elephas* sp.	NY15-65	surface	NY-1	M	-1.4	-0.7
Proboscidea	Elephantidae		*Elephas recki*	NY12FOS-23	surface	NY-1	M, decid?	1.1	-3.4
Proboscidea	Elephantidae		c.f. *Loxodonta*	NY11FOS1a	surface	NY-1	M	-3.1	-3.7
Proboscidea	Elephantidae		*Loxodonta aduarora*	NYA 2017 #113	Exc 5	NY-1	M	0.7	-0.3
Proboscidea				2007-2c	surface	NY-1	TTH	-0.9	-2.5
Carnivora	Felidae		*Megantereon* sp.	KB07-6	surface	NY-2	TTH	-2.7	-3.0
Artiodactyla	Bovidae			NYA 2017 #239	Exc 6	NY-3	M	-1.0	3.5
Artiodactyla	Bovidae			NYA 2017 #185	Exc 6	NY-3	M	1.8	-1.2
Artiodactyla	Bovidae			NYA 2017 #181	Exc 6	NY-3	M3	1.9	-3.7
Artiodactyla	Bovidae	c.f. Hippotragini		NYA 2017 #240	Exc 6	NY-3	TTH	1.4	-0.4
Artiodactyla	Bovidae	c.f. Tragelaphini		NYA 2017 #173	Exc 6	NY-3	LM3	-6.7	-5.1
Artiodactyla	Suidae		*Metridiochoerus sp.*	NYA 2016 #158	surface	NY-3	M3	-0.9	0.2
Perissodactyla	Rhinocerotidae			NYA 2016 #2	Trench 13	NY-3	TTH	-0.4	-0.7
Perissodactyla	Rhinocerotidae			NYA 2016 #1	Trench 13	NY-3	TTH	2.4	-1.7
Artiodactyla	Bovidae	Alcelaphini		NYA 2016 #155	Exc 4	NY-4	M3	0.9	-0.1
Artiodactyla	Bovidae	Antilopini		NYA 2016 #135	Exc 4	NY-4	M3	2.0	1.4
Artiodactyla	Bovidae			NYA 2016 #21	Exc 4	NY-4	TTH	1.4	0.6
Artiodactyla	Hippopotamidae			NYA 2016 #92	Exc 4	NY-4	M	-8.3	-2.8
Artiodactyla	Suidae		*Metridiochoerus* sp.	NYA 2016 #167	Exc 4	NY-4	M3	1.7	-2.2
Artiodactyla	Suidae			NYA 2016 #136	Exc 4	NY-4	TTH	0.7	-
Artiodactyla	Suidae			NYA 2016 #134	Exc 4	NY-4	TTH	1.7	-1.1
Perissodactyla	Equidae			NYA 2016 #173	Exc 4	NY-4	M	1.9	1.7
Perissodactyla	Equidae		*Equus* sp.	NYA 2016 #71	Exc 4	NY-4	M	0.8	0.2
Artiodactyla	Bovidae			NY11FOS5b	surface		PM	-0.9	-0.3
Artiodactyla	Bovidae			NY11FOS5a	surface		UM	3.9	0.5
Artiodactyla	Suidae		*M. modestus*	NYA 2016 #90	surface		M3	1.2	2.2
Artiodactyla	Suidae			NY11FOS3	surface		M3	-0.2	-2.4
Perissodactyla	Equidae			NY11FOS6a	surface		CTH	1.4	-2.9
Perissodactyla	Equidae			NY11FOS2	surface		I	1.7	-1.0
Proboscidea				NY11FOS1b	surface		TTH	0.0	-4.5

Table S14.

Carbon and oxygen isotopic composition of Nyayanga mammal tooth enamel.

A. afarensis	*P. aethiopicus*	*P. boisei*
AL 486 (436?) -1 (M^2)	CH1 (M^1, M^2)	KNM-WT 17400 (M^1, M^2)
AL 200-1a (M^1,M^2)		KNM-ER 1171 (M^2)
AL 199-1 (M^2)		KNM-ER 733 (M^1)
AL 333-86 (M^1)		OH 30 (M^1)
LH 3h (M^1)		
LH 6e (M^1)		
LH 11 (M^2)		
LH 17 (M^1)		
LH 21a (M^1)		
LH 26 (M^2)		

Table S15.

Hominin M^1 and M^2 samples providing comparative measurements for this study.

A. afarensis	*P. aethiopicus*	*P. boisei*
AL 822-1 (M_1)	N/A	OH 38 (M_1)
MAK-VP-1/12 (M_1, M_2)		KNM-ER 802 (M_1, M_2)
AL 1496-1 (M_1, M_2)		KNM-ER 1171 (M_1, M_2)
AL 330-5 (M_1, M_2)		KNM-ER 3737 (M_1)
AL 443-1 (M_1)		KNM-ER 1477 (M_1)
AL 128-23 (M_1, M_2)		KNM-ER 1820 (M_1)
AL 145-35 (M_1, M_2)		KNM-ER 15930 (M_1, M_2)
AL 128-23 (M_1, M_2)		KNM-ER 25520 (M_2)
AL 145-35 (M_1, M_2)		KNM-ER 1816 (M_1, M_2)
AL 188-1 (M_2)		KNM-ER 2597 (M_2)
AL 200-1b (M_1)		KNM-ER 38359 (M_1, M_2)
AL 207-13 (M_2)		KNM-ER 3230 (M_1, M_2)
AL 241-14 (M_2)		KNM-ER 38344 (M_2)
AL 266-1 (M_1, M_2)		KNM-ER 38342 (M_1)
AL 288-1 (M_2)		KNM-ER 38349 (M_2)
AL 333-14 (M_1)		KNM-ER 8556 (M_1, M_2)
AL 333w-1 (M_1, M_2)		
AL 333w-48 (M_2)		
AL 333w-60 (M_1, M_2)		
AL 400-1 (M_2)		
AL 996-1 (M_1, M_2)		
LH 2 (M_1)		
LH 3t (M_1)		

Table S16.

Hominin M_1 and M_2 measurements used for comparison in this study.

Taxon/Specimen	N	BL	MD			
KNM-NG 77315	1	18.1	[17.1]*			
		M^1 BL	M^1 MD	N	M^2 BL	M^2 MD
A. afarensis	6	14.1 (13.1-15.4)	12.7 (11.0-13.9)	4	15.2 (15.0-15.25)	12.9 (12.7-13.3)
P. boisei	5	16.2 (15.4-17.4)	15.0 (13.8-17.4)	2	17.4 (16.3-18.4)	14.9* (14.3-15.5*)
P. aethiopicus	1	14.7	[14.4]	1	17.1	15.7
A. garhi[+]	1	16.5*	14.4*	1	17.7*	14.4*
Mille-Logya[++]		**	**	1	14.0	12.5

Table S17.

Crown metrics for M^1 and M^2 in millimeters. BL: Buccolingual, MD: Mesiodistal.
*Note: up to 0.7 mm of the mesial enamel is missing due to interproximal wear.
[+]From Asfaw et al (*119*)
[++]From Alemseged et al (*18*)

Taxon/Specimen	N	Area	Pro	Par	Met	Hyp	RPro	RPar	RMet	RHyp	Par/Met
KNM-NG 77315	1	278-282	75.7	70.05	61.93	71.8	27.4	25.2	22.2	26.0	1.13
M1											
EAFROB	5	189	54.0	41.0	46.3	42.2	30.0	21.8	24.6	23.2	.88
SAFROB	14	160	45.9	35.7	41.0	37.6	28.7	22.4	25.6	23.4	.87
A afarensis	6	137	40.2	30.6	34.8	31.3	29.5	22.2	25.5	22.9	.87
EAFHOM	8	142	39.9	31.2	36.6	34.4	28.2	22.0	25.8	24.2	.85
M2											
EAFROB	3	220	70.3	66.7	42.3	41.6	32.0	30.2	19.3	19.0	1.6
SAFROB	8	185	56.4	46.4	40.7	41.5	30.7	25.3	22.0	22.3	1.14
A afarensis	7	158	49.2	37.6	33.2	38.4	31.1	23.7	20.9	24.3	1.16
EAFHOM	4	164	55.0	44.7	33.3	31.5	33.2	26.9	20.0	19.1	1.34

Table S18.

Measured crown base areas, measured cusp areas, relative cusp areas, and relative paracone/metacone size of upper first and second molars (in mm^2). With the exception of *A. afarensis*, cusp areas are taken from Wood and Engleman (*118*). EAFROB includes *P. boisei* and *P. aethiopicus*; SAFROB includes *P. robustus*; EAFHOM includes East African *Homo* (*H. rudolfensis*, *H. habilis*, and *H. sp.*); *A.* afarensis data were collected by SEB from calibrated digital occlusal photographs. Pro: protocone area; Par: paracone area; Met: metacone area; Hyp: hypocone area; RPro: relative protocone area; RMet: relative metacone area; RHyp: relative hypocone area. Relative cusp areas are calculated by dividing measured cusp area by total crown base area. Relative paracone/metacone size has been shown to be diagnostic for hominins (*123*).

	Carabelli's feature	Cusp 5
KNM-NG 77315	Weak	absent
M^1		
EAFROB	100.0/weak (3)	100 (3)
SAFROB	71.4/weak (5)	100 (6)
SAFGRA	80.0/weak (5)	50.0 (4)
EAFHOM	20.0/weak (5)	0.0 (3)
A. afarensis	50.0/weak-moderate (6)	50.0 (6)
P. boisei	100.0/weak (2)	66.7 (3)
P. aethiopicus	100.0/weak (1)	-
M^2		
EAFROB	100.0/weak (3)	100 (3)
SAFROB	100.0/weak (3)	87.5 (7)
SAFGRA	100.0/weak (10)	66.7 (12)
EAFHOM	100.0/weak (3)	100 (3)
A. afarensis	33.3/weak (3)	75.0 (4)
P. boisei	100.0/weak (2)	50.0 (2)
P. aethiopicus	100.0/weak (1)	100.00 (1)

Table S19.

Non-metric traits observed on the M^1 and M^2. Frequency of trait expression provided. For Carabelli's feature (on mesiolingual surface) we use weak expression to correspond to grades 1-3 and moderate expression to correspond to grade 4 of the ASU Dental Anthropology System (*120*). Cusp 5 is an accessory cusp/cuspule between the hypocone and metacone. Any expression is considered presence. Numbers in parentheses indicate sample size. Pooled data for EAFROB, SAFROB, SAFGRA and EAFHOM data are from Wood and Engleman, (*118*). EAFROB includes *P. boisei* and *P. aethiopicus*; SAFROB includes *P. robustus*; SAFGRA includes *Au africanus*; EAFHOM includes East African early *Homo* (e.g., *H. rudolfensis, H. habilis* and *H. sp)*. *A. afarensis, P. boisei and P aethiopicus* data were collected by SEB. *P. boisei* and *P aethiopicus* separated here for comparative purposes.

Specimen/Taxon	N	Average Ent/Met	Average Crown Area
KNM-NG 77316	1	91.5	200-226
M_1			
P boisei	3	89.8	221
P aethiopicus	1	94.5	243
P robustus	13	85.0	259
A afarensis	9	73.2	139
Early *Homo*	6	76.8	158
M_2			
P boisei	3	91.9	266
P aethiopicus	1	94.5	--
P robustus	16	78.3	250
A afarensis	11	67.1	161
Early *Homo*	6	69.7	191
Ledi-Geraru	1	65.4	160

Table S20.

Measured crown areas and relevant cusp areas of M_1 and M_2 (mm^2).
Note: The range in crown area for Nyayanga represents the actual measured area and the estimated area, which accommodates mesial interproximal wear. With the exception of Ledi-Geraru, data were collected by SEB from calibrated digital occlusal photographs. Ledi-Geraru data are taken from Villmoare et al. (*21*).

Specimen/Taxa	Cusp 6	Cusp 7
KNM-NG 77316	Present	absent
M_1		
A afarensis		11.1 (18)
P boisei		0.0 (8)
P aethiopicus	--	--
Ledi-Geraru	?	present
EAFHOM	0.0	25.0
EAFROB	100.0	0.0
SAFROB	75.5	15.0
SAFGRA	0.0	0.0
M_2		
A afarensis	38.5 (13)	11.1 (18)
P boisei	81.8 (11)	0.0 (8)
P aethiopicus	--	--
Ledi-Geraru	?	present
EAFHOM	33.3	50.0
EAFROB	100.0	0.0
SAFROB	92.3	0.0
SAFGRA	42.9	37.5

Table S21.

Nyayanga molar non-metric traits and comparative data for lower M_1 and M_2. Any expression of Cusp 6 (accessory cusp between the hypoconulid and entoconid) is considered presence. For Cusp 7, grades 2-7 (small to large lingual accessory cusp independent of the metaconid) are considered present (*120*). Pooled data for EAFROB, SAFROB, SAFGRA and EAFHOM data are from Wood et al 1983. EAFROB includes *P. boisei* and *P. aethiopicus*; SAFROB includes *P. robustus*; SAFGRA includes *Au africanus*; EAFHOM includes East African early *Homo* (e.g., *H. rudolfensis*, *H. habilis* and *H. sp)*. *A. afarensis, P. boisei and P aethiopicus* data were collected by SEB. *P. boisei* and *P aethiopicus* separated here for comparative purposes. Ledi-Geraru data from Villmoare et al (*21*).

References and Notes

1. N. Toth, K. Schick, An overview of the cognitive implications of the Oldowan Industrial Complex. *Azania: Archaeological Research in Africa*. **53**, 3–39 (2018), DOI: https://doi.org/10.1080/0067270X.2018.1439558.

2. M. J. Rogers, S. Semaw, in *Sourcebook of Paleolithic transitions* (Springer, 2009), pp. 155–171.

3. I. Cáceres, N. Kandi, M. Sahnouni, Z. Harichane, J. van der Made, in *Proceedings of the II Meeting of African Prehistory Burgos 15–16 April, 2015*. (Consorcio CENIEH Burgos, Spain, 2017), pp. 173–196.

4. M. Domínguez-Rodrigo, B. Martinez-Navarro, Taphonomic analysis of the early Pleistocene (2.4 Ma) faunal assemblage from AL 894 (Hadar, Ethiopia). *Journal of Human Evolution*. **62**, 315–327 (2012), DOI: https://doi.org/10.1016/j.jhevol.2010.01.010.

5. E. Hovers, in *Developments in Quaternary Sciences* (Elsevier, 2012), vol. 16, pp. 51–68.

6. S. Semaw, P. Renne, J. W. Harris, C. S. Feibel, R. L. Bernor, N. Fesseha, K. Mowbray, 2.5-million-year-old stone tools from Gona, Ethiopia. *Nature*. **385**, 333–336 (1997), DOI: https://doi.org/10.1038/385333a0.

7. D. R. Braun, V. Aldeias, W. Archer, J. R. Arrowsmith, N. Baraki, C. J. Campisano, A. L. Deino, E. N. DiMaggio, G. Dupont-Nivet, B. Engda, Earliest known Oldowan artifacts at> 2.58 Ma from Ledi-Geraru, Ethiopia, highlight early technological diversity. *Proceedings of the National Academy of Sciences*. **116**, 11712–11717 (2019), DOI: https://doi.org/10.1073/pnas.1820177116.

8. Materials and methods 1 to 13 are provided as supplementary materials.

9. M. J. Le Bas, *Carbonatite-nephelinite volcanism: an African case history* (Wiley London, 1977).

10. A. K. Behrensmeyer, R. Potts, T. Plummer, L. Tauxe, N. Opdyke, T. Jorstad, The Pleistocene locality of Kanjera, Western Kenya: stratigraphy, chronology and paleoenvironments. *Journal of Human Evolution*. **29**, 247–274 (1995), DOI: https://doi.org/10.1006/jhev.1995.1059.

11. P. Ditchfield, J. Hicks, T. Plummer, L. C. Bishop, R. Potts, Current research on the Late Pliocene and Pleistocene deposits north of Homa Mountain, southwestern Kenya. *Journal of Human Evolution*. **36**, 123–150 (1999), DOI: https://doi.org/10.1006/jhev.1998.0255.

12. T. Plummer, L. C. Bishop, P. Ditchfield, J. Hicks, Research on Late Pliocene oldowan sites at kanjera south, Kenya. *Journal of Human Evolution*. **36**, 151–170 (1999).

13. L. C. Bishop, T. W. Plummer, D. R. Braun, P. W. Ditchfield, E. Goble Early, F. Hertel, C. Lemorini, J. S. Oliver, R. Potts, T. Vincent, E. Whitfield, R. Kinyanjui, in *African*

Palaeoecology and Human Origins, S. C. Reynolds, R. Bobe, Eds. (Cambridge University Press, Cambridge, In Press).

14. J. G. Ogg, in *Geologic Time Scale 2020* (Elsevier, 2020), pp. 159–192.

15. R. L. Bernor, M. J. Armour-Chelu, H. Gilbert, T. M. Kaiser, E. Schulz, in *Cenozoic mammals of Africa*, L. Werdelin, B. Sanders, Eds. (University of California Press, Berkeley, CA, 2010), pp. 685–722.

16. G. L. Isaac, J. W. K. Harris, E. M. Kroll, in *Koobi Fora Research Project, Volume 5: Plio-Pleistocene Archeology* (Clarendon Press, Oxford, 1997).

17. E. N. DiMaggio, C. J. Campisano, J. Rowan, G. Dupont-Nivet, A. L. Deino, F. Bibi, M. E. Lewis, A. Souron, D. Garello, L. Werdelin, Late Pliocene fossiliferous sedimentary record and the environmental context of early Homo from Afar, Ethiopia. *Science*. **347**, 1355–1359 (2015), DOI: https://doi.org/10.1126/science.aaa1415.

18. Z. Alemseged, J. G. Wynn, D. Geraads, D. Reed, W. A. Barr, R. Bobe, S. P. McPherron, A. Deino, M. Alene, M. J. Sier, Fossils from Mille-Logya, Afar, Ethiopia, elucidate the link between Pliocene environmental changes and Homo origins. *Nature Communications*. **11**, 1–12 (2020), DOI: https://doi.org/10.1038/s41467-020-16060-8.

19. J. G. Wynn, Z. Alemseged, R. Bobe, F. E. Grine, E. W. Negash, M. Sponheimer, Isotopic evidence for the timing of the dietary shift toward C4 foods in eastern African Paranthropus. *Proceedings of the National Academy of Sciences*. **117**, 21978–21984 (2020), DOI: https://doi.org/10.1073/pnas.2006221117.

20. K. D. Zink, D. E. Lieberman, Impact of meat and Lower Palaeolithic food processing techniques on chewing in humans. *Nature*. **531**, 500–503 (2016), DOI: https://doi.org/10.1038/nature16990.

21. B. Villmoare, W. H. Kimbel, C. Seyoum, C. J. Campisano, E. N. DiMaggio, J. Rowan, D. R. Braun, J. R. Arrowsmith, K. E. Reed, Early Homo at 2.8 Ma from Ledi-Geraru, Afar, Ethiopia. *Science*. **347**, 1352–1355 (2015), DOI: https://doi.org/10.1126/science.aaa1343.

22. M. Sahnouni, J. M. Parés, M. Duval, I. Cáceres, Z. Harichane, J. Van der Made, A. Pérez-González, S. Abdessadok, N. Kandi, A. Derradji, 1.9-million-and 2.4-million-year-old artifacts and stone tool–cutmarked bones from Ain Boucherit, Algeria. *Science*. **362**, 1297–1301 (2018), DOI: https://doi.org/10.1126/science.aau0008.

23. T. Plummer, Flaked stones and old bones: biological and cultural evolution at the dawn of technology. *American Journal of Physical Anthropology*. **125**, 118–164 (2004), DOI: https://doi.org/10.1002/ajpa.20157.

24. S. C. Antón, R. Potts, L. C. Aiello, Evolution of early Homo: An integrated biological perspective. *Science*. **345** (2014), doi:https://doi.org/10.1126/science.1236828, DOI: https://doi.org/10.1126/science.1236828.

25. N. J. Van der Merwe, F. T. Masao, M. K. Bamford, Isotopic evidence for contrasting diets of early hominins Homo habilis and Australopithecus boisei of Tanzania. *South African Journal of Science*. **104**, 153–155 (2008), DOI: https://hdl.handle.net/10520/EJC96776.

26. T. D. White, S. H. Ambrose, G. Suwa, D. F. Su, D. DeGusta, R. L. Bernor, J.-R. Boisserie, M. Brunet, E. Delson, S. Frost, Macrovertebrate paleontology and the Pliocene habitat of Ardipithecus ramidus. *Science*. **326**, 67–93 (2009), DOI: https://doi.org/10.1126/science.1175822.

27. T. E. Cerling, E. Mbua, F. M. Kirera, F. K. Manthi, F. E. Grine, M. G. Leakey, M. Sponheimer, K. T. Uno, Diet of Paranthropus boisei in the early Pleistocene of East Africa. *Proceedings of the National Academy of Sciences*. **108**, 9337–9341 (2011), DOI: https://doi.org/10.1073/pnas.1104627108.

28. T. E. Cerling, F. K. Manthi, E. N. Mbua, L. N. Leakey, M. G. Leakey, R. E. Leakey, F. H. Brown, F. E. Grine, J. A. Hart, P. Kaleme, Stable isotope-based diet reconstructions of Turkana Basin hominins. *Proceedings of the National Academy of Sciences*. **110**, 10501–10506 (2013), DOI: https://doi.org/10.1073/pnas.1222568110.

29. M. Sponheimer, Z. Alemseged, T. E. Cerling, F. E. Grine, W. H. Kimbel, M. G. Leakey, J. A. Lee-Thorp, F. K. Manthi, K. E. Reed, B. A. Wood, Isotopic evidence of early hominin diets. *Proceedings of the National Academy of Sciences*. **110**, 10513–10518 (2013), DOI: https://doi.org/10.1073/pnas.1222579110.

30. N. E. Levin, Y. Haile-Selassie, S. R. Frost, B. Z. Saylor, Dietary change among hominins and cercopithecids in Ethiopia during the early Pliocene. *Proceedings of the National Academy of Sciences*. **112**, 12304–12309 (2015), DOI: https://doi.org/10.1073/pnas.1424982112.

31. J. R. Robinson, J. Rowan, C. J. Campisano, J. G. Wynn, K. E. Reed, Late Pliocene environmental change during the transition from Australopithecus to Homo. *Nature Ecology & Evolution*. **1**, 1–7 (2017), DOI: https://doi.org/10.1038/s41559-017-0159.

32. T. Lüdecke, O. Kullmer, U. Wacker, O. Sandrock, J. Fiebig, F. Schrenk, A. Mulch, Dietary versatility of Early Pleistocene hominins. *Proceedings of the National Academy of Sciences*. **115**, 13330–13335 (2018), DOI: https://doi.org/10.1073/pnas.1809439115.

33. J. E. Martin, T. Tacail, J. Braga, T. E. Cerling, V. Balter, Calcium isotopic ecology of Turkana Basin hominins. *Nature Communications*. **11**, 1–7 (2020), DOI: https://doi.org/10.1038/s41467-020-17427-7.

34. S. Semaw, M. J. Rogers, S. W. Simpson, N. E. Levin, J. Quade, N. Dunbar, W. C. McIntosh, I. Cáceres, G. E. Stinchcomb, R. L. Holloway, Co-occurrence of Acheulian and Oldowan artifacts with Homo erectus cranial fossils from Gona, Afar, Ethiopia. *Science Advances*. **6**, eaaw4694 (2020), DOI: https://doi.org/10.1098/rspb.2020.2604.

35. M. M. Skinner, M. G. Leakey, L. N. Leakey, F. K. Manthi, F. Spoor, Hominin dental remains from the Pliocene localities at Lomekwi, Kenya (1982–2009). *Journal of Human Evolution*. **145**, 102820 (2020), DOI: https://doi.org/10.1016/j.jhevol.2020.102820.

36. M. Pickford, The geology and palaeontology of the Kanam erosion gullies (Kenya). *Mainzer Geowissenschaftliche Mitteilungen*. **16**, 209–226 (1987).

37. S. R. Frost, T. Plummer, L. C. Bishop, P. Ditchfield, J. Ferraro, J. Hicks, Partial cranium of Cercopithecoides kimeui Leakey, 1982 from Rawi Gully, Southwestern Kenya. *American Journal of Physical Anthropology*. **122**, 191–199 (2003), DOI: https://doi.org/10.1002/ajpa.10279.

38. Y. Li, H. He, T. W. Plummer, P. W. Ditchfield, C. Deng, Z. Guo, R. Potts, Exploration of apatite (UTh)/He geochronological analysis of volcanic units in fossil-bearing strata of the Homa Peninsula, southwestern Kenya. *Palaeogeography, Palaeoclimatology, Palaeoecology*. **579**, 110599 (2021), DOI: https://doi.org/10.1016/j.palaeo.2021.110599.

39. N. J. Evans, J. P. Byrne, J. T. Keegan, L. E. Dotter, Determination of uranium and thorium in zircon, apatite, and fluorite: Application to laser (U-Th)/He thermochronology. *Journal of Analytical Chemistry*. **60**, 1159–1165 (2005), DOI: https://doi.org/10.1007/s10809-005-0260-1.

40. A. M. Kinyua, T. Plummer, N. Shimizu, W. Melson, R. Potts, Provenance of Kanjera Fossils by X-Ray Fluorescence and Ion Microprobe Analyses. *Advances in X-ray Analysis*. **35**, 1165–1173 (1991), DOI: https://doi.org/10.1154/S0376030800013458.

41. S. Ohde, Instrumental neutron activation analysis of carbonatites from Homa Mountain, Kenya. *Journal of Radioanalytical and Nuclear Chemistry*. **260**, 213–218 (2004), DOI: https://doi.org/10.1023/B:JRNC.0000027084.87098.74.

42. D. Otwoma, J. P. Patel, S. Bartilol, A. O. Mustapha, Estimation of annual effective dose and radiation hazards due to natural radionuclides in mount Homa, southwestern Kenya. *Radiation Protection Dosimetry*. **155**, 497–504 (2013), DOI: https://doi.org/10.1093/rpd/nct031.

43. A. I. R. Herries, M. Kovacheva, M. Kostadinova, Mineral magnetism and archaeomagnetic dating of a mediaeval oven from Zlatna Livada, Bulgaria. *Physics and Chemistry of the Earth, Parts A/B/C*. **33**, 496–510 (2008), DOI: https://doi.org/10.1016/j.pce.2008.02.021.

44. M. Kostadinova, N. Jordanova, D. Jordanova, M. Kovacheva, Preliminary study on the effect of water glass impregnation on the rock-magnetic properties of baked clay. *Studia Geophysica et Geodaetica*. **48**, 637–646 (2004), DOI: https://doi.org/10.1023/B:SGEG.0000037475.67953.9b.

45. J. L. Kirschvink, The least-squares line and plane and the analysis of palaeomagnetic data. *Geophysical Journal International*. **62**, 699–718 (1980), DOI: https://doi.org/10.1111/j.1365-246X.1980.tb02601.x.

46. R. A. Fisher, Dispersion on a sphere. *Proceedings of the Royal Society of London. Series A. Mathematical and Physical Sciences*. **217**, 295–305 (1953), DOI: https://doi.org/10.1098/rspa.1953.0064.

47. Y. Yamamoto, O. Ishizuka, M. Sudo, K. 4 Uto, 40Ar/39Ar ages and palaeomagnetism of transitionally magnetized volcanic rocks in the Society Islands, French Polynesia: Raiatea excursion in the upper-Gauss Chron. *Geophysical Journal International*. **169**, 41–59 (2007), DOI: https://doi.org/10.1111/j.1365-246X.2006.03277.x.

48. T. Harrison, *Paleontology and Geology of Laetoli: Human Evolution in Context: Volume 1: Geology, Geochronology, Paleoecology and Paleoenvironment* (Springer Science & Business Media, 2011).

49. A. L. Deino, in *Paleontology and geology of Laetoli: Human evolution in context* (Springer, Dordrecht, 2011), pp. 77–97.

50. M. Frouin, S. Huot, S. Kreutzer, C. Lahaye, M. Lamothe, A. Philippe, N. Mercier, An improved radiofluorescence single-aliquot regenerative dose protocol for K-feldspars. *Quaternary Geochronology*. **38**, 13–24 (2017), DOI: 10.1016/j.quageo.2016.11.004.

51. M. K. Murari, S. Kreutzer, M. Fuchs, Further investigations on IR-RF: Dose recovery and correction. *Radiation Measurements*. **120**, 110–119 (2018), DOI: 10.1016/j.radmeas.2018.04.017.

52. S. Nomade, A. Gauthier, H. Guillou, J.-F. Pastre, 40Ar/39Ar temporal framework for the Alleret maar lacustrine sequence (French Massif-Central): volcanological and paleoclimatic implications. *Quaternary Geochronology*. **5**, 20–27 (2010), DOI: https://doi.org/10.1016/j.quageo.2009.07.001.

53. E. M. Niespolo, D. Rutte, A. L. Deino, P. R. Renne, Intercalibration and age of the Alder Creek sanidine 40Ar/39Ar standard. *Quaternary Geochronology*. **39**, 205–213 (2017), DOI: https://doi.org/10.1016/j.quageo.2016.09.004.

54. L. C. Bishop, in *Cenozoic mammals of Africa* (University of California Press, Berkeley, CA, 2010), vol. 821, pp. 821–842.

55. N. G. Jablonski, S. R. Frost, in *Cenozoic Mammals of Africa, eds Werdelin L, Sanders WJ* (Univ California Press, Berkeley, CA, 2010).

56. W. J. Sanders, E. Gheerbrant, J. M. Harris, H. Saegusa, C. Delmer, in *Cenozoic Mammals of Africa* (University of California Press, Berkeley, CA, 2010), pp. 161–251.

57. M. Dominguez-Rodrigo, T. R. Pickering, E. Baquedano, A. Mabulla, D. F. Mark, C. Musiba, H. T. Bunn, D. Uribelarrea, V. Smith, F. Diez-Martin, First partial skeleton of a 1.34-million-year-old Paranthropus boisei from Bed II, Olduvai Gorge, Tanzania. *PLoS One*. **8**, e80347 (2013), DOI: https://doi.org/10.1371/journal.pone.0080347.

58. M. G. Leakey, Extinct large colobines from the Plio-Pleistocene of Africa. *American Journal of Physical Anthropology*. **58**, 153–172 (1982), DOI: https://doi.org/10.1002/ajpa.1330580207.

59. J. M. Harris, F. H. Brown, M. G. Leakey, *Stratigraphy and paleontology of Pliocene and Pleistocene localities west of Lake Turkana, Kenya* (Natural History Museum of Los Angeles County, 1988).

60. N. P. Toth, thesis, University of California, Berkeley (1982).

61. N. Toth, Behavioral inferences from early stone artifact assemblages: an experimental model. *Journal of Human Evolution*. **16**, 763–787 (1987), DOI: https://doi.org/10.1016/0047-2484(87)90023-6.

62. D. Stout, S. Semaw, M. J. Rogers, D. Cauche, Technological variation in the earliest Oldowan from Gona, Afar, Ethiopia. *Journal of Human Evolution*. **58**, 474–491 (2010), DOI: https://doi.org/10.1016/j.jhevol.2010.02.005.

63. D. R. Braun, J. W. Harris, in *Oldowan: Rather more than smashing stones*, J. Moreno, R. Torcal, I. Saniz, Eds. (University of Barcelona Press, 2003), pp. 117–144.

64. D. R. Braun, Examining flake production strategies: examples from the Middle Paleolithic of Southwest Asia. *Lithic Technology*. **30**, 107–125 (2005), DOI: https://doi.org/10.1080/01977261.2005.11721029.

65. A. Mackay, A method for estimating edge length from flake dimensions: use and implications for technological change in the southern African MSA. *Journal of Archaeological Science*. **35**, 614–622 (2008), DOI: http://dx.doi.org/10.1016/j.jas.2007.05.013.

66. I. de la Torre, R. Mora, M. Domínguez-Rodrigo, L. de Luque, L. Alcalá, The Oldowan industry of Peninj and its bearing on the reconstruction of the technological skills of Lower Pleistocene hominids. *Journal of Human Evolution*. **44**, 203–224 (2003), DOI: https://doi.org/10.1016/S0047-2484(02)00206-3.

67. J. Mercader, P. Akuku, N. Boivin, R. Bugumba, P. Bushozi, A. Camacho, T. Carter, S. Clarke, A. Cueva-Temprana, P. Durkin, Earliest Olduvai hominins exploited unstable environments~ 2 million years ago. *Nature Communications*. **12**, 1–15 (2021), DOI: https://doi.org/10.1038/s41467-020-20176-2.

68. H. T. Bunn, thesis, University of California, Berkeley (1982).

69. H. T. Bunn, Archaeological evidence for meat-eating by Plio-Pleistocene hominids from Koobi Fora and Olduvai Gorge. *Nature*. **291**, 574–577 (1981), DOI: https://doi.org/10.1038/291574a0.

70. R. Potts, P. Shipman, Cutmarks made by stone tools on bones from Olduvai Gorge, Tanzania. *Nature*. **291**, 577–580 (1981), DOI: https://doi.org/10.1038/291577a0.

71. R. J. Blumenschine, C. W. Marean, S. D. Capaldo, Blind tests of inter-analyst correspondence and accuracy in the identification of cut marks, percussion marks, and carnivore tooth marks on bone surfaces. *Journal of Archaeological Science*. **23**, 493–507 (1996), DOI: https://doi.org/10.1006/jasc.1996.0047.

72. R. J. Blumenschine, M. M. Selvaggio, Percussion marks on bone surfaces as a new diagnostic of hominid behaviour. *Nature*. **333**, 763–765 (1988), DOI: https://doi.org/10.1038/333763a0.

73. T. R. Pickering, C. P. Egeland, Experimental patterns of hammerstone percussion damage on bones: implications for inferences of carcass processing by humans. *Journal of Archaeological Science*. **33**, 459–469 (2006), DOI: https://doi.org/10.1016/j.jas.2005.09.001.

74. J. S. Oliver, *Diagnosing bone fracture to assess early hominin behaviour, meat-eating, and socioecology at FLK-Zinjanthropus, Olduvai Gorge, Tanzania* (Liverpool John Moores University (United Kingdom), 2015).

75. Y. Fernandez-Jalvo, P. Andrews, *Atlas of taphonomic identifications: 1001+ images of fossil and recent mammal bone modification* (Springer, 2016).

76. M. Domínguez-Rodrigo, E. Baquedano, Distinguishing butchery cut marks from crocodile bite marks through machine learning methods. *Scientific Reports*. **8**, 1–8 (2018), DOI: https://doi.org/10.1038/s41598-018-24071-1.

77. L. R. Binford, *Bones: ancient men and modern myths* (Academic press, 2014).

78. M. M. Selvaggio, Carnivore tooth marks and stone tool butchery marks on scavenged bones: archaeological implications. *Journal of Human Evolution*. **27**, 215–228 (1994), DOI: https://doi.org/10.1006/jhev.1994.1043.

79. C. Delaney-Rivera, T. W. Plummer, J. A. Hodgson, F. Forrest, F. Hertel, J. S. Oliver, Pits and pitfalls: taxonomic variability and patterning in tooth mark dimensions. *Journal of Archaeological Science*. **36**, 2597–2608 (2009), DOI: https://doi.org/10.1016/j.jas.2009.08.001.

80. G. J. Linares Matás, J. Yravedra, 'We hunt to share': social dynamics and very large mammal butchery during the Oldowan–Acheulean transition. *World Archaeology*, 1–31 (2022), DOI: https://doi.org/10.1080/00438243.2022.2030793.

81. C. Lemorini, T. W. Plummer, D. R. Braun, A. N. Crittenden, P. W. Ditchfield, L. C. Bishop, F. Hertel, J. S. Oliver, F. W. Marlowe, M. J. Schoeninger, Old stones' song: use-wear experiments and analysis of the Oldowan quartz and quartzite assemblage from Kanjera South (Kenya). *Journal of Human Evolution*. **72**, 10–25 (2014), DOI: https://doi.org/10.1016/j.jhevol.2014.03.002.

82. C. Lemorini, L. C. Bishop, T. W. Plummer, D. R. Braun, P. W. Ditchfield, J. S. Oliver, Old stones' song—second verse: use-wear analysis of rhyolite and fenetized andesite

artifacts from the Oldowan lithic industry of Kanjera South, Kenya. *Archaeological and Anthropological Sciences*. **11**, 4729–4754 (2019), DOI: https://doi.org/10.1007/s12520-019-00800-z.

83. C. Hamon, *Broyage et abrasion au Néolithique ancien. Caractérisation technique et fonctionnelle des outils en grès du Bassin parisien. British Archaeological Reports* (2006), vol. 1551.

84. M. J. Jackson, M. P. Hitchiner, *High performance grinding and advanced cutting tools* (Springer Science & Business Media, 2012).

85. J. L. Adams, S. Delgado, L. Dubreuil, C. Hamon, H. Plisson, R. Risch, F. Sternke, L. J. Costa, L. Eigeland, in *Functional analysis of macro-lithic artifacts.* (Archaeopress Oxford, 2009), pp. 43–66.

86. L. Dubreuil, D. Savage, S. Delgado-Raack, H. Plisson, B. Stephenson, I. de la Torre, in *Use-wear and residue analysis in archaeology* (Springer, 2015), pp. 105–158.

87. A. Pedergnana, A. Ollé, A. A. Evans, A new combined approach using confocal and scanning electron microscopy to image surface modifications on quartzite. *Journal of Archaeological Science: Reports*. **30**, 102237 (2020), DOI: https://doi.org/10.1016/j.jasrep.2020.102237.

88. V. Rots, Hafting and raw materials from animals: Guide to the identification of hafting traces on stone tools. *Anthropozoologica*. **43**, 43–66 (2008).

89. A. van Gijn, *Flint in focus: lithic biographies in the Neolithic and Bronze Age* (Sidestone Press, Leiden, 2010).

90. D. Stapert, Some natural surface modifications on flint in the Netherlands. *Palaeohistoria*, 7–41 (1976).

91. H. Plisson, M. Mauger, Chemical and mechanical alteration of microwear polishes: an experimental approach. *Helinium*. **28**, 3–16 (1988).

92. I. Levi-Sala, *Processes of polish formation on flint tool surface. British Archaeological Reports International Series, vol. 411. Archaeopress* (Oxford, 1988).

93. J. J. Flenniken, J. C. Haggarty, Trampling as an agency in the formation of edge damage: an experiment in lithic technology. *Northwest Anthropological Research Notes*. **13**, 208–214 (1979).

94. S. McBrearty, L. Bishop, T. Plummer, R. Dewar, N. Conard, Tools underfoot: human trampling as an agent of lithic artifact edge modification. *American Antiquity*. **63**, 108–129 (1998).

95. T. E. Cerling, J. Quade, Y. Wang, J. R. Bowman, Carbon isotopes in soils and palaeosols as ecology and palaeoecology indicators. *Nature*. **341**, 138–139 (1989), DOI: https://doi.org/10.1038/341138a0.

96. T. E. Cerling, J. G. Wynn, S. A. Andanje, M. I. Bird, D. K. Korir, N. E. Levin, W. Mace, A. N. Macharia, J. Quade, C. H. Remien, Woody cover and hominin environments in the past 6 million years. *Nature*. **476**, 51–56 (2011).

97. T. E. Cerling, J. M. Harris, Carbon isotope fractionation between diet and bioapatite in ungulate mammals and implications for ecological and paleoecological studies. *Oecologia*. **120**, 347–363 (1999), DOI: https://doi.org/10.1007/s004420050868.

98. B. H. Passey, T. F. Robinson, L. K. Ayliffe, T. E. Cerling, M. Sponheimer, M. D. Dearing, B. L. Roeder, J. R. Ehleringer, Carbon isotope fractionation between diet, breath CO2, and bioapatite in different mammals. *Journal of Archaeological Science*. **32**, 1459–1470 (2005), DOI: https://doi.org/10.1016/j.jas.2005.03.015.

99. T. E. Cerling, S. A. Andanje, S. A. Blumenthal, F. H. Brown, K. L. Chritz, J. M. Harris, J. A. Hart, F. M. Kirera, P. Kaleme, L. N. Leakey, Dietary changes of large herbivores in the Turkana Basin, Kenya from 4 to 1 Ma. *Proceedings of the National Academy of Sciences*. **112**, 11467–11472 (2015), DOI: https://doi.org/10.1073/pnas.1513075112.

100. J. V. Tejada-Lara, B. J. MacFadden, L. Bermudez, G. Rojas, R. Salas-Gismondi, J. J. Flynn, Body mass predicts isotope enrichment in herbivorous mammals. *Proceedings of the Royal Society B*. **285**, 20181020 (2018), DOI: https://doi.org/10.1098/rspb.2018.1020.

101. A. Zazzo, M. Balasse, B. H. Passey, A. P. Moloney, F. J. Monahan, O. Schmidt, The isotope record of short-and long-term dietary changes in sheep tooth enamel: implications for quantitative reconstruction of paleodiets. *Geochimica et Cosmochimica Acta*. **74**, 3571–3586 (2010), DOI: https://doi.org/10.1016/j.gca.2010.03.017.

102. B. J. Tipple, S. R. Meyers, M. Pagani, Carbon isotope ratio of Cenozoic CO2: A comparative evaluation of available geochemical proxies. *Paleoceanography*. **25** (2010), doi:https://doi.org/10.1029/2009PA001851, DOI: https://doi.org/10.1029/2009PA001851.

103. M. J. Kohn, Predicting animal δ18O: accounting for diet and physiological adaptation. *Geochimica et Cosmochimica Acta*. **60**, 4811–4829 (1996), DOI: https://doi.org/10.1016/S0016-7037(96)00240-2.

104. N. E. Levin, T. E. Cerling, B. H. Passey, J. M. Harris, J. R. Ehleringer, A stable isotope aridity index for terrestrial environments. *Proceedings of the National Academy of Sciences*. **103**, 11201–11205 (2006), DOI: https://doi.org/10.1073/pnas.0604719103.

105. S. A. Blumenthal, N. E. Levin, F. H. Brown, J.-P. Brugal, K. L. Chritz, J. M. Harris, G. E. Jehle, T. E. Cerling, Aridity and hominin environments. *Proceedings of the National Academy of Sciences*. **114**, 7331–7336 (2017), DOI: https://doi.org/10.1073/pnas.1700597114.

106. M. P. Veldhuis, E. S. Kihwele, J. Cromsigt, J. O. Ogutu, J. G. C. Hopcraft, N. Owen-Smith, H. Olff, Large herbivore assemblages in a changing climate: incorporating water dependence and thermoregulation. *Ecology Letters*. **22**, 1536–1546 (2019), DOI: https://doi.org/10.1111/ele.13350.

107. E. S. Kihwele, V. Mchomvu, N. Owen-Smith, R. S. Hetem, M. C. Hutchinson, A. B. Potter, H. Olff, M. P. Veldhuis, Quantifying water requirements of African ungulates through a combination of functional traits. *Ecological Monographs*. **90**, e01404 (2020), DOI: https://doi.org/10.1002/ecm.1404.

108. S. A. Blumenthal, T. E. Cerling, T. M. Smiley, C. E. Badgley, T. W. Plummer, Isotopic records of climate seasonality in equid teeth. *Geochimica et Cosmochimica Acta*. **260**, 329–348 (2019), DOI: https://doi.org/10.1016/j.gca.2019.06.037.

109. K. T. Uno, F. Rivals, F. Bibi, M. Pante, J. Njau, I. de la Torre, Large mammal diets and paleoecology across the Oldowan–Acheulean transition at Olduvai Gorge, Tanzania from stable isotope and tooth wear analyses. *Journal of Human Evolution*. **120**, 76–91 (2018), DOI: https://doi.org/10.1016/j.jhevol.2018.01.002.

110. J. Rowan, E. M. Locke, J. R. Robinson, C. J. Campisano, J. G. Wynn, K. E. Reed, Fossil Giraffidae (Mammalia, Artiodactyla) from Lee Adoyta, Ledi-Geraru, and Late Pliocene Dietary Evolution in Giraffids from the Lower Awash Valley, Ethiopia. *Journal of Mammalian Evolution*. **24**, 359–371 (2017), DOI: https://doi.org/10.1007/s10914-016-9343-z.

111. D. Geraads, Perissodactyla (Rhinocerotidae and Equidae) from Kanapoi. *Journal of Human Evolution*. **140**, 102373 (2020), DOI: https://doi.org/10.1016/j.jhevol.2017.07.013.

112. T. W. Plummer, E. M. Finestone, in *Rethinking Human Evolution*, J. H. Schwartz, Ed. (MIT Press, Cambridge, Massachusetts, 2018), pp. 267–296.

113. E. S. Vrba, *The significance of bovid remains as indicators of environment and predation patterns. In (AK Behrensmeyer & AP Hill, Eds) Fossils in the Making* (Chicago: University of Chicago Press, 1980).

114. P. Shipman, J. Harris, in *Evolutionary History of the'Robust'Australopithecines. F. Grine, eds. New York, Aldine de Gruyter* (1988), pp. 343–383.

115. F. Bibi, J. Rowan, K. Reed, Late Pliocene Bovidae from Ledi-Geraru (Lower Awash Valley, Ethiopia) and their implications for Afar paleoecology. *Journal of Vertebrate Paleontology*. **37**, e1337639 (2017), DOI: https://doi.org/10.1080/02724634.2017.1337639.

116. B. A. Wood, S. A. Abbott, Analysis of the dental morphology of Plio-pleistocene hominids. I. Mandibular molars: crown area measurements and morphological traits. *Journal of Anatomy*. **136**, 197 (1983), DOI: PMCID: PMC1171940.

117. B. A. Wood, S. A. Abbott, S. H. Graham, Analysis of the dental morphology of Plio-Pleistocene hominids. II. Mandibular molars--study of cusp areas, fissure pattern and cross sectional shape of the crown. *Journal of Anatomy*. **137**, 287 (1983), DOI: PMCID: PMC1262088.

118. B. A. Wood, C. A. Engleman, Analysis of the dental morphology of Plio-Pleistocene hominids. V. Maxillary postcanine tooth morphology. *Journal of Anatomy*. **161**, 1 (1988), DOI: PMCID: PMC1262088.

119. B. Asfaw, T. White, O. Lovejoy, B. Latimer, S. Simpson, G. Suwa, Australopithecus garhi: a new species of early hominid from Ethiopia. *Science*. **284**, 629–635 (1999), DOI: https://doi.org/10.1126/science.284.5414.629.

120. C. G. I. Turner, C. R. Nichol, G. R. Scott, in *Advances in Dental Anthropology*, M. A. Kelley, C. S. Larsen, Eds. (Wiley-Liss, 1991), pp. 13–31.

121. S. E. Bailey, A morphometric analysis of maxillary molar crowns of Middle-Late Pleistocene hominins. *Journal of Human Evolution*. **47**, 183–198 (2004), DOI: https://doi.org/10.1016/j.jhevol.2004.07.001.

122. S. Molnar, Human tooth wear, tooth function and cultural variability. *American Journal of Physical Anthropology*. **34**, 175–189 (1971), DOI: https://doi.org/10.1002/ajpa.1330340204.

123. R. Quam, S. Bailey, B. Wood, Evolution of M1 crown size and cusp proportions in the genus Homo. *Journal of Anatomy*. **214**, 655–670 (2009), DOI: https://doi.org/10.1111/j.1469-7580.2009.01064.x.

124. A. Ortiz, M. M. Skinner, S. E. Bailey, J.-J. Hublin, Carabelli's trait revisited: An examination of mesiolingual features at the enamel–dentine junction and enamel surface of Pan and Homo sapiens upper molars. *Journal of Human Evolution*. **63**, 586–596 (2012), DOI: https://doi.org/10.1016/j.jhevol.2012.06.003.

125. A. D. Beynon, B. A. Wood, Variations in enamel thickness and structure in East African hominids. *American Journal of Physical Anthropology*. **70**, 177–193 (1986), DOI: https://doi.org/10.1002/ajpa.1330700205.

126. F. E. Grine, R. L. Jacobs, K. E. Reed, J. M. Plavcan, The enigmatic molar from Gondolin, South Africa: implications for Paranthropus paleobiology. *Journal of human evolution*. **63**, 597–609 (2012), DOI: http://dx.doi.org/10.1016/j.jhevol.2012.06.005.

127. T. W. Plummer, P. W. Ditchfield, L. C. Bishop, J. D. Kingston, J. V. Ferraro, D. R. Braun, F. Hertel, R. Potts, Oldest evidence of toolmaking hominins in a grassland-dominated ecosystem. *PLoS One*. **4**, e7199 (2009), DOI: https://doi.org/10.1371/journal.pone.0007199.

128. N. E. Levin, J. Quade, S. W. Simpson, S. Semaw, M. Rogers, Isotopic evidence for Plio–Pleistocene environmental change at Gona, Ethiopia. *Earth and Planetary Science Letters*. **219**, 93–110 (2004), DOI: https://doi.org/10.1016/S0012-821X(03)00707-6.

129. R. L. Quinn, C. J. Lepre, C. S. Feibel, J. D. Wright, R. A. Mortlock, S. Harmand, J.-P. Brugal, H. Roche, Pedogenic carbonate stable isotopic evidence for wooded habitat preference of early Pleistocene tool makers in the Turkana Basin. *Journal of Human Evolution*. **65**, 65–78 (2013), DOI: https://doi.org/10.1016/j.jhevol.2013.04.002.

130. S. Harmand, J. E. Lewis, C. S. Feibel, C. J. Lepre, S. Prat, A. Lenoble, X. Boës, R. L. Quinn, M. Brenet, A. Arroyo, 3.3-million-year-old stone tools from Lomekwi 3, West Turkana, Kenya. *Nature*. **521**, 310–315 (2015), DOI: https://doi.org/10.1038/nature14464.

131. J. D. Kingston, in *Paleontology and geology of Laetoli: Human evolution in context* (Springer, 2011), pp. 293–328.

132. J. G. Wynn, K. E. Reed, M. Sponheimer, W. H. Kimbel, Z. Alemseged, Z. K. Bedaso, C. J. Campisano, Dietary flexibility of Australopithecus afarensis in the face of paleoecological change during the middle Pliocene: Faunal evidence from Hadar, Ethiopia. *Journal of Human Evolution*. **99**, 93–106 (2016), DOI: https://doi.org/10.1016/j.jhevol.2016.08.002.

133. D. B. Patterson, D. R. Braun, K. Allen, W. A. Barr, A. K. Behrensmeyer, M. Biernat, S. B. Lehmann, T. Maddox, F. K. Manthi, S. R. Merritt, Comparative isotopic evidence from East Turkana supports a dietary shift within the genus Homo. *Nature Ecology & Evolution*. **3**, 1048–1056 (2019), DOI: https://doi.org/10.1038/s41559-019-0916-0.

134. E. W. Negash, Z. Alemseged, R. Bobe, F. Grine, M. Sponheimer, J. G. Wynn, Dietary trends in herbivores from the Shungura Formation, southwestern Ethiopia. *Proceedings of the National Academy of Sciences*. **117**, 21921–21927 (2020), DOI: https://doi.org/10.1073/pnas.2006982117.

135. H. T. Bunn, Patterns of skeletal representation and hominid subsistence activities at Olduvai Gorge, Tanzania, and Koobi Fora, Kenya. *Journal of Human Evolution*. **15**, 673–690 (1986), DOI: https://doi.org/10.1016/S0047-2484(86)80004-5.